

Research

Studies of Corrosion of Cladding Materials in Simulated BWR-environment Using Impedance Measurements

Part I: Measurements in the Pre-transition Region

Stefan Forsberg
Elisabet Ahlberg
Ulf Andersson

September 2004

SKI Perspective

Fuel rod cladding waterside corrosion is one of the phenomena that limits the life time of nuclear fuel. Corrosion performance depends on the cladding material properties well as operating conditions during the irradiation of the fuel. The corrosion resistance of the cladding is affected by its chemical composition and the manufacturing process. Fuel rod power history, coolant temperature and water chemistry are among the operational parameters that influence corrosion. In an ideal situation, the oxide film formed on the surface of a material protects the material against further degradation. The degree of protection depends on the properties of the oxide. Since these properties change as the oxide grows, the oxidation process has stages of different growth rates. In order to understand the mechanisms it is therefore important to monitor the corrosion process of the material through the different stages. Available methods to measure oxide thickness, however, are designed to measure oxide in the late stages of oxidation when the oxide has grown thick, and they do not allow measurement simultaneously with growth.

The project was initiated to qualify a technique for measuring oxide in-situ in an autoclave in the different stages of growth. The technique is based on electrochemical impedance spectroscopy and allows, in addition to the oxide layer thickness, the measurement of several physical properties that characterise the oxide layer. The results of the project are presented in two separate reports. They concern measurements in the pre- and post-transition corrosion regimes, respectively.

SKI has participated in the project in order to encourage efforts to increase the understanding of corrosion mechanisms for fuel rod cladding and other Zirconium components. This in turn will support the ability to make fair judgements about consequences from changes in the operation of power plants and to validate the potential improvements of new cladding materials. An additional incentive for supporting this research is that it contributes to the development of knowledge and competence in the Swedish nuclear industry, institutes and universities.

Responsible for the project at SKI have been Ingrid Töcksberg and Jan-Erik Lindbäck.
SKI reference: 14.6-010346
Project number: 21085

Studsvik reference: STUDSVIK/N(K)-03/017
2004-09-02, N64051, SKI/KP/STUDSVIK-B47:2

Research

Studies of Corrosion of Cladding Materials in Simulated BWR-environment Using Impedance Measurements

Part I: Measurements in the Pre-transition Region

Stefan Forsberg
Elisabet Ahlberg
Ulf Andersson

Studsvik Nuclear AB
SE-611 82 Nyköping
Sweden

September 2004

This report concerns a study which has been conducted for the Swedish Nuclear Power Inspectorate (SKI). The conclusions and viewpoints presented in the report are those of the author/authors and do not necessarily coincide with those of the SKI.

Stefan Forsberg
Elisabet Ahlberg
Ulf Andersson

Studies of corrosion of cladding materials in simulated BWR-environment using impedance measurements

Part I: Measurements in the pre-transition region

Abstract

The corrosion of three Zircaloy 2 cladding materials, LK2, LK2+ and LK3, have been studied in-situ in an autoclave using electrochemical impedance spectroscopy. Measurements were performed in simulated BWR water at temperatures up to 288°C. The impedance spectra were successfully modelled using equivalent circuits. When the oxide grew thicker during the experiments, a change-over from one to two time constants was seen, showing that a layered structure was formed. Oxide thickness, oxide conductivity and effective donor density were evaluated from the impedance data. The calculated oxide thickness at the end of the experiments was consistent with the value obtained from SEM. It was shown that the difference in oxide growth rate between the investigated materials is small in the pre-transition region. The effective donor density, which is a measure of electronic conductivity, was found to be lower for the LK3 material compared to the other two materials.

Sammanfattning

Korrosionen hos tre Zircaloy-2 kapslingsmaterial, LK2, LK2+ och LK3, har studerats in-situ i en autoklav med användande av elektrokemisk impedansspektroskopi. Föreliggande rapport redovisar resultaten från mätningar i förtransitionsområdet. Mätningarna har genomförts i simulerat BWR-vatten vid temperaturer upp till 288°C. Uppmätta impedansspektra har modellerats med hjälp av ekvivalenta elektriska kretsar. När oxidtjockleken ökar under experimentet syns en förändring från en till två tidskonstanter i uppmätta spektra. Detta visar att oxiden skiktas och består av ett inre och ett yttre skikt. Oxidtjocklek, oxidkonduktivitet och antal laddningsbärare har kunnat beräknas från uppmätta impedansdata. Den beräknade oxidtjockleken vid experimentets slut överensstämde med tjockleken uppmätt i SEM. Skillnaden i oxidtillväxthastighet befanns vara liten mellan de tre undersökta materialen i förtransitionsområdet. Antalet laddningsbärare, som är ett mått på elektronledningsförmågan, var lägre för LK3-materialet jämfört med de andra två materialen. Föreliggande arbete har tydligt visat att impedansspektroskopi kan användas för in-situ studier av korrosion av kapslingsmaterial i förtransitionsområdet vid temperaturer upp till 288°C.

List of contents

	Page
1	Introduction 1
2	Theory and evaluation of impedance data 2
2.1	Basic theory of AC impedance 2
2.2	Representation of impedance data 4
2.3	Equivalent circuit analysis 5
2.3.1	Impedance spectra of some simple electrical circuits 6
2.3.2	Equivalent circuits used in the present work 8
2.3.3	Oxide properties from equivalent circuit analysis 9
2.4	Oxide thickness from α -corrected capacitance 10
2.5	Mott-Schottky plots and calculation of effective donor density 12
2.5.1	Calculation of oxide capacitance from Mott-Schottky plots 14
2.6	The electrolyte double layer and the double layer capacitance 15
2.7	The Arrhenius equation and conductivity 17
3	Experimental 18
3.1	Materials 18
3.2	Experimental set-up and procedure 19
3.3	Chemistry 20
3.4	Post-experiment examinations 20
4	Results 21
4.1	The LK2 material 21
4.2	The LK2+ material 33
4.3	The LK3 material 44
5	Discussion 53
6	Conclusions 58
	Acknowledgements 59
	References 60
	Appendices
A	Data from potential measurements
B	Measured impedance spectra
C	Parameter values from equivalent circuit analysis
D	Values of α -corrected (extrapolated) capacitance and accompanying values of the dispersion factor

1 Introduction

Zirconium alloys are widely used as fuel cladding material in nuclear power plants because of their low thermal neutron cross section, mechanical properties and corrosion resistance. In pressurized water reactors (PWRs) Zircaloy 4 and in boiling water reactors (BWRs) Zircaloy 2 are used for fuel tubes. Corrosion performance is a very important parameter and a lot of work to improve the corrosion resistance has been done. The cladding material's resistance to corrosion may limit the lifetime of the fuel in the core. The corrosion performance is a function of the material properties (alloy composition and heat treatment) and the environment, such as temperature and water chemistry. Irradiation has also an impact on the corrosion of the cladding.

Impedance measurements can be used to investigate, in-situ, the physical properties of the oxide formed on the zirconium alloy. Information on the following properties can be obtained from the measurements:

- Number of layers in the oxide
- Oxide thickness
- Oxide conductivity
- Oxide porosity
- Semi-conducting properties of the oxide

Both conductivity and porosity are important in regard to the corrosion process. Several measurements have been conducted at room temperature. However, this condition is far from actual plant conditions. Equipment for in-situ impedance measurements of cladding materials at high temperature in simulated nuclear reactor water has previously been designed and built at Studsvik [1]. Initial measurements were performed in both simulated PWR water (with boron, lithium and hydrogen addition) and simulated BWR water (with oxygen or hydrogen addition) up to 290°C. An equivalent circuit for a two-layer oxide film was successfully fitted to the measured impedance. It was also shown that the impedance of water could be separated from the other impedances.

In the present work, impedance measurements were performed on three Zircaloy 2 materials, LK2, LK2+ and LK3, in simulated BWR water at high temperatures. These materials have different size distributions of secondary phase particles [2] and show differences in corrosion performance in actual plant. The purpose of the work was to qualify impedance measurements for in-situ studies of corrosion of cladding materials. Measurements have been conducted in both the pre-transition and the post-transition stage. This report presents the results from the measurements on specimens that have not been pre-oxidized (pre-transition stage). The work is a co-operation between Studsvik Nuclear AB and Department of Chemistry at Göteborg University. At Göteborg University, impedance measurements are performed on the same materials in simulated PWR water.

2 Theory and evaluation of impedance data

The impedance technique involves a potentiostat and a frequency response analyzer (FRA). By use of these devices the electrochemical potential of a working electrode is modulated sinusoidally with respect to a reference electrode, usually at the open circuit potential. The response of the current is monitored which allows the impedance to be obtained.

2.1 Basic theory of AC impedance

If a sinusoidal voltage is applied across an electrochemical cell, the resulting current will also be sinusoidal and usually out of phase with the voltage. If the voltage is given by

$$E = \Delta E \sin(\omega t) \quad (\text{Eq 1})$$

the resulting current will have the value

$$I = \Delta i \sin(\omega t + \phi) \quad (\text{Eq 2})$$

where

E or I	= instantaneous voltage or current
ΔE or Δi	= maximum amplitude of voltage or current
ω	= frequency in radians/sec = $2\pi f$
f	= frequency in Hz
ϕ	= phase shift (or phase angle or phase) in radians

Figure 1 represents typical plots of a voltage sine wave applied across a given circuit and the resultant AC current waveform. Voltage and current differ not only in amplitude, but also in phase. In this Figure, current leads voltage by phase angle $\phi = \pi/2$. For a DC circuit (a special case of AC where the frequency equals 0 Hz) Ohm's Law defines a resistance:

$$E = IR \quad (\text{Eq 3})$$

One can apply a DC voltage (E) to a circuit, measure the resulting current (I) and compute the resistance (R). For AC, where the frequency is non-zero, the analogous equation is

$$E = IZ \quad (\text{Eq 4})$$

In this equation E and I are waveform amplitudes for potential and current, respectively, and Z is defined as "impedance," the AC equivalent of resistance. The impedance is a frequency dependent number which has a magnitude ($=\Delta E/\Delta i$) and phase ($=\phi$).

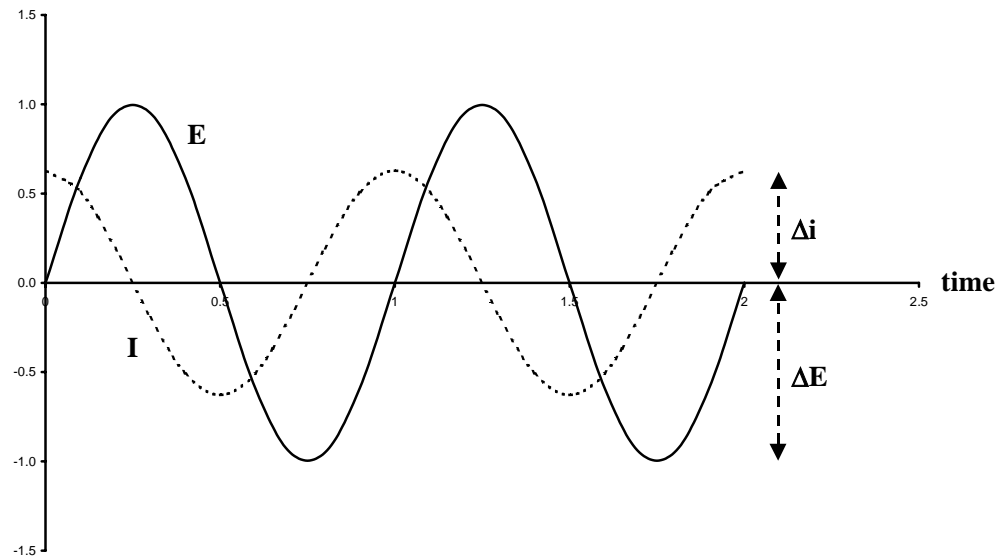


Figure 1

AC waveforms for an applied potential and a resultant current.

Vector analysis provides a convenient method of describing an AC waveform. It permits a description of the wave in terms of its amplitude and its phase. The impedance vector (quotient of the voltage and current vectors) can be graphically described in different ways. In Figure 2a, the impedance vector is unambiguously defined by the phase angle, ϕ , and the magnitude, $|Z|$. Another approach, which is often more convenient for numerical analysis, is shown in Figure 2b. Here the axes are defined as real, Z' , and imaginary, Z'' . The mathematical convention for expressing quantities in this coordinate system is to multiply the Z'' coordinate value by $\sqrt{-1}$, symbolized by "j" [3].

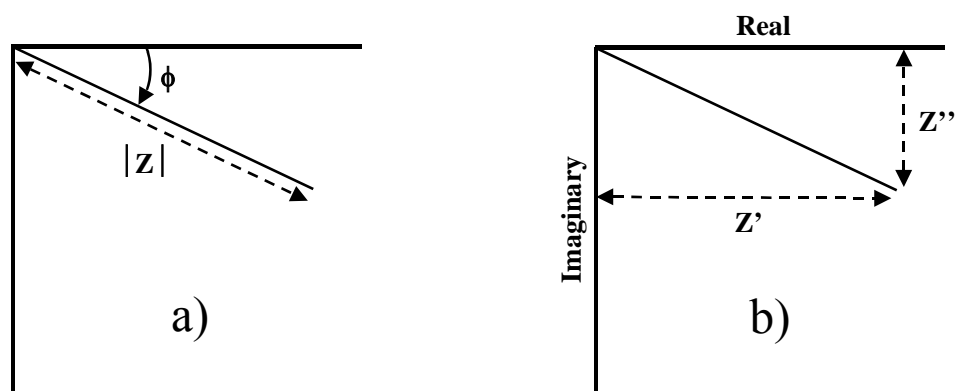


Figure 2

a) Impedance vector in terms of phase angle, ϕ , and magnitude, $|Z|$.

b) Impedance vector in terms of coordinates: real, Z' , and imaginary, Z'' .

Using this convention, the impedance vector can be defined as the sum of its real and imaginary components:

$$Z = Z' + j Z'' \quad (\text{Eq 5})$$

where $j = \sqrt{-1}$. From analytical geometry, the absolute magnitude of the impedance vector can be expressed as

$$|Z| = \sqrt{(Z')^2 + (Z'')^2} \quad (\text{Eq 6})$$

and

$$\tan \phi = \frac{Z''}{Z'} \Rightarrow \phi = \text{Arc tan} \frac{Z''}{Z'} \quad (\text{Eq 7})$$

$$Z' = |Z| \cos \phi \quad (\text{Eq 8})$$

$$Z'' = |Z| \sin \phi \quad (\text{Eq 9})$$

2.2 Representation of impedance data

The experimental impedance data can be plotted in various ways. An effective way of displaying the impedance is through a complex plane plot or 'Nyquist plot,' in which the imaginary part of the impedance (Z'') is plotted against the real part (Z'). The Nyquist plot has the frequency only as an implicit variable, and a better representation of the frequency variation of the impedance can be found through 'Bode plots' of $\log |Z|$ and phase angle (ϕ) vs $\log \omega$ (or $\log f$). In the present work, Bode diagrams are used to display impedance data. An example of a Bode plot is given in Figure 3. This diagram shows measurements made on an oxidized Zircaloy cladding at room temperature. The impedance response is mainly due to the impedance of the oxide on the Zircaloy sample. If the oxide is layered, there will be several maxima (or time constants - see section 2.3 below) in the phase angle plot, each corresponding to a specific layer. In Figure 3 it is obvious that the oxide is layered and that the properties (e.g. porosity) changes when moving from the inner layer (I) to the outer layer (III). In low conductivity water, a time constant related to the impedance of water is sometimes visible at high frequencies.

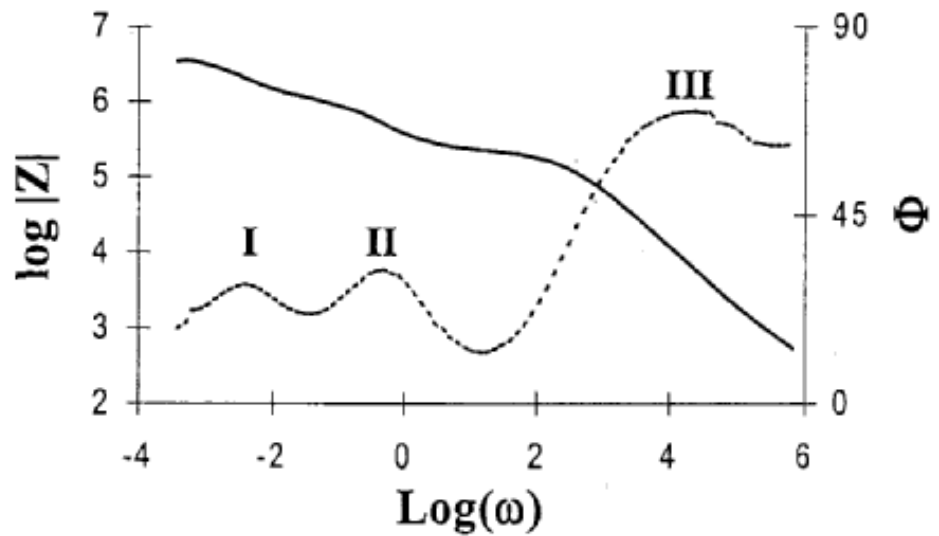


Figure 3

Impedance spectrum of oxidized Zircaloy sample measured in 0.5 M H₂SO₄ at room temperature. Dashed line = phase angle and solid line = log |Z|. Note that the negative of the phase angle is displayed in this figure.

2.3 Equivalent circuit analysis

The measured impedance spectrum can be described or modelled using a so-called equivalent electrical circuit. The impedance of some circuit elements and combinations of elements are given in Table 1. In the present work, the program LEVM 6.0 [4], incorporated into the commercial software Z-plot, was used for the equivalent circuit analysis. The analysis starts with proposing the equivalent circuit to be used. Using NonLinear Least Squares Fit (NLLSF) techniques, all parameters (e.g. R, C_Q and α) in the equivalent circuit model are adjusted simultaneously in order to obtain the optimum fit to the measured impedance data. The Constant Phase Element (CPE) listed in Table 1 is a very general diffusion related element, which is frequently encountered in solid state electrochemistry. It may be viewed as a non-ideal (leaking) capacitor. The impedance equation for the CPE is in fact a very general formula. For α = 0 it represents a resistance with R = 1/C_Q, for α = 1 a capacitance with C = C_Q, for α = 0.5 a Warburg impedance and for α = -1 an inductance with L = 1/C_Q. In general, semi-infinite diffusion is described by a Warburg impedance [4].

A parallel combination of R and C or R and Q is called a time constant. For a parallel combination of R and C, the time constant is obtained by

$$\tau = C R \quad (\text{Eq 10})$$

Table 1

AC impedance for circuit elements and combination of elements [5].

Circuit element	Symbol	AC impedance equation
Resistor	R	$Z = R$
Capacitor	C	$Z = -\frac{j}{\omega C} = \frac{1}{j\omega C}$
Constant Phase Element (CPE)	Q	$Z = \frac{1}{(j\omega)^\alpha C_Q}$
Series combination of R and C		$Z = R - \frac{j}{\omega C}$
Parallel combination of R and C		$Z = \frac{R - j\omega CR^2}{1 + \omega^2 C^2 R^2}$
Parallel combination of R and Q		$Z = \frac{R}{1 + (j\omega)^\alpha C_Q R}$

where

R = resistance (ohm)

C = capacitance (farad)

 $j = \sqrt{-1}$ ω = frequency (radians/sec) = $2\pi f$ C_Q = general parameter for CPE α = dispersion factor

and for a parallel combination of R and Q by

$$\tau = (C_Q R)^{1/\alpha} \quad (\text{Eq 11})$$

When the capacitance is expressed in farad and the resistance in ohm, the resulting unit for the time constant is seconds. A time constant will produce a maximum in the phase angle in a Bode plot. When the oxide on a Zircaloy sample is layered, one will need one time constant for each layer in order to describe the impedance. For example, in Figure 3 three time constants (I-III) are easily distinguished. The time constant thus gives the resistance and capacitance of the oxide layer, and this information can be used to calculate the oxide thickness and conductivity (see below).

2.3.1 Impedance spectra of some simple electrical circuits

A series combination of a resistor and a capacitor will produce the impedance spectrum shown in Figure 4. The electrical circuit is also displayed in this figure. At high frequencies, the impedance is only due to

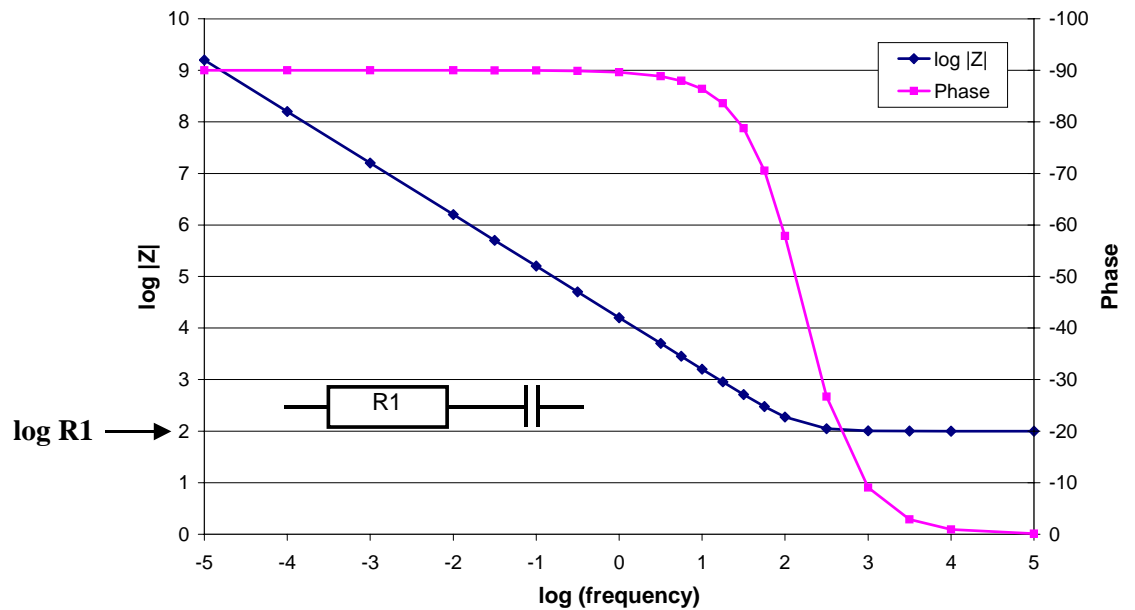


Figure 4
Impedance spectrum of a series combination of R and C.

the resistor so that $|Z| \rightarrow R1$ and phase $\rightarrow 0$. At low frequencies, the impedance is due to the capacitor. In this case phase $\rightarrow -90^\circ$ and from Eq 6 and Table 1 we see that

$$|Z| = \sqrt{(R1)^2 + (-1/(\omega C))^2} \approx \frac{1}{\omega C} = \frac{1}{2\pi f C} \quad (\text{Eq 12})$$

at these low frequencies. Taking the logarithm and rearranging one finds

$$\log |Z| = -\log 2\pi C - \log f \quad (\text{Eq 13})$$

Thus, a plot of $\log |Z|$ versus $\log f$ will produce a straight line of slope -1.

If a second resistor is connected in parallel with the capacitor, this will produce the impedance spectrum shown in Figure 5. This is the way one usually models an electrochemical reaction. At high frequencies, the impedance corresponds to the impedance of resistor R1 so that $|Z| \rightarrow R1$ and phase $\rightarrow 0$. At low frequencies, the impedance corresponds to a series connection of R1 and R2 so that $|Z| \rightarrow R1+R2$ and phase $\rightarrow 0$. In the mid-frequency region, we have the capacitive region, where the capacitor influences the impedance. Here, a linear section of slope -1 is found in the plot of $\log |Z|$ versus $\log f$, and the phase angle goes through a maximum.

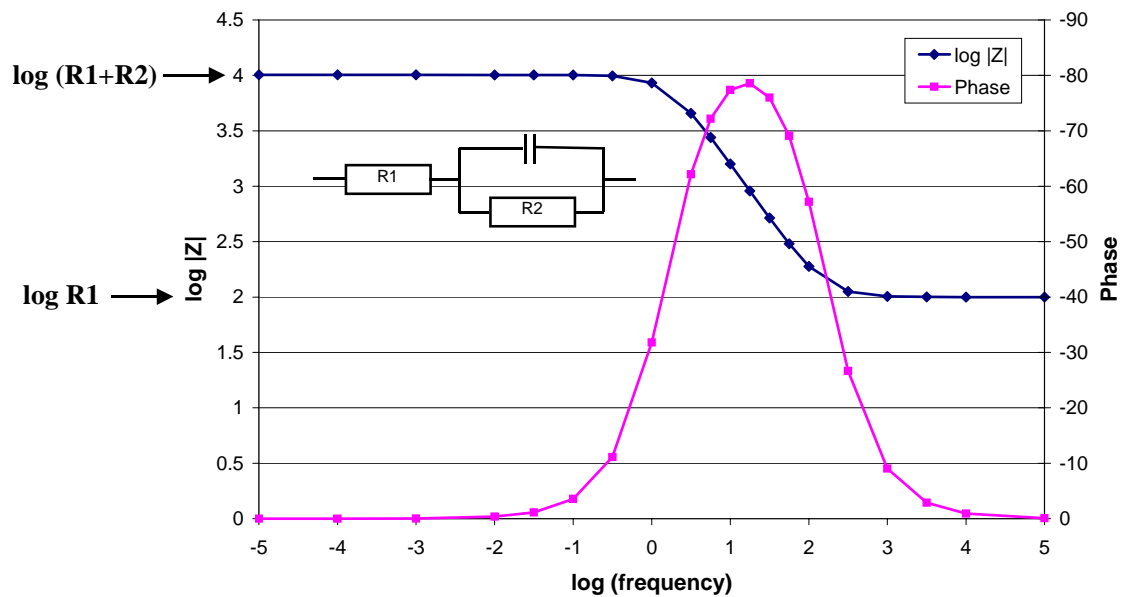


Figure 5

Impedance spectrum of a resistor connected in series with a parallel RC-unit.

2.3.2 Equivalent circuits used in the present work

Generally, oxides in the pre-transition stage are relatively non-porous and can be characterized by one or two time constants. In the present work, mainly two types of equivalent circuits have been used. These are shown in Figure 6. In this figure, only a resistance is used for the impedance of the electrolyte. In low conductivity water (without addition of supporting electrolyte or at low temperature) a parallel combination of R and C, i.e. a time constant, is needed to describe the impedance of water. In our measurements, the impedance exhibits some frequency dispersion, i.e. the capacitance of the oxide varies with frequency. Therefore, constant phase elements were used instead of capacitors. When written as in Figure 6b, Q1 is the total capacitance of the oxide (inner and outer layer) and Q2 is the capacitance of the inner layer.

The most difficult part of an equivalent circuit analysis is to find a suitable circuit. Sometimes impedance measurements give results that are hard to fit to an electrical circuit. These difficulties arise because the simple equivalent circuits do not fully describe the physical phenomena of an electrochemical system. Yet simple equivalent circuit models are frequently good approximations to real systems and data can often be fitted to yield results of reasonable accuracy.

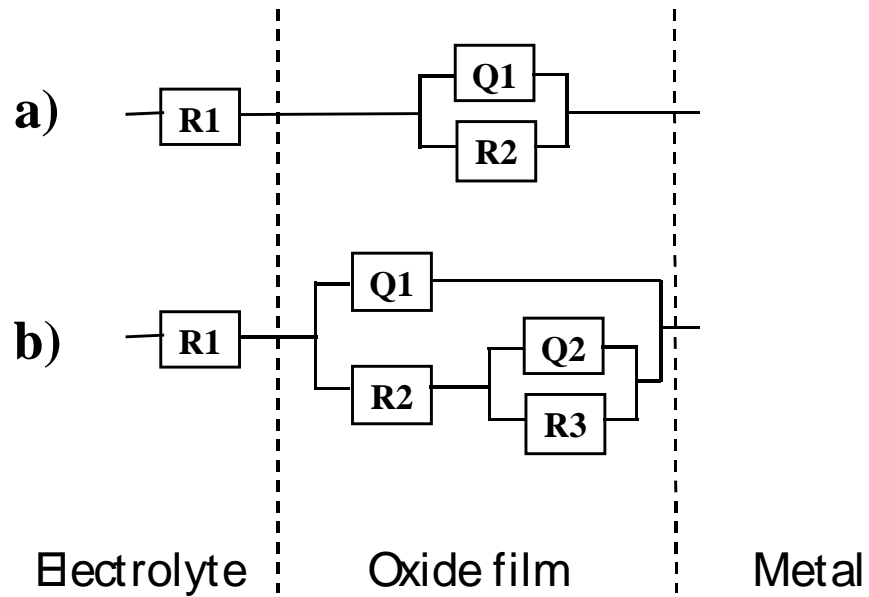


Figure 6
Equivalent circuit of a) one-layer oxide film and b) two-layer oxide film in high conductivity electrolyte.

2.3.3 Oxide properties from equivalent circuit analysis

From the values obtained in the equivalent circuit analysis, the following oxide properties have been evaluated.

Oxide thickness

The oxide behaves like a capacitor in the impedance measurements and the overall thickness can be calculated by the expression for a parallel plate capacitor [6-8]:

$$d = \frac{\varepsilon \varepsilon_0 A}{C_Q^{1/\alpha}} \quad (\text{Eq 14})$$

where

- d = oxide thickness
- ε = dielectric constant of ZrO_2 (= 22)
- ε_0 = permittivity of a vacuum (= 8.854×10^{-12} F/m)
- A = area of Zircaloy sample (= 6.635×10^{-4} m²)
- C_Q = capacitance (of Q1 in Figure 6)
- α = dispersion factor (of Q1 in Figure 6)

In Eq 14, the capacitance has been corrected for the dispersion factor α . It should be pointed out that when α becomes too low ($< \sim 0.85$), Eq 14 cannot be used to calculate the oxide thickness. In this case, the calculated thickness will be too large.

Oxide conductivity

The conductivity is inversely proportional to the resistance and can be calculated by the following formula

$$\sigma = \frac{d}{RA} = \frac{\epsilon\epsilon_0}{RC_Q^{1/\alpha}} \quad (\text{Eq 15})$$

where

σ = specific conductivity of the oxide
 R = resistance of the oxide (= $R_2 + R_3$ in Figure 6)
 $d, A, \epsilon, \epsilon_0, C_Q$ and α as in Equation 14.

Inhomogeneity

The dispersion coefficient is a measure of inhomogeneity. This may be interpreted as the extent or nature of the porosity of the oxide.

2.4 Oxide thickness from α -corrected capacitance

At frequencies where the impedance spectrum can be modelled by an RC series equivalent circuit we can write (see Eq 5 and Table 1)

$$Z = Z' + j Z'' = R - j/\omega C \quad (\text{Eq 16})$$

Hence, at these frequencies, a capacitance can be calculated from the imaginary component using

$$C = -\frac{1}{\omega Z''} = -\frac{1}{2\pi f Z''} \quad (\text{Eq 17})$$

As we have seen above, a series combination of R and C will produce a straight line of slope -1 in the $\log |Z|$ vs $\log f$ plot. When dealing with real systems (which require parallel RC-units), linear sections of slope -1 are found at frequencies corresponding to maxima of the phase angle (capacitive region - see also section 2.3.1). In these regions, a plot of $\log C$ vs $\log f$ will produce a straight line.

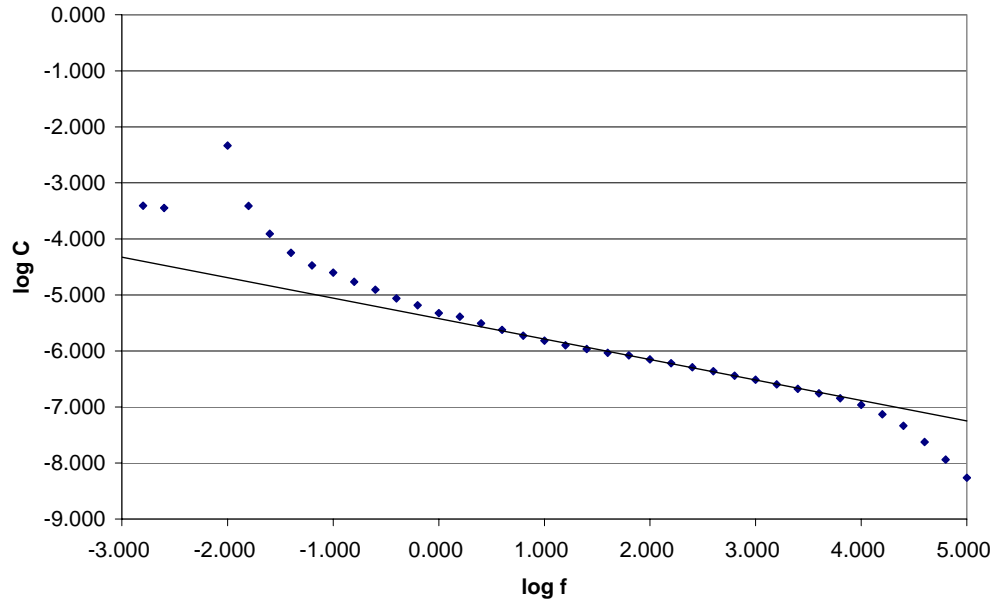


Figure 7

An example of a plot of $\log C$ versus $\log f$. The capacitance is calculated from Eq 17.

An example of this is shown in Figure 7. An α -corrected capacitance, $C_{\alpha\text{-corr}}$, is obtained by extrapolating the linear section to high frequencies. In the present work, $C_{\alpha\text{-corr}}$ was calculated by extrapolating to 10^5 Hz [9]. The $C_{\alpha\text{-corr}}$ -value should agree reasonably well with $C_Q^{1/\alpha}$ from the equivalent circuit analysis. Also, from the linear section of the $\log C$ vs $\log f$ plot, α can be calculated according to the following equation:

$$\alpha = 1 + S \quad (\text{Eq 18})$$

where S = slope. By assuming that the measured capacitance originates almost entirely from a simple parallel plate capacitor with ZrO_2 acting as a dielectric, the oxide thickness can be calculated from

$$d = \frac{\varepsilon \varepsilon_0 A}{C_{\alpha\text{-corr}}} \quad (\text{Eq 19})$$

where ε , ε_0 and A have the same meaning as in Eq 14.

2.5 Mott-Schottky plots and calculation of effective donor density

Information about the electronic conductivity through the ZrO₂ lattice can be obtained from capacitance vs voltage (CV) profiles. During these experiments, the impedance is measured as a function of the voltage, without anodizing the sample (i.e. without affecting the thickness of the oxide film). In the present work, the voltage was varied between -1 and +1 V vs open circuit potential (OCP). The capacitance is calculated from the imaginary component of the impedance at a fixed frequency in the capacitive region (around the maximum in the phase angle) using Eq 17. From this data, so-called Mott-Schottky plots of C^{-2} vs voltage, V , can be constructed. An example of a Mott-Schottky plot is presented in Figure 8. The relation between capacitance, C , and voltage, V , can be written [10-12]

$$C^{-2} = C_{ox}^{-2} + \left(\frac{2}{\varepsilon\varepsilon_0 e N_D A^2} \right) \left(V - V_{fb} - \frac{k_B T}{e} \right) \quad (\text{Eq 20})$$

where

C_{ox}	= oxide capacitance
e	= elementary charge of the electron (= 1.602×10^{-19} C)
N_D	= effective donor density
k_B	= Boltzmann constant (= 1.38066×10^{-23} J K ⁻¹)
T	= absolute temperature
V_{fb}	= flat band potential (= -1.4 V vs SCE = -1.1585 V vs SHE)

and ε , ε_0 and A have their usual meaning. Eq 20 predicts a linear relationship between C^{-2} and V , where the slope, S , is given by

$$S = \frac{2}{\varepsilon\varepsilon_0 e N_D A^2} \quad (\text{Eq 21})$$

Eqs 20 and 21 are valid for n-type semiconductors. For p-type semiconductors, the sign of the slope will change. As can be seen from Eq 21, the slope of the Mott-Schottky plot, dC^{-2}/dV , is not influenced by the oxide capacitance. Solving for the donor density, one obtains

$$N_D = \frac{2}{\varepsilon\varepsilon_0 e S A^2} \quad (\text{Eq 22})$$

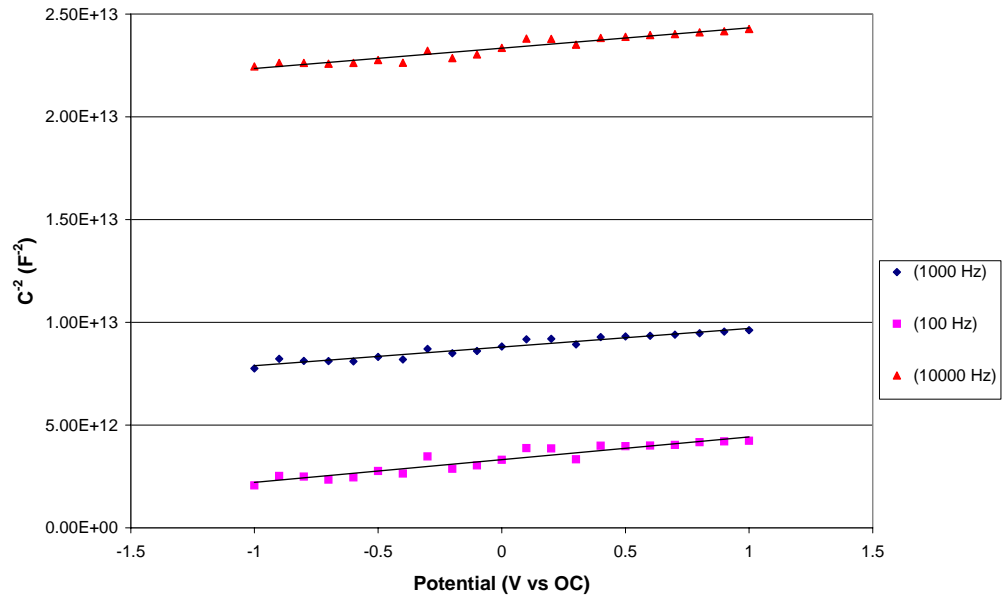


Figure 8

Examples of Mott-Schottky plots constructed at three different frequencies in the capacitive region.

When using SI-units, the resulting unit for N_D is m^{-3} . N_D may be interpreted as the concentration of mobile electrons in the conduction band.

According to Goossens et al. [10], the observed dependence of C^{-2} on applied voltage can be understood by regarding the measured capacitance, C , as resulting from a series combination of a potential independent oxide capacitance, C_{ox} , and a potential dependent space charge capacitance, C_{sc} . In that case

$$C^{-1} = C_{\text{ox}}^{-1} + C_{\text{sc}}^{-1} \quad (\text{Eq 23})$$

The space charge region is a non-neutral region that can be formed in the oxide film either at the film/solution interface or at the metal/film interface. Together with the capacitance of the oxide and the space charge region, one should also consider the capacitance of the Helmholtz layer, C_{H} , in the oxide/solution interface. Thus, the total capacitance is given by

$$C^{-1} = C_{\text{ox}}^{-1} + C_{\text{sc}}^{-1} + C_{\text{H}}^{-1} \quad (\text{Eq 4})$$

It turns out, however, that in most cases C_{H} is much larger than C_{ox} or C_{sc} so that Eq 24 reduces to Eq 23.

2.5.1 Calculation of oxide capacitance from Mott-Schottky plots

From Eq 20, the intercept of the Mott-Schottky plot on the potential axis ($C^{-2} = 0$; $V = V_0$) is given by

$$V_0 = V_{fb} + \frac{k_B T}{e} - \frac{\epsilon \epsilon_0 e N_D A^2}{2C_{ox}^2} = V_{fb} + \frac{k_B T}{e} - \frac{1}{S C_{ox}^2} \quad (\text{Eq 25})$$

where S = slope of the Mott-Schottky plot. Solving for the oxide capacitance, one obtains

$$C_{ox} = \sqrt{\frac{1}{S (V_{fb} - V_0 + k_B T / e)}} \quad (\text{Eq 26})$$

In the present work, the flat band potential given in Eq 20, is considered to be independent of temperature. As can be seen in Figure 8, the lines at different frequencies are parallel, and they will therefore intersect the potential axis at different positions. In the present work, a α -corrected capacitance was derived according to the procedure described in section 2.4 above. The Mott-Schottky plot constructed from this α -corrected capacitance was used to calculate V_0 (and also S) in Eq 26. If flat band potential is given vs SHE, V_0 should also be given vs SHE.

Goossens et al. [10] found, in their room temperature measurements, that C_{ox} is practically identical to the measured total capacitance, C. This justifies our previous assumption to consider the measured capacitance as originating almost entirely from a simple parallel plate capacitor with ZrO_2 acting as a dielectric. The additional space charge capacitance makes only a minor contribution to the total measured capacitance. That is, C_{sc} is considerably larger than C_{ox} ($C_{sc} \gg C_{ox}$), so that Eq 23 reduces to

$$C^{-1} = C_{ox}^{-1} + C_{sc}^{-1} \approx C_{ox}^{-1} \quad (\text{Eq 27})$$

Therefore, in this case, the total measured capacitance, C, can be used to calculate the oxide thickness. Still it is possible to calculate the number of charge carriers from the slope, since the slope is independent of the total oxide capacitance.

2.6 The electrolyte double layer and the double layer capacitance

When a metal electrode is brought into contact with a solution, a charged double layer will form at the phase boundary. The electrode surface will acquire a charge (positive or negative) and an excess of ions of charge opposite to that on the electrode surface will be found in the solution close to the electrode. As explained in chapter 3.4 in Hamann et. al. [13], the simplest view of the phase boundary is to imagine that these ions approach the surface of the electrode as closely as possible. The double layer then consists of two parallel layers of charge, one on the electrode surface and one comprising ions at the distance of closest approach. If we identify the solvent side of the double layer with the centre of charge of the (possibly solvated) ions present in excess, the separation of the charged layers will be half the diameter of the (possibly solvated) ions. This model is known as the Helmholtz layer model and the plane passing through the centre of charge of the ions is termed the Helmholtz plane. It is clear that the Helmholtz layer will behave as a parallel plate capacitor and the capacitance should be given by

$$C_H = \frac{\varepsilon'_{H_2O} \varepsilon_0}{a/2} \quad (\text{Eq 28})$$

where ε'_{H_2O} is the dielectric constant of water in the Helmholtz layer and a is the diameter of the (possibly solvated) ions. The situation is, however, complicated by the fact that the water dipoles cannot re-orient freely in the Helmholtz layer and, therefore, the dielectric constant of water will be considerably lowered.

The Helmholtz model is however incomplete since, at low electrolyte concentrations, ions will tend to release from the compact Helmholtz layer [14]. As discussed in Ref. [13], Gouy and Chapman proposed a model that led to the picture of a diffuse double layer, consisting of ions of both charges, in a spatially quite extended region near the electrode surface. Ions of charge opposite to that on the electrode surface are present in excess compared to the bulk of the electrolyte, and ions of the same charge as the electrode surface are present in lower concentration compared to the bulk. Later, Stern pointed out that the most realistic model is a combination of the Helmholtz layer and the diffuse layer models. Thus, the double layer is divided into two layers that lie in series with each other, and the expression for the total double layer capacitance will be

$$\frac{1}{C} = \frac{1}{C_H} + \frac{1}{C_{dl}} \quad (\text{Eq 29})$$

where C_{dl} is the capacitance of the diffuse layer, which is given by

$$C_{dl} = \frac{\varepsilon_{H_2O} \varepsilon_0}{L_D} \quad (\text{Eq 30})$$

where L_D is the so-called Debye length. It follows that the potential drop between the interior of the electrode and the interior of the solution can be divided into two contributions, the potential drop across the Helmholtz layer and the potential drop across the diffuse layer. The Debye length is the distance from the Helmholtz plane to the point at which the diffuse layer potential has dropped to a value $1/e$ of its total change from Helmholtz plane to bulk solution. It may be considered as a measure of the thickness of the double layer. According to section 2.2.3.2 in Ref. [4], the Debye length is given by

$$L_D = \frac{1}{\sqrt{\frac{F^2}{\varepsilon_{H_2O} \varepsilon_0 RT} \sum z_i^2 c_i}} \quad (\text{Eq 31})$$

where F is the Faraday constant ($= 96\,485 \text{ C mol}^{-1}$) and z_i and c_i is the charge and concentration (in mol m^{-3}) of the ions. The sum includes all ions. Using SI-units, the resulting unit for L_D is metre (m).

From Eq 31 it can be seen that the thickness of the double layer depends primarily on the ionic strength of the solution. The diffuse double layer may, in dilute solutions, extend more than 10 nm, whereas at high ionic strengths, the thickness of the double layer is not much greater than the Helmholtz layer (the latter is around 0.1 – 0.2 nm). It follows that, for high ionic strengths, the diffuse double layer will be small so that C_{dl} becomes large (Eq 30) and can be neglected in the expression for the total capacitance of the double layer (Eq 29). Under these circumstances, the entire potential drop is accommodated across the Helmholtz layer, and the diffuse double layer can be neglected. In dilute solutions, on the other hand, the capacitance of the diffuse layer must be taken into account. When L_D increases, C_{dl} decreases and becomes increasingly significant in the expression for the total double layer capacitance (Eq 29). As a result, in more dilute solutions, the value of C decreases.

2.7 The Arrhenius equation and conductivity

The Arrhenius equation was originally developed to describe the temperature dependence of the rate constant of a chemical reaction. Later it has been found that this type of equation can be used to describe the temperature dependence of a variety of phenomena. According to West [15], for example, the temperature dependence of ionic conductivity in a solid is usually given by the Arrhenius equation

$$\sigma = A e^{-E_A/RT} \quad (\text{Eq 32})$$

where

σ	= conductivity (unit $\Omega^{-1} \text{ m}^{-1}$)
A	= pre-exponential factor (constant)
E_A	= activation energy (unit J mol^{-1})
R	= gas constant = $8.31451 \text{ J mol}^{-1} \text{ K}^{-1}$
T	= absolute temperature (unit K)

The pre-exponential factor, A , contains several constants, including the vibrational frequency of the potentially mobile ions. Taking the logarithm of Eq 32 one obtains

$$\log \sigma = \log A - \frac{E_A \log e}{R} \frac{1}{T} \quad (\text{Eq 33})$$

Therefore, graphs of $\log \sigma$ against T^{-1} should give straight lines of slope $-E_A \log e/R$. Such graphs are called Arrhenius plots. In the present work, the impedance has been measured at some different temperatures between room temperature and 288°C . From these data Arrhenius plots have been constructed.

3 Experimental

3.1 Materials

The materials used for the present investigations were three different Zircaloy-2 tubes: LK2, LK2+ and LK3. Sandvik Steel AB manufactured the tubes, and their chemical composition is given in Table 2. The main difference between the three materials is the size distribution of second phase particles (SPP). The size distribution of SPPs in the LK2, LK2+ and LK3 fuel cladding before and after different amounts of irradiation in Forsmark 3 power plant has been measured by Nystrand and Lundström [2]. The results show that the LK2 non-irradiated material has the smallest particle diameter and the LK3 material has the largest particle diameter. The particle density in all three materials decreases with irradiation time. After a burn-up of about 40 MWd/kgU, the LK3 fuel cladding had 18 % of the particles left, the LK2+ had 9 % left and the LK2 fuel cladding had no particles left. The SPPs increases the corrosion resistance. The disappearance of the SPPs in the LK2 material at high burn-ups is therefore expected to increase the corrosion rate of this material.

Six Westinghouse Atom SVEA-96 fuel rods with LK2, LK2+ and LK3 cladding, irradiated for three and four years in Forsmark 3, have earlier been examined in Studsvik. This examination showed that the LK3 material had the best corrosion resistance (thinnest oxide) and the LK2 material the least corrosion resistance (thickest oxide) [2]. The difference in corrosion behaviour was, however, not so significant as the difference in hydrogen uptake. The LK3 material had the lowest hydrogen uptake and the LK2 material the highest hydrogen uptake. Thus, the size distribution of SPPs seems to be important in regard to the in-reactor fuel cladding corrosion behaviour and hydrogen uptake.

The tubes used for the present experiments are 22 mm long and the diameter is 9.6 mm. Thus, the area exposed in the impedance measurements was 6.6 cm². For the measurements reported here, un-oxidized samples of the different materials were used.

Table 2

Chemical composition of Zircaloy-2 tubes.

Sample	Lot No.	Alloying elements (wt.-%)			
		Sn	Fe	Cr	Ni
LK2	44-222	1.5	0.12	0.10	0.05
LK2+	99-107	1.3	0.18	0.10	0.05
LK3	99-108	1.3	0.18	0.10	0.05

3.2 Experimental set-up and procedure

The impedance measurements were carried out in an autoclave at temperatures up to 288°C. A schematic picture of the experimental set-up is shown in Figure 9. High purity, degassed water with a conductivity of less than 0.07 $\mu\text{S}/\text{cm}$ was pre-heated before it entered the autoclave (except for the room temperature measurements). A continuous water flow of about 2 litres per hour was used during the experiments. As shown in Figure 9, dosage of chemicals to the water was possible. The autoclave and other wetted surfaces at high temperature were made of titanium in order to avoid influence from corrosion products of stainless steel.

A two-electrode cell was used for the impedance measurements. The counter (outer) electrode was a platinum cylinder and the working (inner) electrode was the Zircaloy cylinder. The distance between these electrodes was small, about 0.3 mm. The counter electrode (CE) and working electrode (WE) were insulated from the autoclave using Teflon (PTFE). The equipment was designed to avoid water penetration into the Zircaloy cylinder. The autoclave was also equipped with a Ag/AgCl reference electrode, used to measure the potentials of the platinum and Zircaloy electrodes. The instrumentation used for the impedance measurements was an EG&G Princeton Applied Research Potentiostat Model 273A, and a Solartron SI 1255 frequency response analyzer. Data on electrode potentials, autoclave temperature and ambient temperature conductivity of pure water were collected using a Hewlett Packard data acquisition unit 34970A.

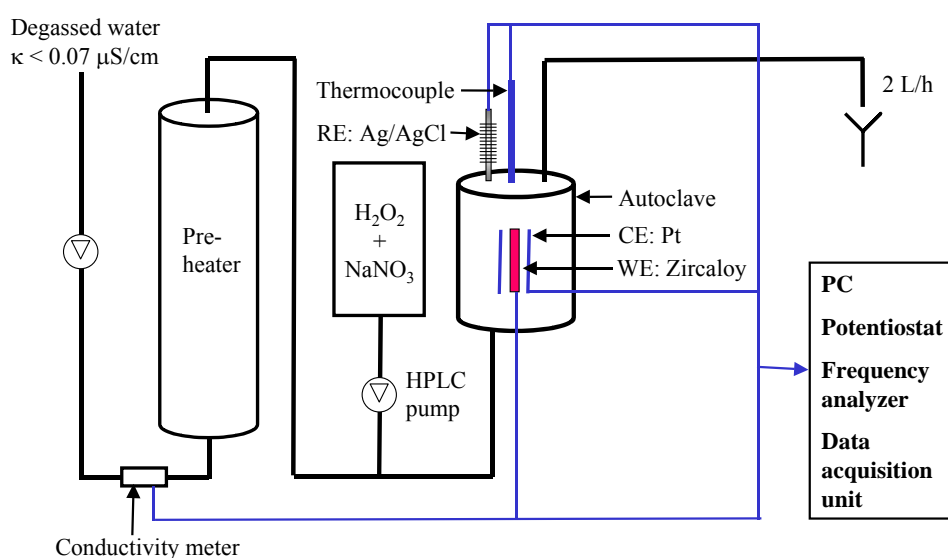


Figure 9
Schematic picture of the experimental set-up used for the impedance measurements.

At the start of an experiment, the electrodes were mounted in the autoclave, the water flow was started and the pressure was raised to 90 bar. Impedance measurements were then usually performed at room temperature, and at a few other temperatures, before raising the temperature to 288°C. During the measurements, an AC voltage (usually 10 mV) was applied between the CE and WE at the open circuit potential. Measurements were carried out in the frequency range 0.001 Hz – 100 000 Hz. The samples were kept for a prolonged time at 288°C. This time varied between the samples and was 47 days for LK2, 45 days for LK2+ and 127 days for the LK3 material. During this period, impedance measurements were usually carried out once a day. A few measurements were also carried out when lowering the temperature at the end of the experiment (except for the LK2+ sample). In addition to this, measurements were also performed at applied voltage in the range –1 to +1 V versus open circuit potential in order to obtain information about the electronic conductivity (see section 2.5).

3.3 Chemistry

In order to simulate the oxidizing in-core environment of a BWR, 500 ppb hydrogen peroxide (H_2O_2) was dosed to the water in the present experiments. Some of the H_2O_2 decomposed. According to calculations using PEROX [16], 110 ppb H_2O_2 remained at the Zircaloy sample and 180 ppb O_2 was formed.

Experiments were at first conducted without addition of supporting electrolyte. It was found, however, that some diffusion process in the water was rate limiting at this low ionic strength, so that it was not possible to study the properties of the oxide. Therefore, in order to increase the conductivity of the water, NaNO_3 was added to a concentration of 0.2 mM. Using the limiting ionic conductivities for Na^+ and NO_3^- at 25°C [13], a conductivity of 24.3 $\mu\text{S}/\text{cm}$ is calculated. The ambient temperature conductivity was also measured at one occasion, and was found to be 22.9 $\mu\text{S}/\text{cm}$.

3.4 Post-experiment examinations

The oxide thickness at the end of each experiment was measured using scanning electron microscopy (SEM). A few mm of the Zircaloy tube was embedded in an epoxy resin, and the surface was coated with a thin layer (approx. 50 Å) of gold. The study was performed in a JEOL JSM 6300 scanning electron microscope in backscattered electron image mode. The oxide thickness was measured using a Noran/Voyager image analysis system.

The hydrogen contents of the Zircaloy samples were determined at the end of the experiments using the instrument ELTRA OH 900. The samples are melted so that the hydrogen is released as hydrogen gas. The total hydrogen contents is measured using a thermo conducting detector, TCD.

4 Results

In the present work, the oxidation of three different Zircaloy-2 materials, LK2, LK2+ and LK3, have been studied in situ in an autoclave using electrochemical impedance spectroscopy (EIS). The results are accounted for below. During these experiments, the potentials of the platinum and Zircaloy electrodes as well as the potential of the autoclave (titanium) have been continuously monitored. Potentials measured are presented in Appendix A. All impedance spectra measured are given in Appendix B, and the results from the equivalent circuit analysis is tabulated in Appendix C. Values of the α -corrected (extrapolated) capacitance and the dispersion factor, derived according to the procedure given in section 2.4, are tabulated in Appendix D.

4.1 The LK2 material

Impedance measurements were carried out in the temperature range 20 - 288°C on a material that had not been pre-oxidized. Dosage of H₂O₂ (500 ppb) and NaNO₃ (0.2 mM) were made throughout this experiment. The potentials measured are shown in Figure A.1 in Appendix A.1. The autoclave temperature is also displayed in this figure. It can be seen that the potential of the Zircaloy electrode is 300 – 500 mV lower than the potentials of the platinum electrode and the autoclave. Also, the Zircaloy potential increases with time at the beginning of the experiment.

All impedance spectra measured are given in Appendix B.1–B.9. The numbers in the legends correspond to the date when the measurement was performed. For example, "zry0111" is a measurement conducted January 11 (2002). During the period January 31 – March 18, the temperature was 288°C. Impedance spectra measured at three different temperatures at the beginning of the experiment are shown in Figure 10. It can be seen that the impedance decreases as the temperature increases, especially at low and high frequencies. From the phase angle plot it can be seen that the time constant (maximum in phase angle) is displaced to higher frequencies with increasing temperature.

All impedance spectra have been modelled using the equivalent circuits described in section 2.3.2. At room temperature, a time constant (parallel combination of R and C), instead of a pure resistance, is needed to describe the impedance of the electrolyte. The results from the equivalent circuit analysis are tabulated in Appendix C.1. The temperature of the measurements is also given. At the beginning of the experiment, only one time constant is required to describe the impedance of the oxide. An example of such a spectrum, measured at room temperature, is presented in

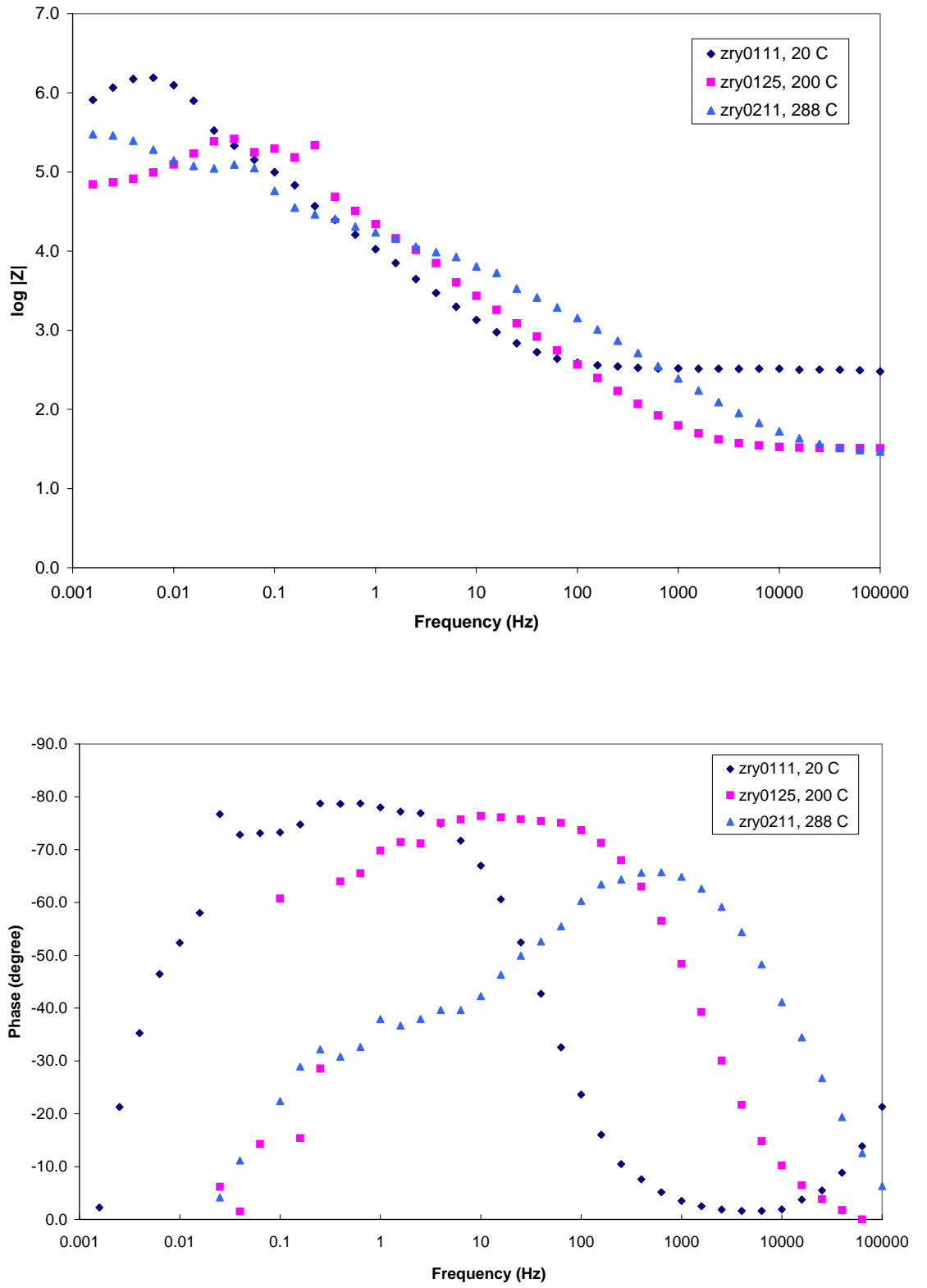


Figure 10
Impedance spectra of the LK2 material at three different temperatures at the beginning of the experiment.

Figure 11. The triangles are experimental data and the lines are the result from the equivalent circuit analysis. The time constant discernible at high frequencies ($>10^4$ Hz) is due to the impedance of the electrolyte. In all measurements made at 288°C, two time constants are required to describe the impedance of the oxide. This shows that the oxide is composed of an inner and an outer layer. An example of a spectrum measured at 288°C is presented in Figure 12. When lowering the temperature at the end of the experiment, the impedance spectra at 200° and 100°C were distorted. There was a discontinuity in the impedance at 10 Hz and the data exhibited a large spread below this frequency. Equivalent circuit analysis was not successful at these two temperatures.

Oxide thickness and conductivity

The calculated oxide thickness and conductivity are shown as functions of test time in Figure 13. The oxide thickness was calculated from the fit parameters of the equivalent circuit analysis (Eq 14) and from a α -corrected (extrapolated) capacitance. Values of the α -corrected capacitance and the dispersion factor, derived according to the procedure in section 2.4, are tabulated in Appendix D.1. The conductivity was calculated from Eq 15. The test time at 288°C is indicated in Figure 13. The calculated thickness from the fit parameters is somewhat scattered but amounts to approximately 800 nm at the end of the experiment. The calculation based on the α -corrected capacitance predicts a thickness of about 600 nm at the end of the experiment, except for the last three measurements when the temperature was lowered. Here, the calculated thickness is somewhat higher.

After the experiment, the material was investigated by light optical microscopy (LOM) and scanning electron microscopy (SEM) – see Figures 14 and 15. The oxide thickness deduced from the SEM investigation is compared with the calculated thickness from the impedance measurements in Table 3. The measured hydrogen content is also given in this table. It can be seen that the calculated thickness from the impedance measurements is in good agreement with the thickness measured by SEM.

Table 3

Oxide thickness and hydrogen content of the materials at the end of the experiments.

Material	Test time at 288°C (days)	Oxide thickness (nm)		Hydrogen content (ppm)
		EIS	SEM	
LK2	47	600-800	600-700	71
LK2+	46	600-850	600-700	64
LK3	127	930-1030 ^a	1000-1200	79

^a Based only on the α -corrected (extrapolated) capacitance.

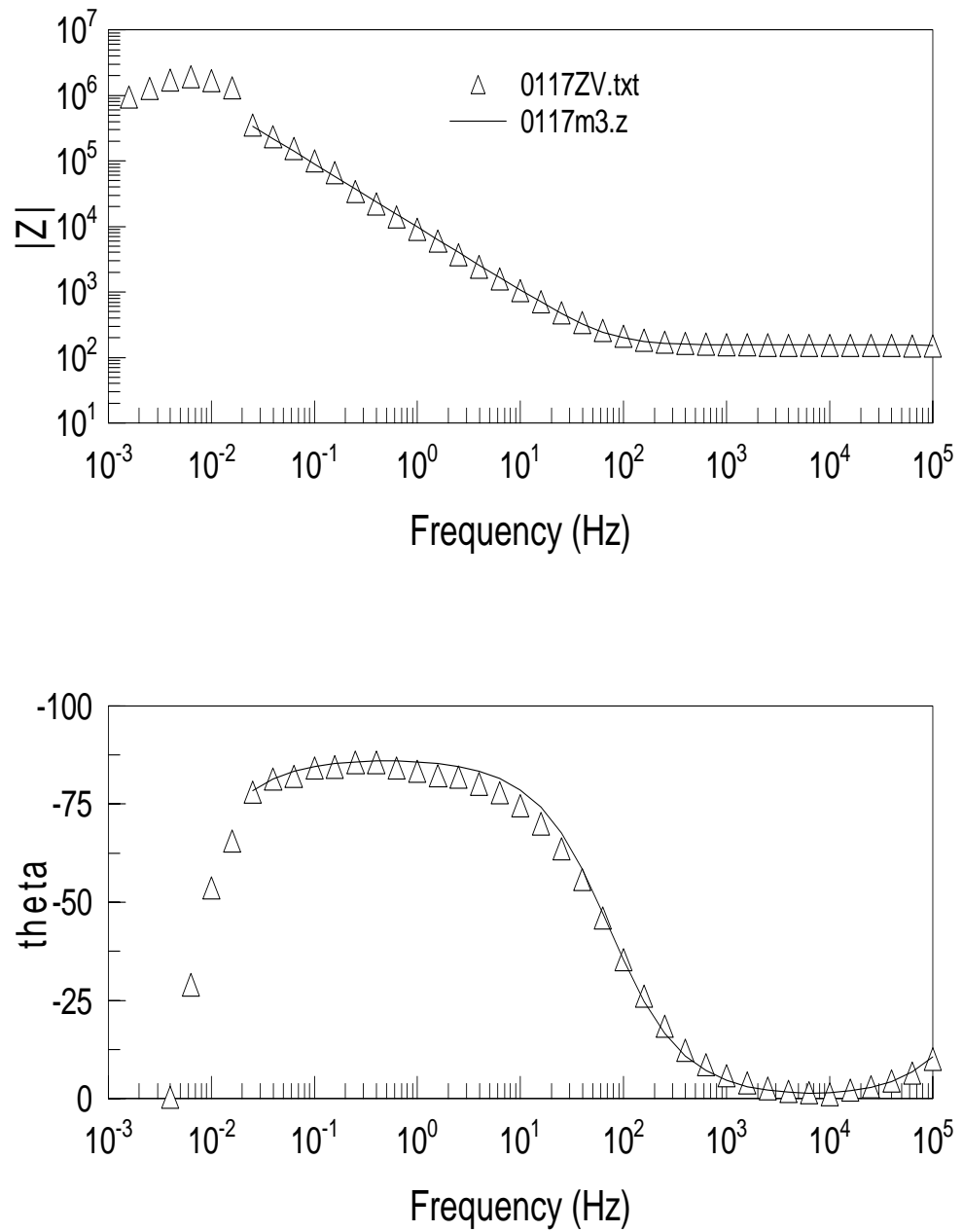


Figure 11

Impedance spectrum of the LK2 material measured at room temperature and the result of the equivalent circuit analysis.

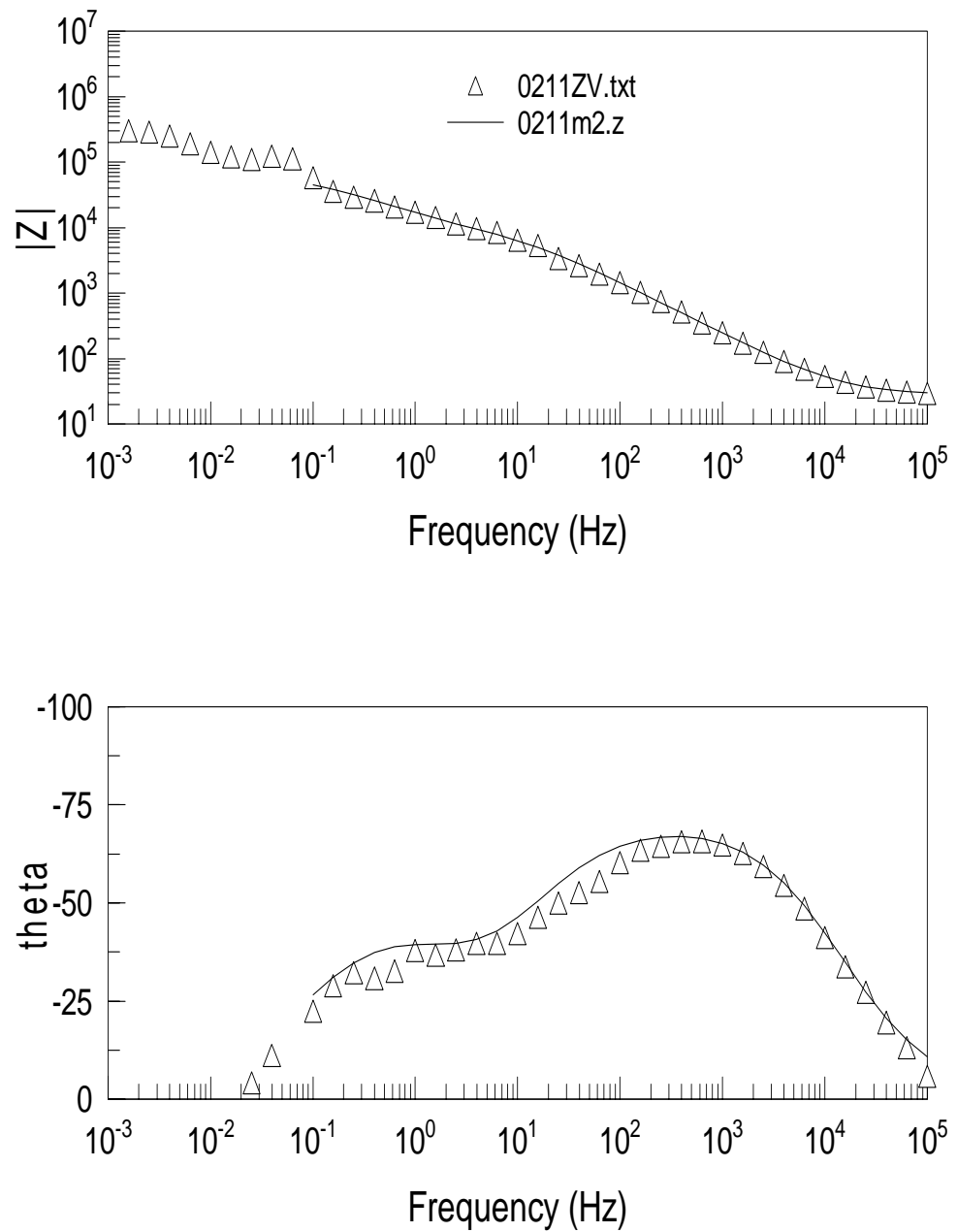


Figure 12

Impedance spectrum of the LK2 material measured at 288°C and the result of the equivalent circuit analysis.

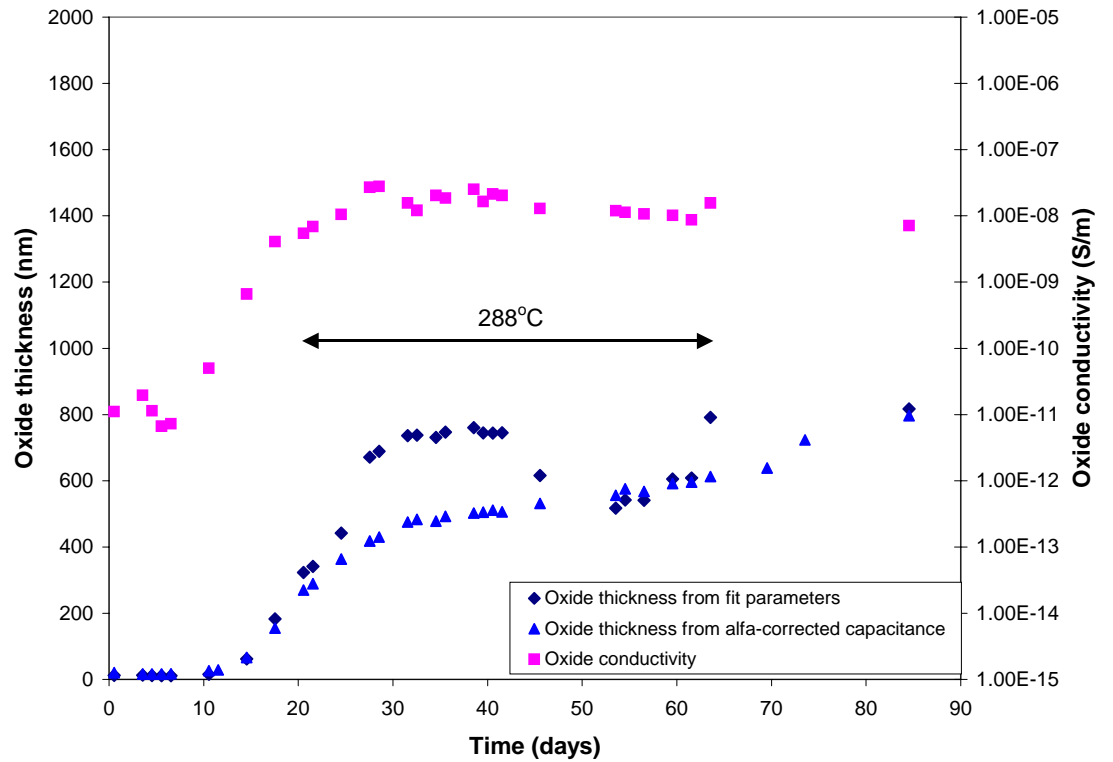


Figure 13
Calculated oxide thickness and conductivity for the LK2 material.

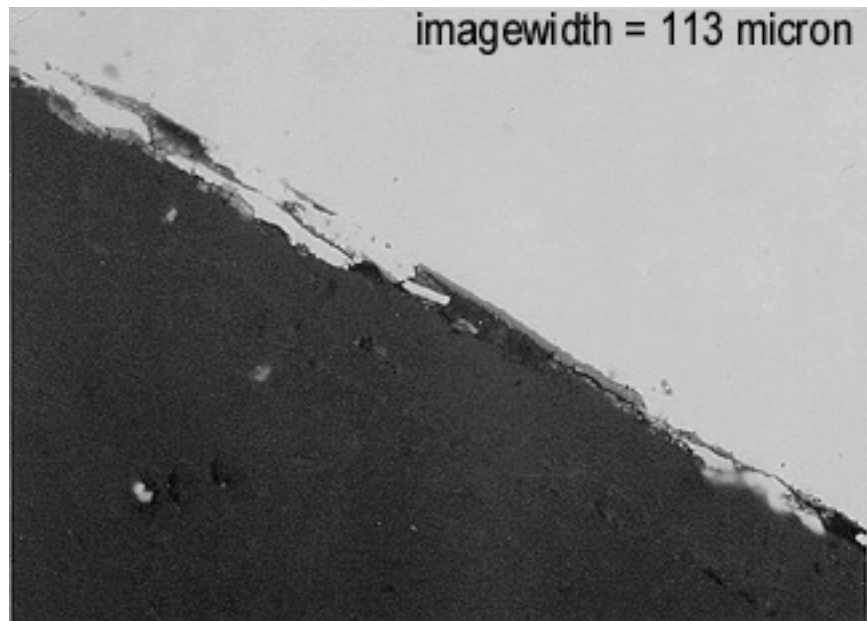


Figure 14
Light optical micrograph of the LK2 material after experiment.

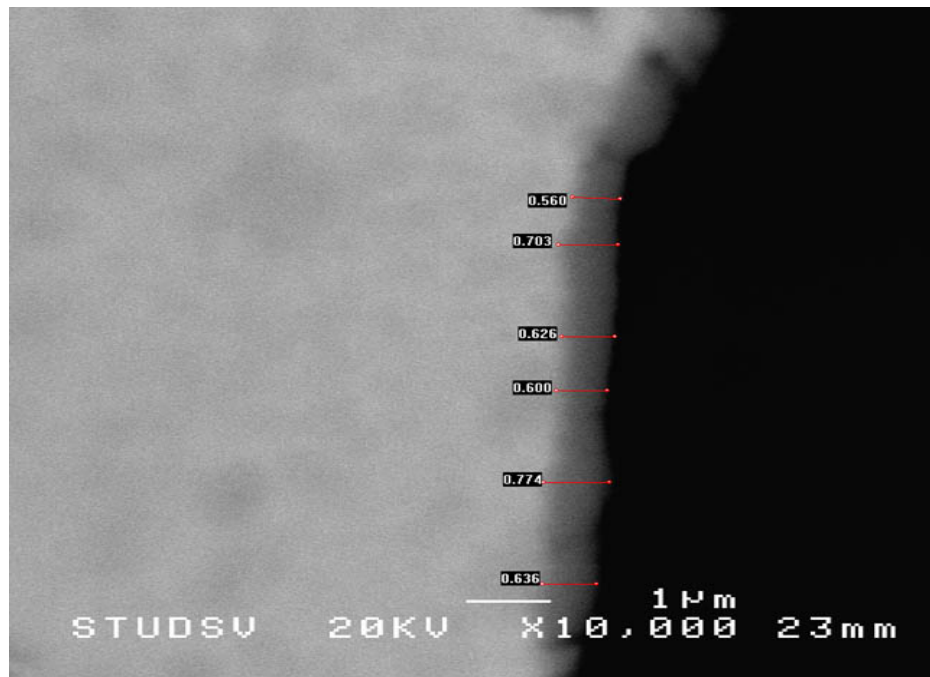


Figure 15

SEM micrograph of the LK2 material after the experiment.

Also, the thickness calculated from the α -corrected (extrapolated) capacitance seems to be slightly more reliable than the thickness calculated from the fit parameters. Yamamoto and Pein [1] report an oxide thickness of $1.7 \mu\text{m}$ for a LK2 material after 46 days at 288°C . In their experiment, hydrogen, lithium hydroxide and boric acid were added during part of the test in order to simulate PWR water chemistry.

The oxide growth in the present work was fitted to the function $d = a + b t^c$ where a , b and c are constants and t is time (in days). The result is shown in Figure 16 and the resulting function is

$$d = 142 + 111 \cdot t^{0.377} \quad (\text{Eq 34})$$

Since the growth rate is expected to be dependent on the temperature, the first and last measurements at temperatures less than 288°C were not used in the fit. Eq 34 predicts a oxide thickness of 960 nm after 200 days at 288°C . According to the discussion in Oskarsson et al. [6], the initial growth of the oxide is governed by a parabolic growth behaviour. This is a natural consequence of oxygen diffusion through the growing oxide layer being the rate limiting process. However, the exponent $\frac{1}{3}$ rather than $\frac{1}{2}$ on the time

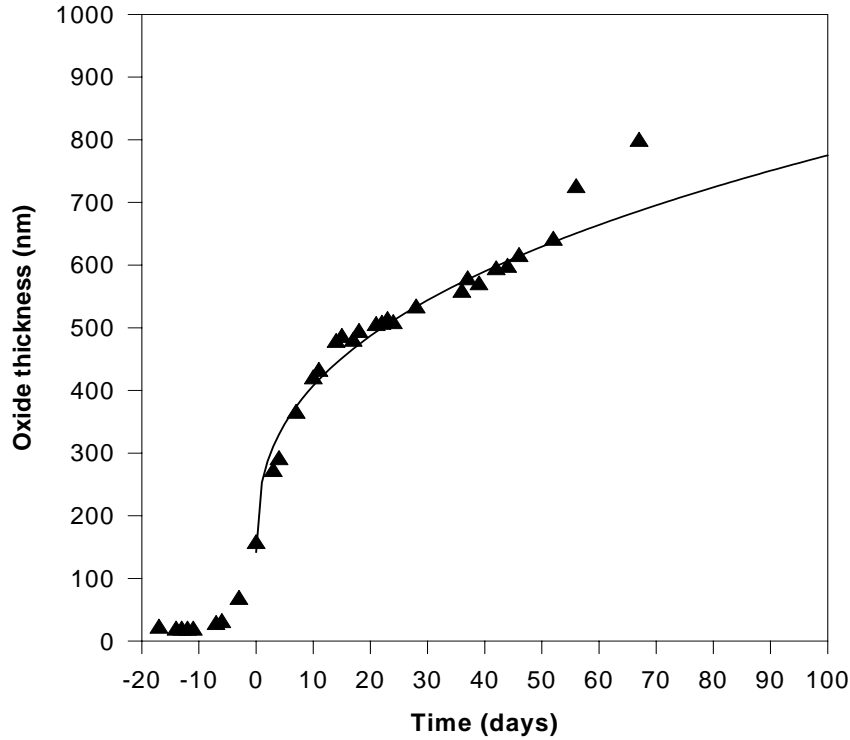


Figure 16

Curve fitted to the oxide growth at 288°C for the LK2 material.

indicates that the grain structure coarsens with growth so that the available grain boundary area for diffusion decreases with growth (oxygen diffusion takes place mainly at the grain boundaries). At a certain thickness of the oxide, typically about 2 μm , the growth rate becomes linear with time. This is the so-called transition [17].

An Arrhenius plot of the oxide conductivity as a function of inverse temperature at the beginning of the experiment is shown in Figure 17. The activation energy for conduction deduced from this diagram is 34.4 kJ mol^{-1} . The conductivity is based on the oxide thickness and resistance resulting from the equivalent circuit analysis. It should be pointed out, however, that data at the lowest frequencies were usually not considered during the analysis due to large spread at these frequencies. Hence, the resistance is afflicted with some uncertainty.

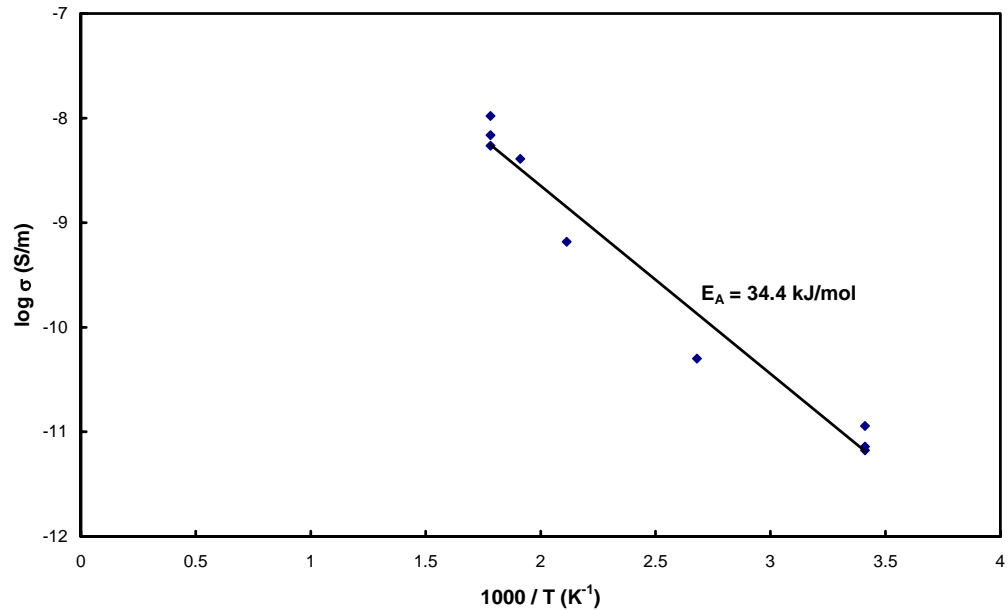


Figure 17

Oxide conductivity as a function of inverse temperature for the LK2 material at the beginning of the experiment.

Effective donor density and oxide capacitance

Capacitance versus voltage profiles were measured at two occasions at 288°C and at three occasions when lowering the temperature at the end of the experiment. Mott-Schottky plots (MS-plots) at three different frequencies from the measurements at 288°C are shown in Figure 18 and 19. The effective donor densities derived from these plots are given in Table 4. In Figures 18 and 19, MS-plots based on α -corrected capacitances are also shown. The latter plots were used to derive values of the oxide capacitance (see below). When lowering the temperature, the data points in the MS-plots were scattered, especially at 100 Hz and 10 000 Hz. Calculations of effective donor densities at these two frequencies were therefore not successful. MS-plots at 1000 Hz from the measurements at 200°, 100° and 20°C are displayed in Figure 20. The corresponding effective donor density is tabulated in Table 4. The effective donor densities at 200° and 100° are lower than the values at 288°C, whereas the value at 20°C is somewhat higher. It must be pointed out, however, that there is a greater spread of the data points at these three temperatures compared to 288°C, making the derived values of the donor densities more uncertain. The values found in the present work may be compared with the value $4.8 \times 10^{26} \text{ m}^{-3}$ found for anodic oxide films formed on zirconium in 1 M H_3PO_4 at room temperature [10]. The reason for the discrepancy is not clear but may be connected to how the oxide was produced. In the work by Goossens et al. [10], the oxide film was grown on Zr potentiodynamically.

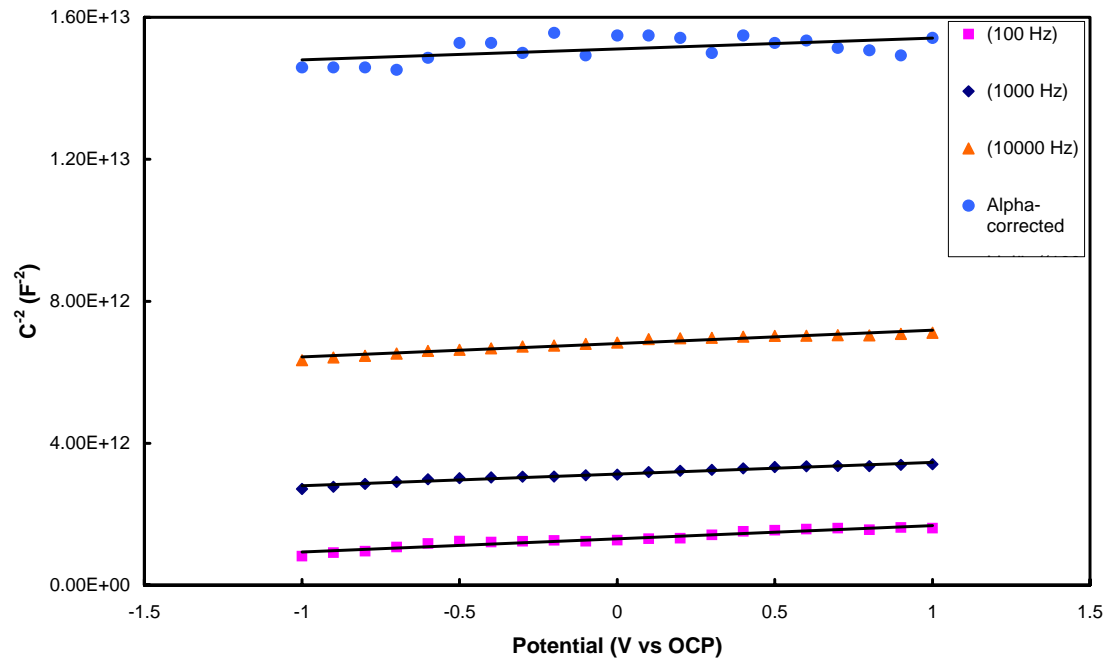


Figure 18

Mott-Schottky plots for the LK2 material at $288^\circ C$. The measurements were conducted at a total test time of 43 days.

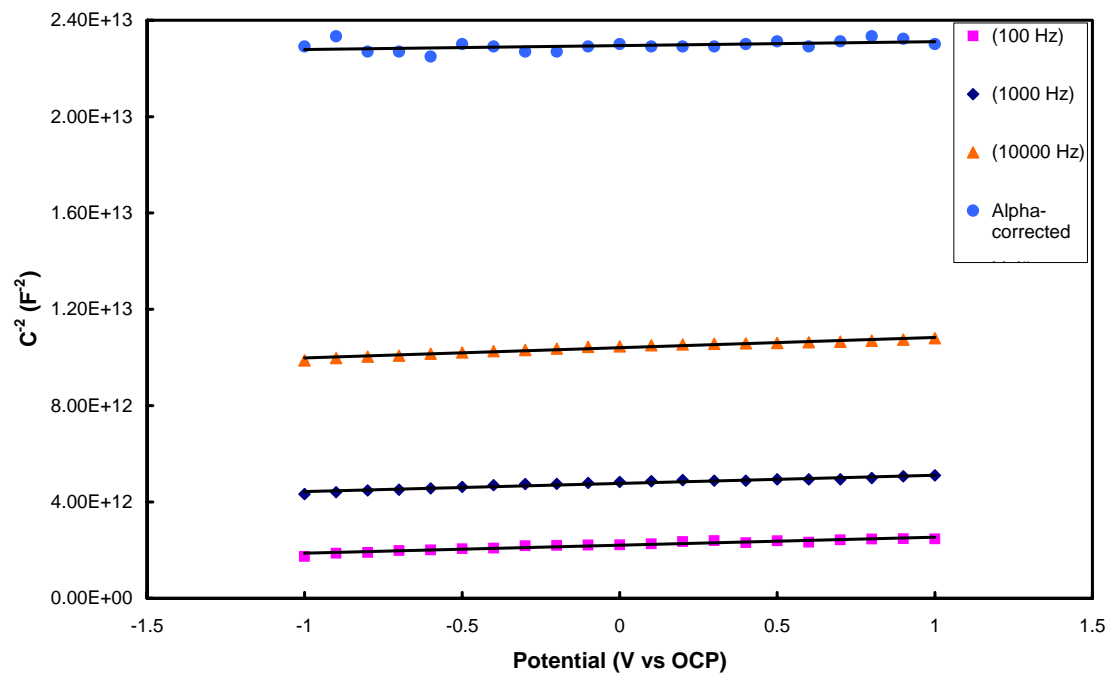


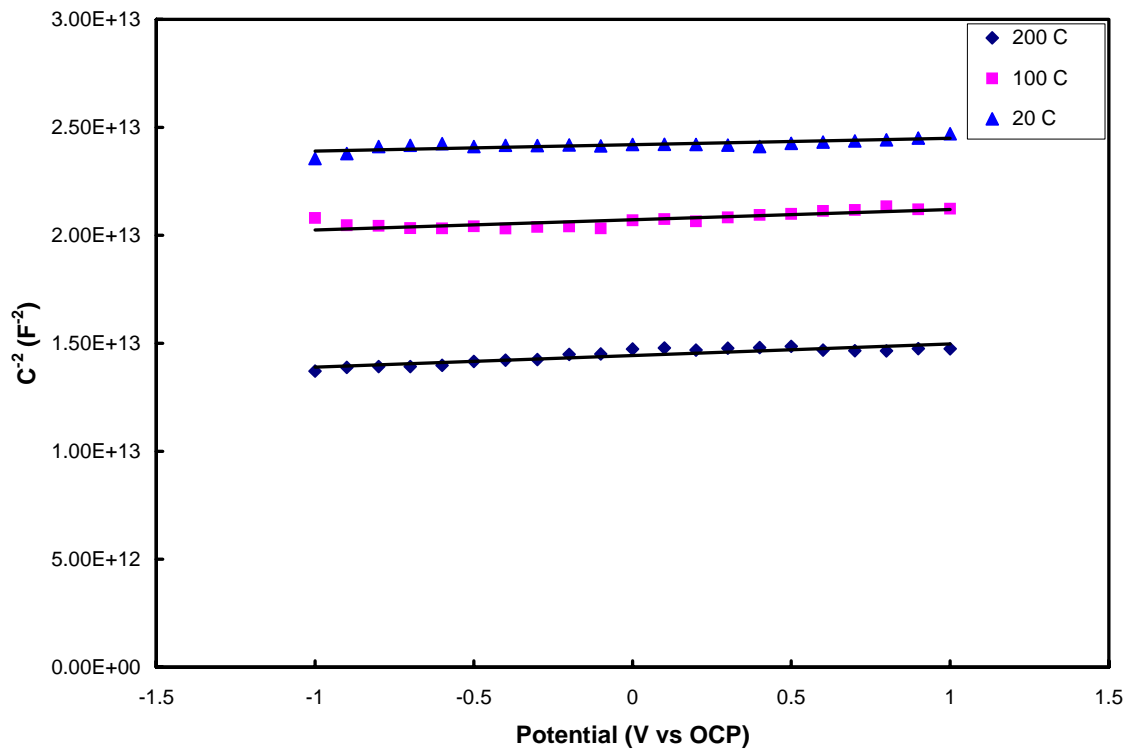
Figure 19

Mott-Schottky plots for the LK2 material at $288^\circ C$. The measurements were conducted at a total test time of 67 days.

Table 4

Calculated effective donor density for the LK2 material.

Test time (days)	Temperature (°C)	Frequency (Hz)	Effective donor density $N_D \times 10^{-23} \text{ (m}^{-3}\text{)}$
43	288	100	3.894
43	288	1000	4.406
43	288	10 000	3.857
67	288	100	4.343
67	288	1000	4.265
67	288	10 000	3.423
70	200	1000	2.698
74	100	1000	3.069
84	20	1000	4.885

**Figure 20**

Mott-Schottky plots for the LK2 material at 200°, 100° and 20°C. The frequency is 1000 Hz.

The oxide capacitance can be calculated from the slope of the Mott-Schottky plot and its intercept on the potential axis using Eq 26. The intercept and slope were calculated from the MS-plot constructed from α -corrected (extrapolated) capacitances, as explained in section 2.5.1. The oxide capacitance derived from the measurements at 288°C is given in Table 5. The oxide capacitance may also be obtained by considering the total measured capacitance as originating from a series combination of the oxide capacitance and the double layer capacitance of the electrolyte. Thus, we may write

$$\frac{1}{C_{tot}} = \frac{1}{C_{ox}} + \frac{1}{C_{dl}} \quad (\text{Eq 35})$$

where

C_{tot} = total measured capacitance

C_{ox} = oxide capacitance

C_{dl} = electrolyte double layer capacitance

The total measured capacitance given in Table 5 is the α -corrected (extrapolated) capacitance derived according to the procedure described in section 2.4. By identifying C_{dl} with the diffuse layer capacitance, one calculates a value of $1.062 \times 10^{-2} \text{ F/m}^2$ for this capacitance in our electrolyte at 288°C, using Eq 30 and 31 in section 2.6. The oxide capacitance obtained from Eq 35 is given in Table 5. The oxide thickness can be calculated from the oxide capacitance using the expression for a parallel plate capacitor

$$d = \frac{\epsilon \epsilon_0 A}{C_{ox}} \quad (\text{Eq 36})$$

where ϵ , ϵ_0 and A have their usual meaning (see for example Eq 14).

Table 5

Oxide capacitance and derived values of the oxide thickness for the LK2 material at 288°C.

Test time (days)	Total capacitance $C_{tot} \times 10^7$ (F)	Oxide capacitance $C_{ox} \times 10^7$ (F)		Oxide thickness (nm)		
		From MS	From C_{dl}	From C_{tot}	From C_{ox}^a	From C_{ox}^b
43	2.553	2.599	2.649	506	497	488
67	2.109	2.095	2.174	613	617	594

^a Oxide capacitance from Mott-Schottky plot

^b Oxide capacitance from C_{dl} (Eq 35)

From Table 5 it can be seen that the values of the oxide capacitance derived by the two methods described above are in very good agreement. Further, since the oxide capacitance, C_{ox} , is practically identical to the measured total capacitance, C_{tot} , the error when using C_{tot} instead of C_{ox} for the calculation of oxide thickness is negligible.

4.2 The LK2+ material

Impedance measurements were carried out in the temperature range 20 - 288°C on a material that had not been pre-oxidized. Dosage of H_2O_2 (500 ppb) and $NaNO_3$ (0.2 mM) were made throughout this experiment, except for a period of 9 days when the HPLC-pump malfunctioned. The potentials measured are shown in Figure A.2 in Appendix A.1. The autoclave temperature is also displayed in this figure. The period (May 15 to May 24, 2002) when the HPLC-pump malfunctioned is easily distinguishable since the potentials were lower. Due to problems with the potential measurement, the temperature was lowered and the experiment was interrupted for a period of 12 days (May 30 to June 11). During this break, the reference electrode was exchanged for a new one.

All impedance spectra measured in this experiment are displayed in Appendix B.10 - B.15. As before, the numbers in the legends correspond to the date when the measurement was performed. During the period May 1 to June 27, the temperature was 288°C. Impedance spectra at three different temperatures at the beginning of the experiment are shown in Figure 21. It can be seen that the impedance decreases with increasing temperature, especially at low and high frequencies. Also, in conformity with the LK2 data, the time constant is displaced to higher frequencies with increasing temperature. A change-over from one to two time constants takes place after a certain time. After the interruption, however, again only one time constant is discernible in the impedance spectra.

All impedance spectra have been modelled using the equivalent circuits described in section 2.3.2. At room temperature, a time constant (parallel combination of R and C), instead of a pure resistance, is needed to describe the impedance of the electrolyte. The results from the equivalent circuit analysis are tabulated in Appendix C.2. The temperature at each measurement is also given. As stated above, at the beginning of the experiment, only one time constant is required to describe the impedance of the oxide. An example of a spectrum measured at room temperature at the beginning of the experiment is presented in Figure 22. The time constant discernible at high frequencies ($>10^4$ Hz) is due to the impedance of the electrolyte. When raising the temperature to 288°C, two time constants

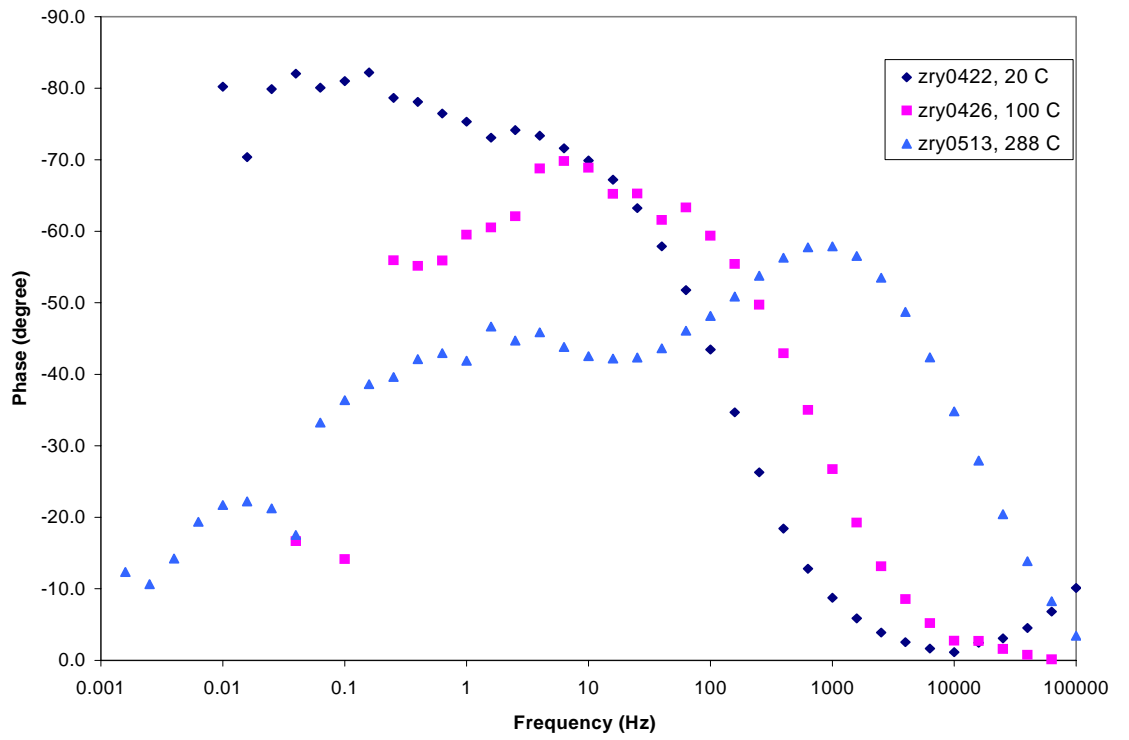
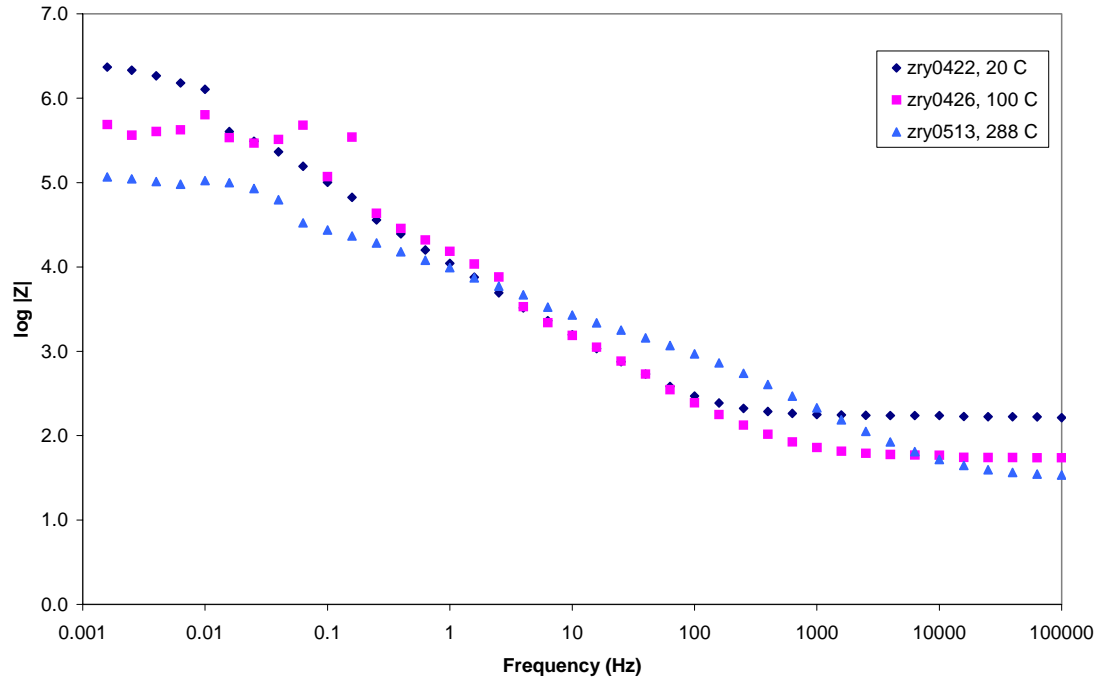


Figure 21
Impedance spectra of the LK2+ material at three different temperatures at the beginning of the experiment.

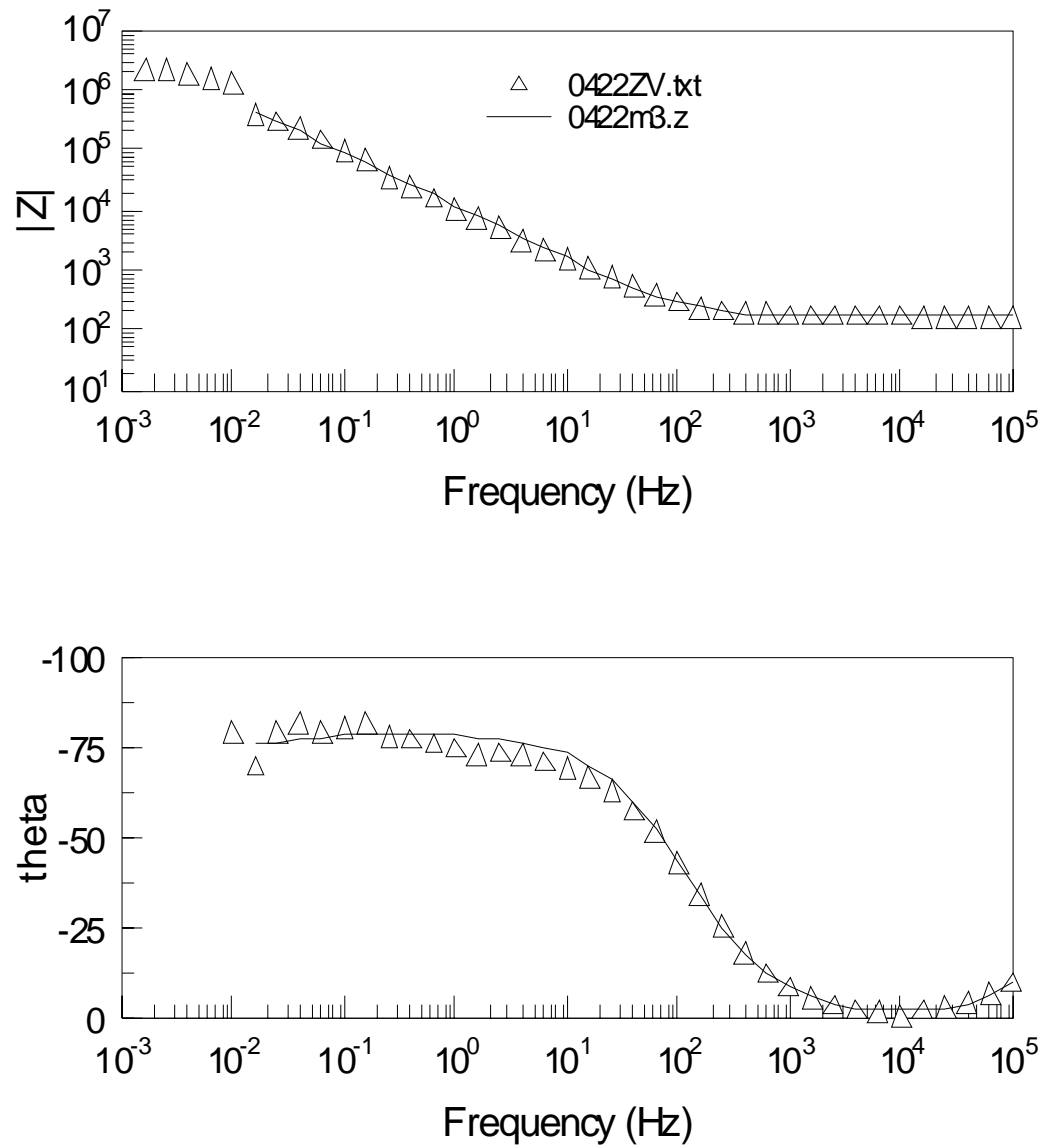


Figure 22

Impedance spectrum of the LK2+ material measured at room temperature and the result of the equivalent circuit analysis.

are required to describe the impedance of the oxide before the interruption (except for the first measurement) whereas only one is required after the interruption. Two examples of spectra measured at 288°C, before and after the interruption, are given in Figures 23 and 24, respectively. No measurements were conducted when lowering the temperature at the end of the experiment.

Oxide thickness and conductivity

The calculated oxide thickness and conductivity are shown as functions of test time in Figure 25. The oxide thickness was calculated from the fit parameters of the equivalent circuit analysis (Eq 14) and from an α -corrected (extrapolated) capacitance. Values of the α -corrected capacitance and the dispersion factor, derived according to the procedure in section 2.4, are tabulated in Appendix D.2. The conductivity was calculated from Eq 15. The test time at 288°C is indicated in Figure 25. The thickness calculated from the fit parameters is somewhat scattered but amounts to approximately 850 nm at the end of the experiment whereas the thickness calculated from the α -corrected capacitance is 600 nm at the end of the experiment.

After the experiment, the material was investigated by light optical microscopy (LOM) and scanning electron microscopy (SEM) – see Figures 26 and 27. The oxide thickness deduced from the SEM investigation is compared with the calculated thickness from the impedance measurements in Table 3. The measured hydrogen content is also given in this table. It can be seen that the calculated thickness from the impedance measurements are in good agreement with the thickness measured by SEM. The thickness calculated from the α -corrected (extrapolated) capacitance seem to be slightly more reliable than the thickness calculated from the fit parameters.

The time dependence of the oxide growth is described by the following equation

$$d = 115 + 111 t^{0.394} \quad (\text{Eq 37})$$

where t is time in days. When fitting this function to the calculated oxide thickness, data at the beginning of the experiment at temperatures lower than 288°C were not used. The calculated oxide thickness together with the result from the curve fit are shown in Figure 28. Eq 37 predicts a oxide thickness of 1010 nm after 200 days at 288°C.

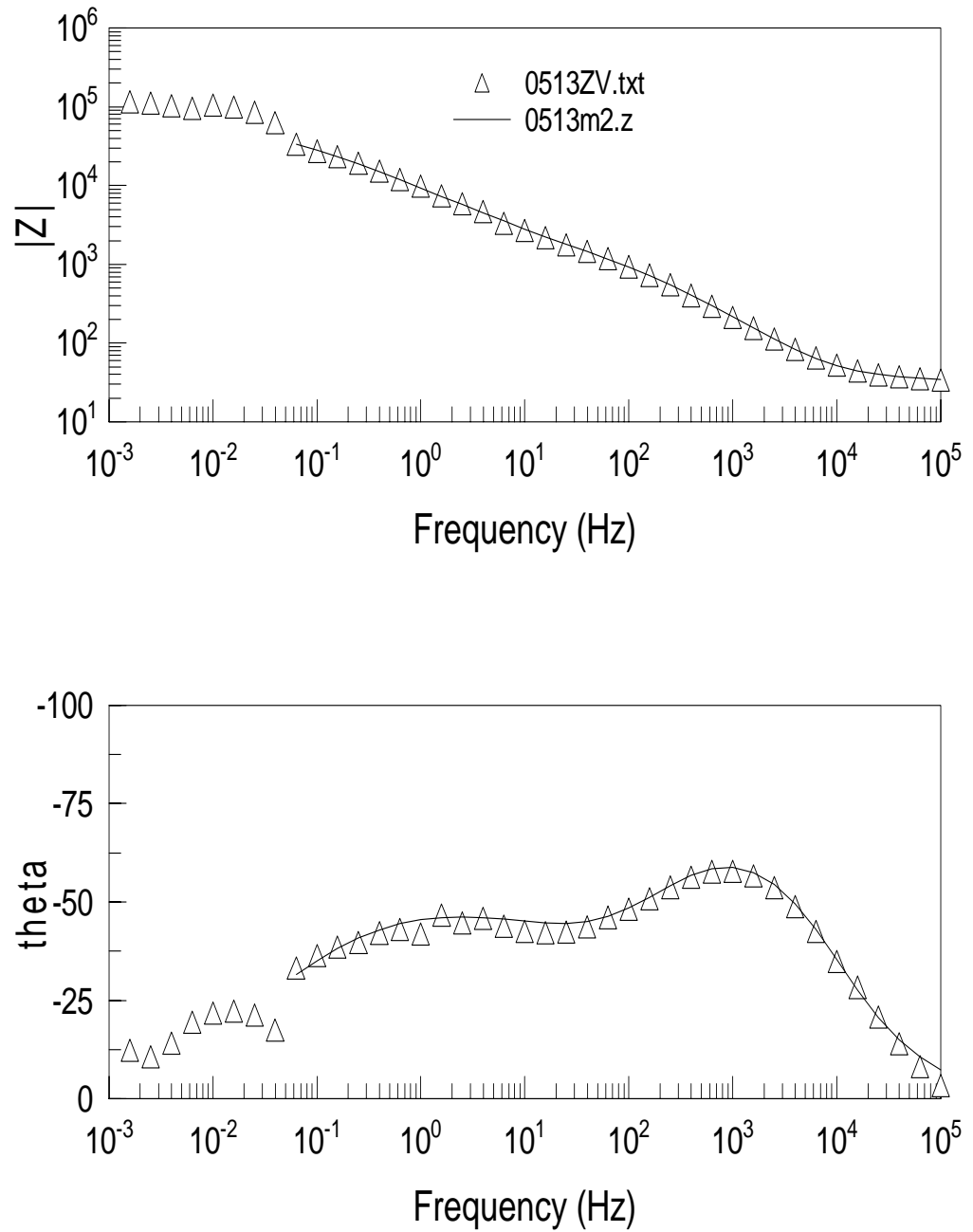


Figure 23

Impedance spectrum of the LK2+ material measured at 288°C and the result of the equivalent circuit analysis. The measurement was performed before the interruption.

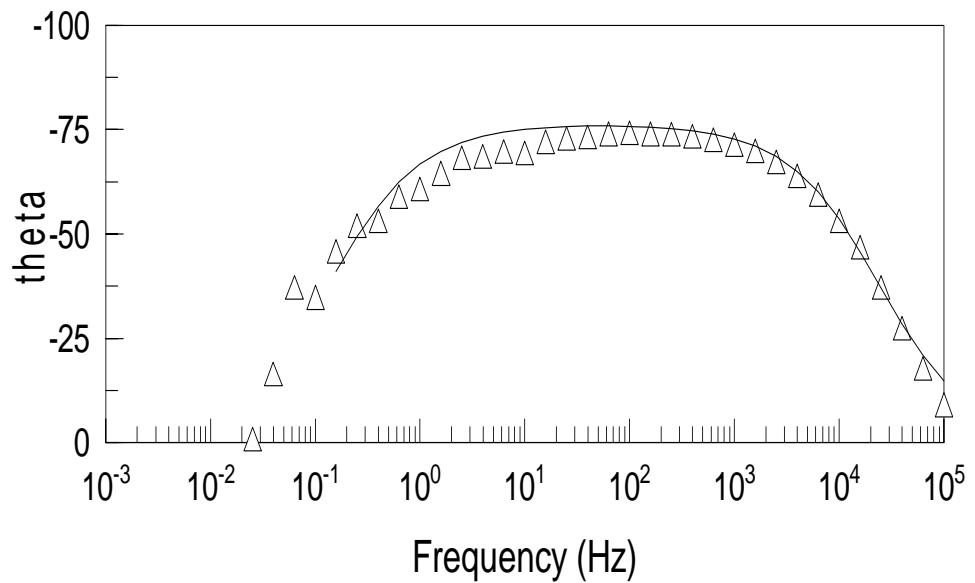
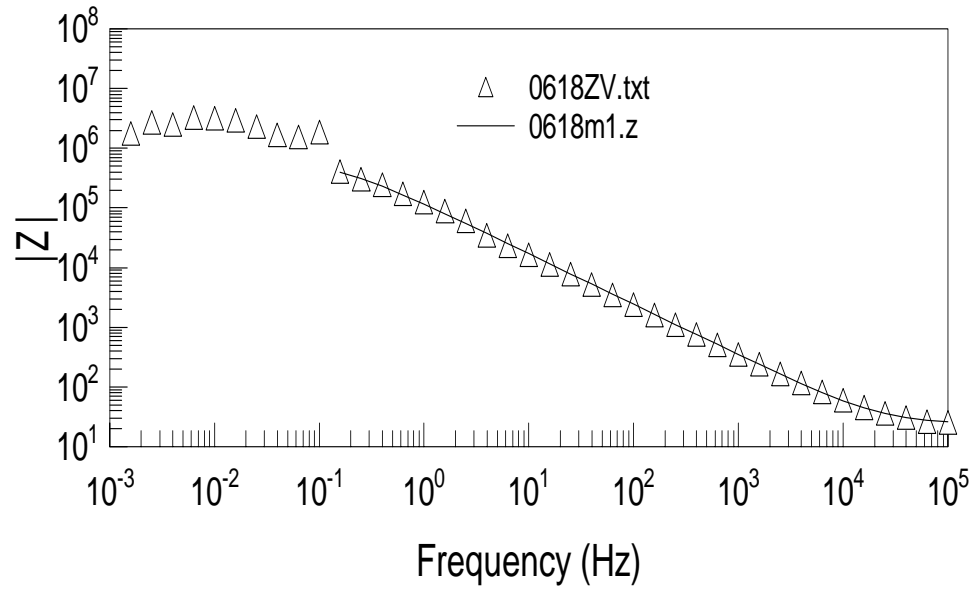


Figure 24

Impedance spectrum of the LK2+ material measured at 288°C and the result of the equivalent circuit analysis. The measurement was performed after the interruption.

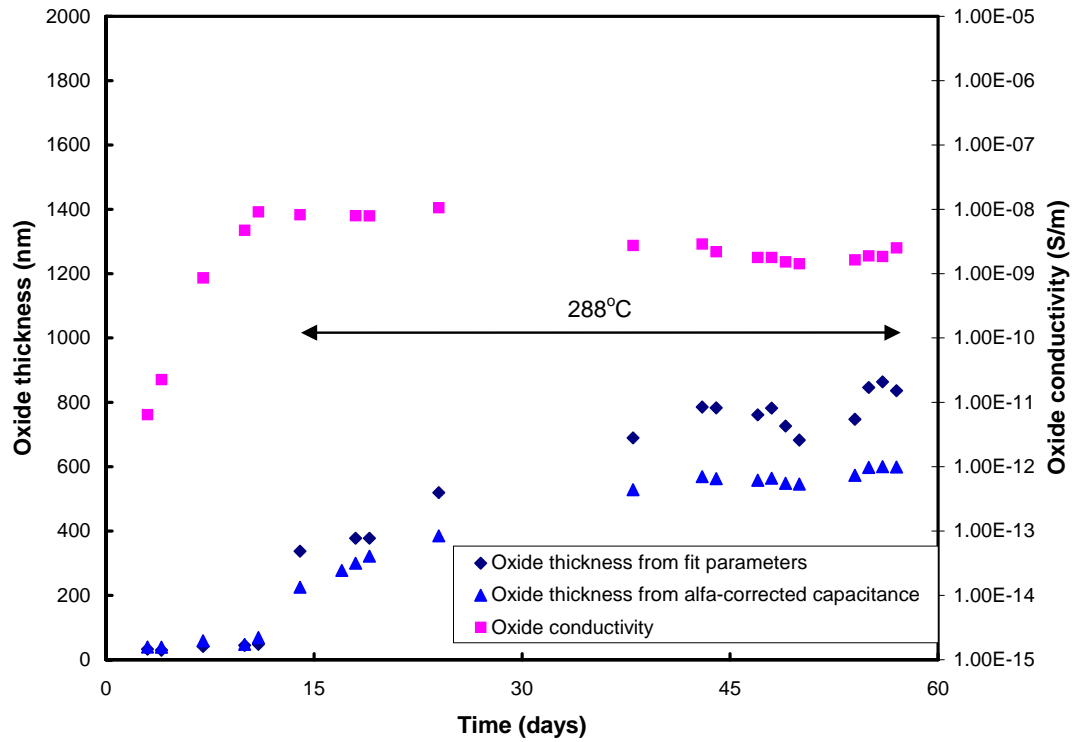


Figure 25

Calculated oxide thickness and conductivity for the LK2+ material.

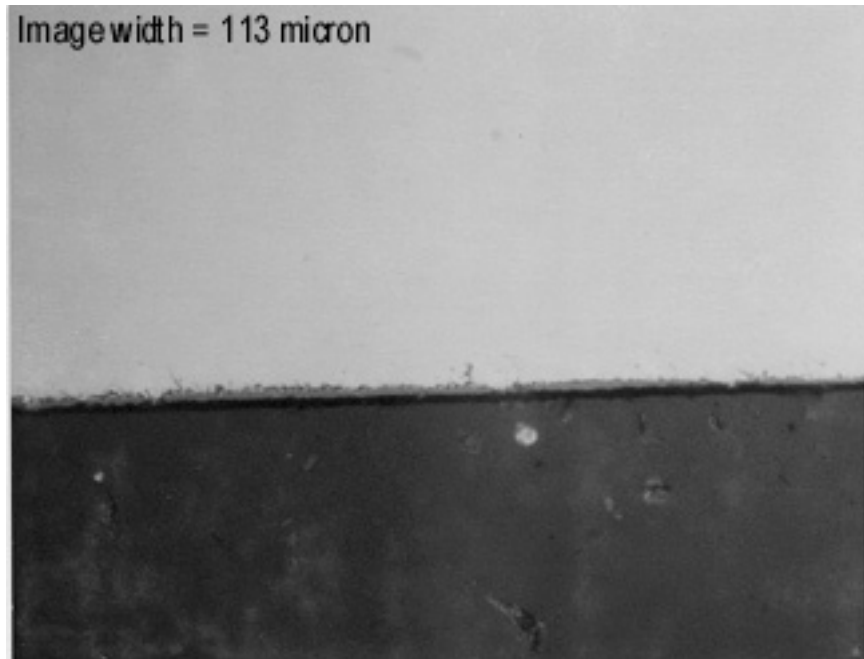


Figure 26

Light optical micrograph of the LK2+ material after the experiment.

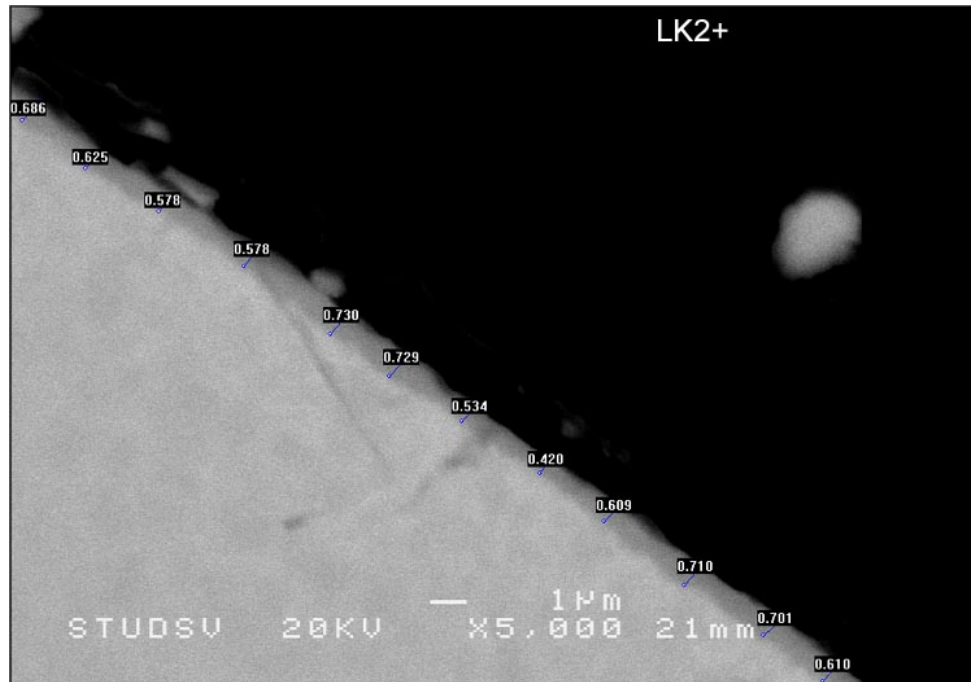


Figure 27
SEM micrograph of the LK2+ material after the experiment.

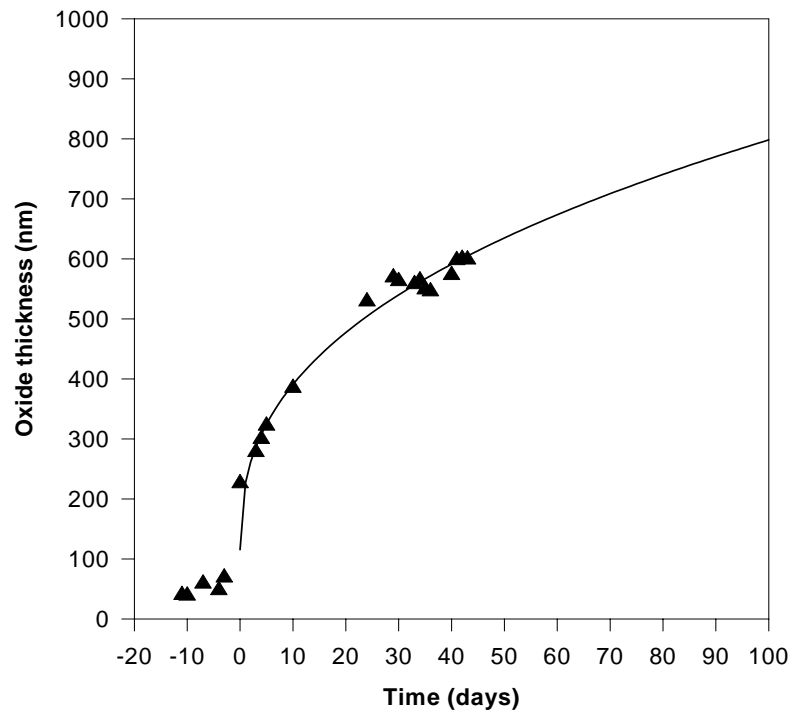


Figure 28
Curve fitted to the oxide growth at 288°C for the LK2+ material.

The Arrhenius plot, based on the calculated oxide conductivity at the beginning of the experiment, is shown in Figure 29. The activation energy for conduction calculated from the slope is 33.4 kJ mol^{-1} .

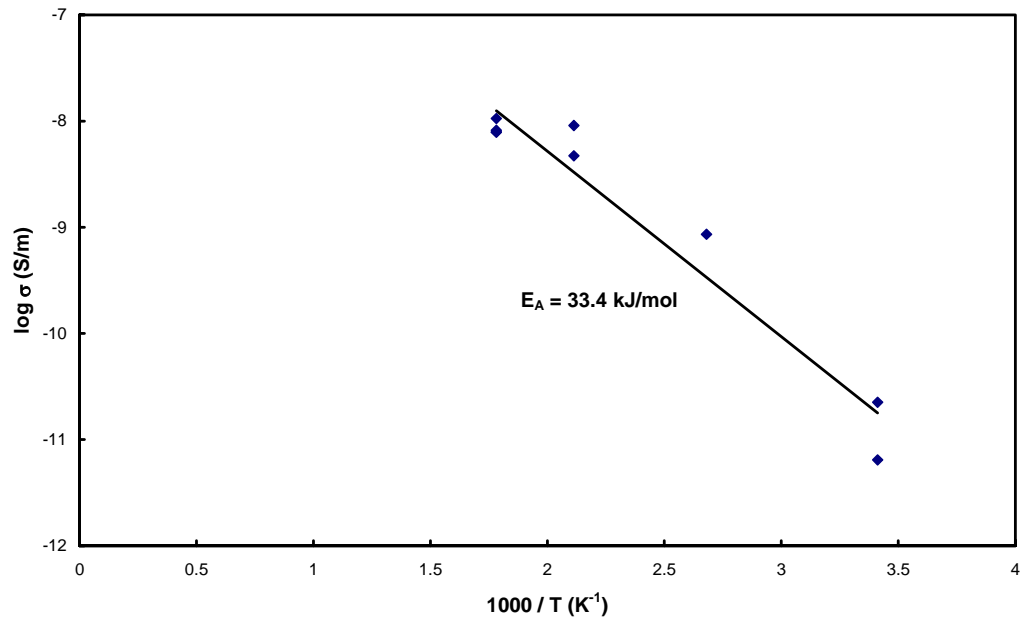


Figure 29

Oxide conductivity as a function of inverse temperature for the LK2+ material at the beginning of the experiment.

Effective donor density and oxide capacitance

The impedance was measured as a function of voltage on one occasion at the end of the experiment. The temperature was 288°C. Mott-Schottky plots (MS-plots) at three different frequencies constructed from these measurements are shown in Figure 30. The effective donor densities derived from these plots are given in Table 6. The line at 100 Hz is somewhat curved, and therefore the donor density calculated at this frequency may be less reliable than at the other values. In Figure 30, the MS-plot based on α -corrected capacitances is also shown.

The oxide capacitance, C_{ox} , calculated from the slope of the Mott-Schottky plot and its intercept on the potential axis using Eq 26 is given in Table 7. The intercept and slope was calculated from the MS-plot constructed from α -corrected (extrapolated) capacitances, as explained in section 2.5.1. The plot made from the α -corrected capacitances was, however, not linear over the whole potential region considered. Therefore, only potentials of 0 V and over were used to calculate the slope and intercept of the MS-plot.

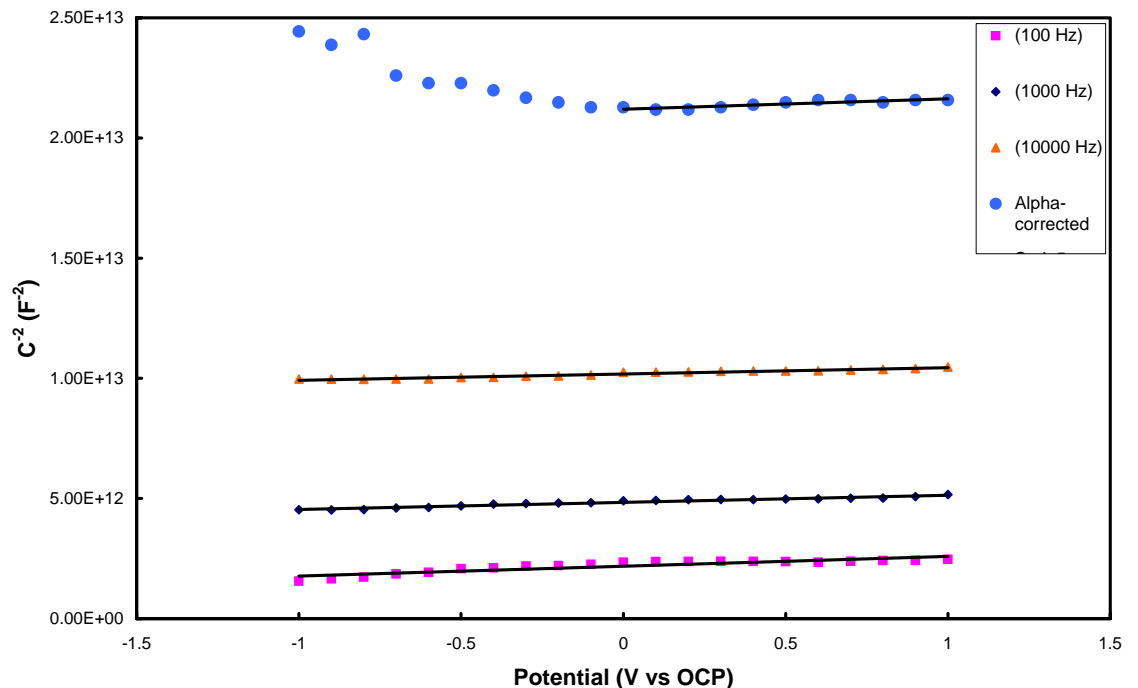


Figure 30

Mott-Schottky plots for the LK2+ material at 288°C. The measurements were conducted at a total test time of 56 days.

Table 6

Effective donor density calculated for the LK2+ material.

Test time (days)	Temperature (°C)	Frequency (Hz)	Effective donor density $N_D \times 10^{-23} \text{ (m}^{-3}\text{)}$
56	288	100	3.557
56	288	1000	4.837
56	288	10 000	5.537

The oxide capacitance obtained by considering the total measured capacitance, C_{tot} , as originating from a series combination of the oxide capacitance and the double layer capacitance of the electrolyte, C_{dl} , is also given in Table 7 (for details see section 4.1). The total measured capacitance, given in Table 7, is the α -corrected (extrapolated) capacitance derived according to the procedure described in section 2.4. The values of the oxide capacitance derived by the two methods described above are in very good agreement.

The oxide thickness calculated from the total capacitance and the oxide capacitance, using the expression for a parallel plate capacitor (Eqs 9 and 36), are also given in Table 7. Since the oxide capacitance, C_{ox} , is practically identical to the measured total capacitance, C_{tot} , the error when using C_{tot} instead of C_{ox} for the calculation of oxide thickness is very small.

Table 7

Oxide capacitance and derived values of the oxide thickness for the LK2+ material at 288°C.

Test time (days)	Total capacitance $C_{tot} \times 10^7 \text{ (F)}$	Oxide capacitance $C_{ox} \times 10^7 \text{ (F)}$		Oxide thickness (nm)		
		From MS	From C_{dl}	From C_{tot}	From C_{ox}^a	From C_{ox}^b
56	2.153	2.199	2.221	600	588	582

^a Oxide capacitance from Mott-Schottky plot

^b Oxide capacitance from C_{dl} (Eq 35)

4.3 The LK3 material

This experiment was started in the spring of 2001 without dosage of H_2O_2 and NaNO_3 . Like the other two materials, the LK3 material had not been pre-oxidized. Impedance measurements were performed at 288°C and the impedance data were fitted to equivalent circuits. Only one time constant was needed to describe the impedance of the oxide and, due to the low conductivity of the electrolyte, a time constant was also needed to describe the impedance of the water. It was found that, in this electrolyte, the dispersion factor was in all cases around 0.5. This indicates that some diffusion process, probably in the electrolyte double layer, is rate limiting for the total process. This low value of the dispersion factor means that the oxide growth could not be studied in-situ, since the calculated oxide thickness is much too large. During the summer the temperature was lowered and no measurements were performed. When the experiment was re-started in the autumn of 2001 it was decided to add H_2O_2 to a concentration of 500 ppb in order to simulate the oxidizing environment in the core of a BWR. In this electrolyte, the dispersion factor was still too low (0.66 - 0.69), so that the oxide thickness could not be calculated from the fit parameters of the equivalent circuit analysis. Therefore, at the end of this experiment it was decided to add NaNO_3 in order to increase the conductivity of the electrolyte. Unlike the other two experiments reported here, the concentration of NaNO_3 was 0.15 mM.

The potentials measured during this experiment are shown in Figure A.3 in Appendix A.2. The autoclave temperature is also displayed. The points of time when the dosages of H_2O_2 (September 24) and NaNO_3 (November 12) were started are easily distinguished from this figure since the potentials increase. The dip in potentials during a short period of time in November is due to the fact that the HPLC-pump used for dosage of H_2O_2 and NaNO_3 was out of order.

All impedance spectra measured after the re-start of the experiment in August of 2001 are given in Appendix B.16 - B.25. No measurements were performed when raising the temperature at the beginning of the experiment or before the dosage of H_2O_2 was started. As before, the numbers in the legends correspond to the date when the measurement was performed. During the period August 31 – November 28, the temperature was 288°C . Impedance spectra measured before and after the addition of supporting electrolyte (NaNO_3) was started are shown in Figure 31. The dosage of NaNO_3 was started on the 12th of November, after the impedance measurement had been conducted. It can be seen that the impedance at high frequencies (where we see the impedance of the electrolyte) decreases when the addition is started. Also, the time constant visible at frequencies higher than 10 kHz disappears.

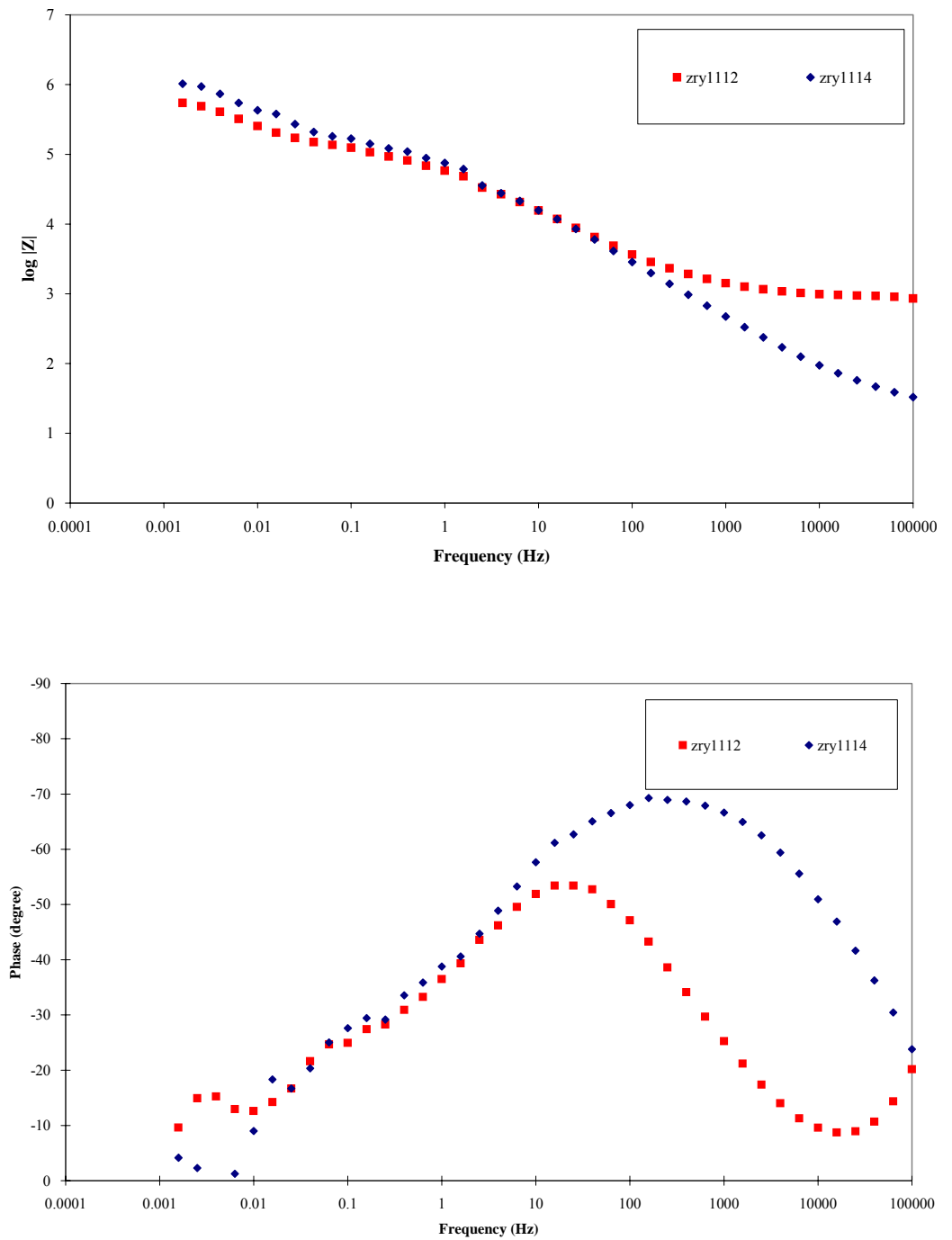


Figure 31

Impedance spectra of the LK3 material before and after the addition of supporting electrolyte (NaNO_3) was started.

All impedance spectra have been modelled using the equivalent circuits described in section 2.3.2. Due to the low conductivity of the water before the addition of NaNO_3 was started, a time constant (parallel combination of R and C), instead of a pure resistance, is needed to describe the impedance of the electrolyte. The results from the equivalent circuit analysis are tabulated in Appendix C.3. The temperature of the measurements are also given. At the beginning of the experiment, only one time constant is required to describe the impedance of the oxide. An example of such a spectrum is presented in Figure 32. As before, the triangles are experimental data and the lines are the result of the equivalent circuit analysis. Later in the experiment, two time constants are required to describe the impedance of the oxide. This shows that the oxide is composed of an inner and an outer layer. An example of such a spectrum is presented in Figure 33. Compared to the other two materials investigated, the LK3 material becomes layered much later in the experiment. Thus, the second time constant appears in the impedance spectra after a test time of 83 days at 288°C . Both spectra shown in Figure 32 and 33 are measured before the dosage of supporting electrolyte was started, and the time constant discernible at high frequencies ($>10^4$ Hz) is due to the impedance of the electrolyte. When lowering the temperature at the end of the experiment, the impedance spectra at 250° , 200° , 150° and 100°C were distorted. There was a discontinuity in the impedance at about 10 Hz and the data exhibited a large spread below this frequency. Equivalent circuit analysis at these four temperatures were not successful. Also, in the two last measurements at 288°C , only one time constant was used to describe the impedance of the oxide due to the great spread of the impedance data at low frequencies.

Oxide thickness and conductivity

The calculated oxide thickness and conductivity are shown as a function of test time in Figure 34. The test time at 288°C is also indicated in the figure. The oxide thickness was calculated from the fit parameters of the equivalent circuit analysis (Eq 14) and from an α -corrected (extrapolated) capacitance. Values of the α -corrected capacitance and the dispersion factor, derived according to the procedure in section 2.4, are tabulated in Appendix D.3. Before the addition of supporting electrolyte, the calculated oxide thickness from the fit parameters is very large (approximately $10\ \mu\text{m}$) and falls outside the scale of the diagram in Figure 34. The reason for this is the low value of the dispersion factor, which means that Eq 14 cannot be used to calculate the thickness. When NaNO_3 is added, the calculated thickness using Eq 14 is $1.9 - 3\ \mu\text{m}$. At the end of the experiment, the calculated thickness based on the α -corrected capacitance is $2.2\ \mu\text{m}$ before NaNO_3 is added and $0.9 - 1.0\ \mu\text{m}$ after the addition is started, except for the last measurements when the temperature is lowered. Here the calculated thickness is somewhat higher. Since the oxide thickness calculated from the fit parameters is too large, the conductivity displayed in Figure 34 is based on the thickness derived from the α -corrected capacitance.

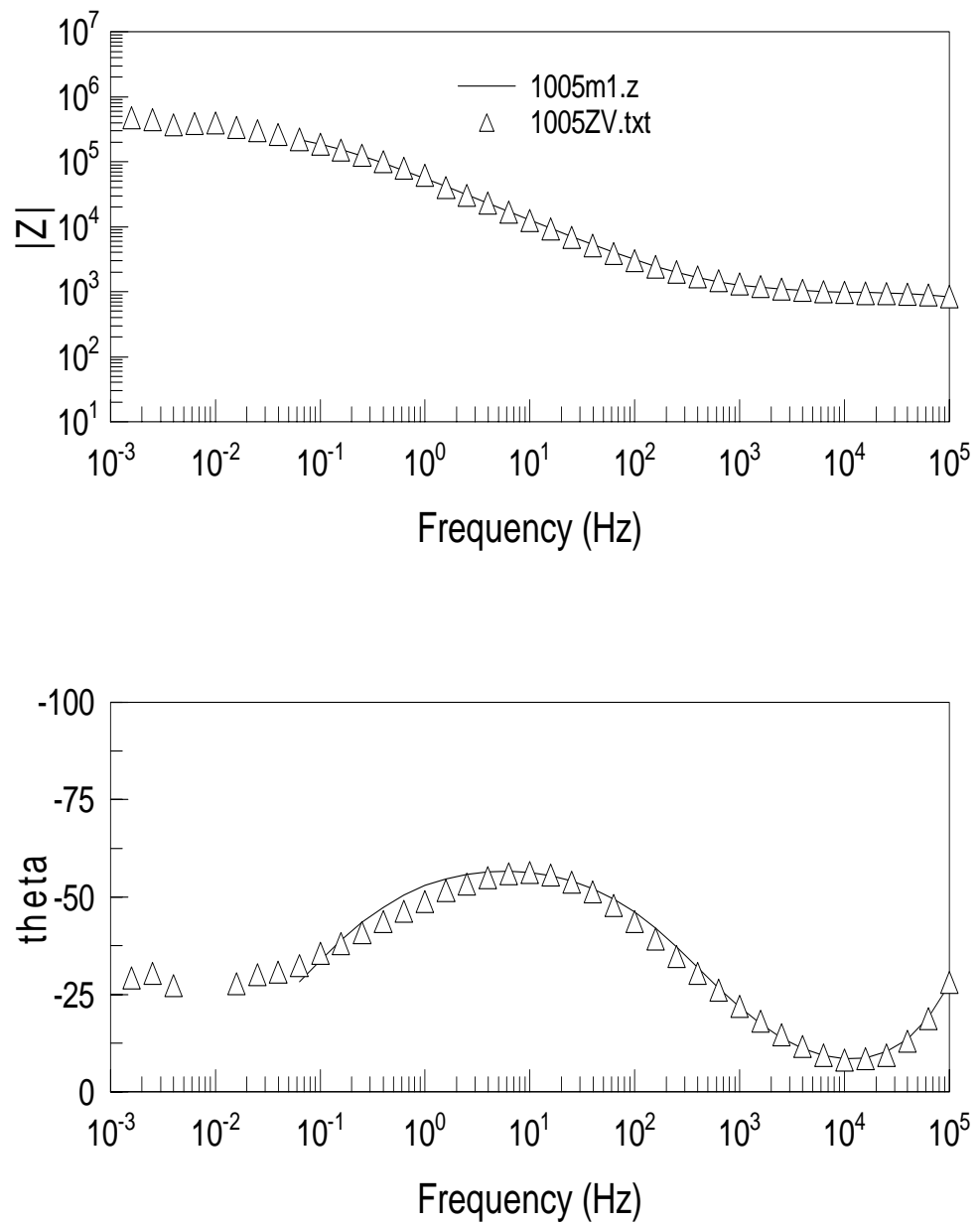


Figure 32

Impedance spectrum of the LK3 arterial, measured before the oxide becomes layered, and the result of the equivalent circuit analysis. The temperature is 288°C .

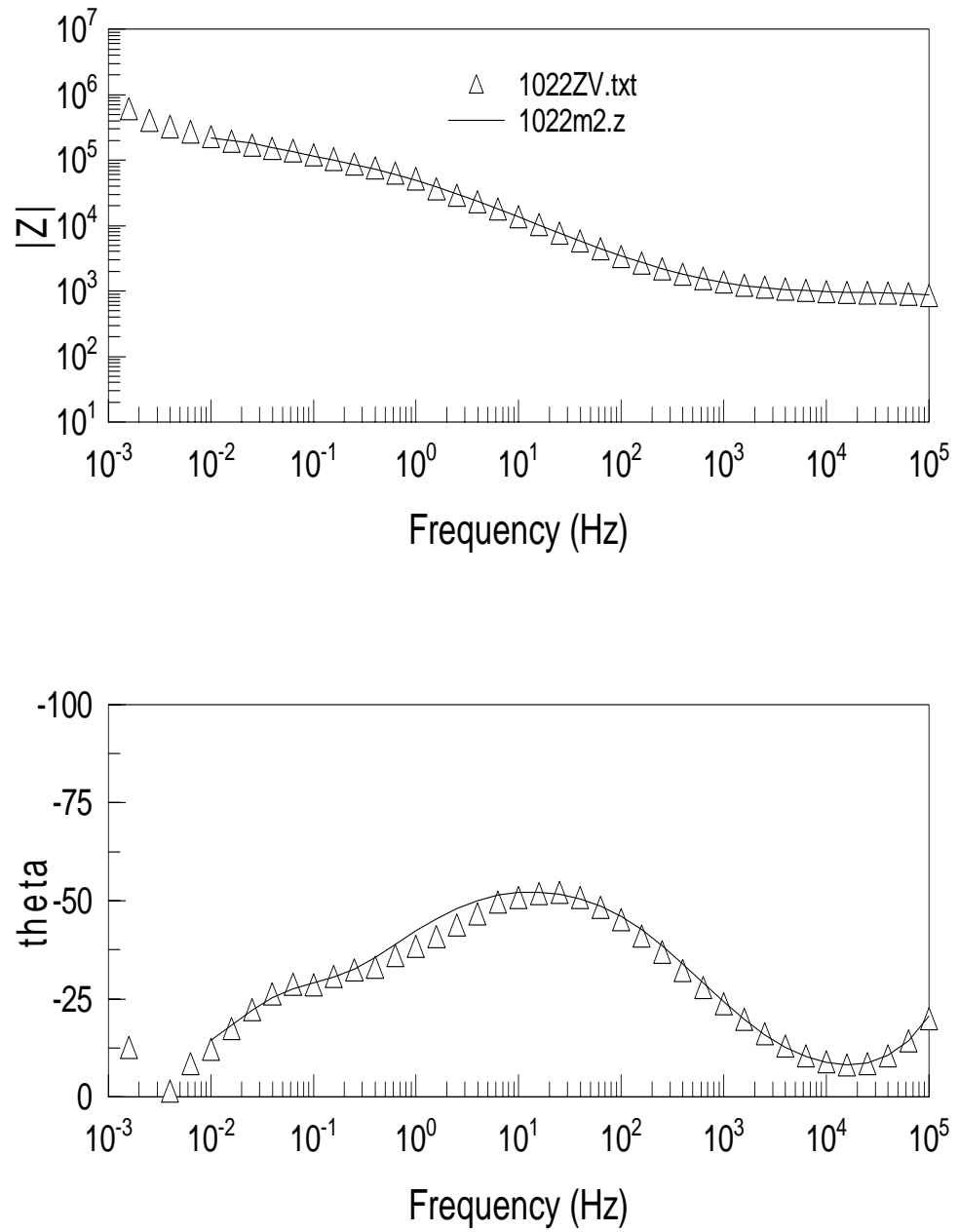


Figure 33

Impedance spectrum of the LK3 arterial, measured after the oxide becomes layered, and the result of the equivalent circuit analysis. The temperature is 288°C.

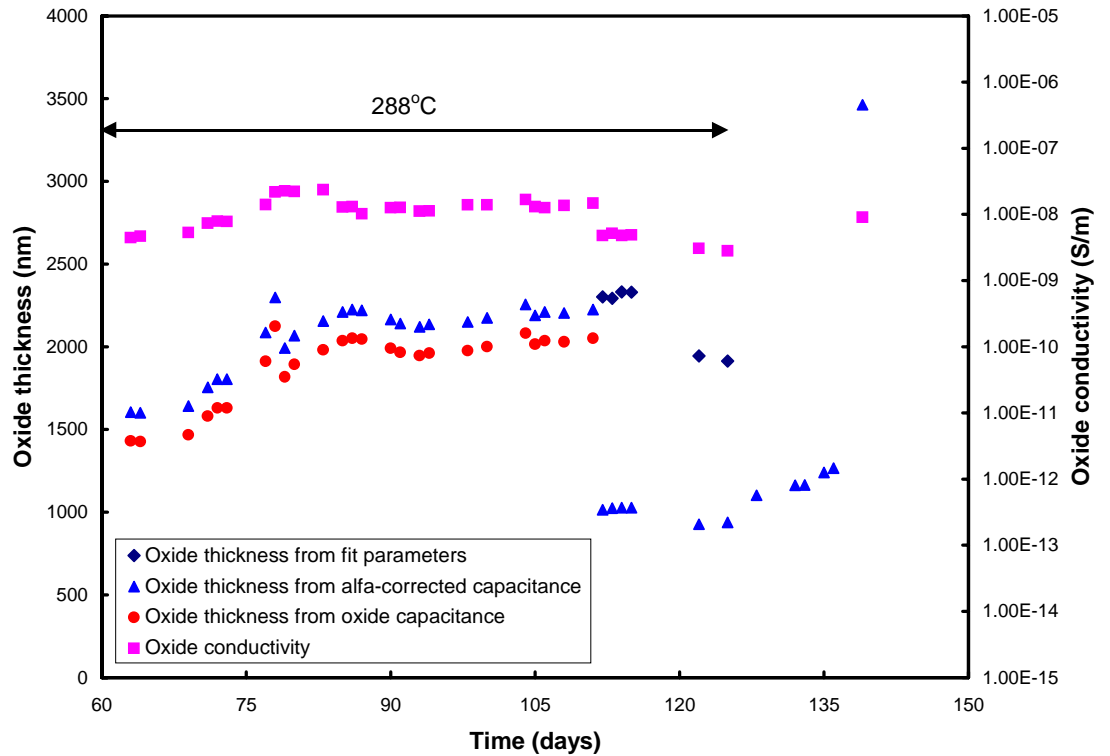


Figure 34
Calculated oxide thickness and conductivity for the LK3 arterial.

Before the addition of supporting electrolyte is started, the ionic strength of the solution is very low. This means that the electrolyte double layer will be quite extended. This in turn means that the value of the double layer capacitance will be small so that it may make significant contribution to the total measured capacitance. By considering the total measured capacitance (α -corrected capacitance) as originating from a series combination of the oxide capacitance and the double layer capacitance, values of the oxide capacitance may be calculated using Eq 5, as described in section .1. Using Eqs 0 and 1 in section .6, one calculates a value of $1.12 \times 10^{-3} \text{ F/m}^2$ for the double layer (diffuse layer) capacitance in pure water at 288°C (compared to the value $10.6 \times 10^{-3} \text{ F/m}^2$ reported in section .1). The oxide thickness calculated from the oxide capacitance using the expression for a parallel plate capacitor (Eq 6) is displayed in Figure 4. It can be seen that, before the addition of NaNO_3 is started, the calculated thickness is lowered by about 170 m by taking the double layer capacitance into account.

After the experiment, the material was investigated by scanning electron microscopy (SEM) – see Figure 5. The oxide thickness deduced from the SEM investigation (about 1 μm) is compared with the calculated thickness from the impedance measurements in Table . The measured hydrogen content is also given in this table. The thickness calculated from the fit parameters is too large, even when supporting electrolyte is added. This may result from the low value of the dispersion factor (0.77-0.80). A possible explanation is that the concentration of NaNO_3 (0.15 mM at room temperature) was lower in this experiment compared to the other to experiments reported here. It can further be concluded, that the thickness calculated from the α -corrected (extrapolated) capacitance is too large before the addition of NaNO_3 is started, also when the electrolyte double layer capacitance is taken into consideration. After the addition is started, however, the calculation is in very good agreement with the result from the SEM investigation.

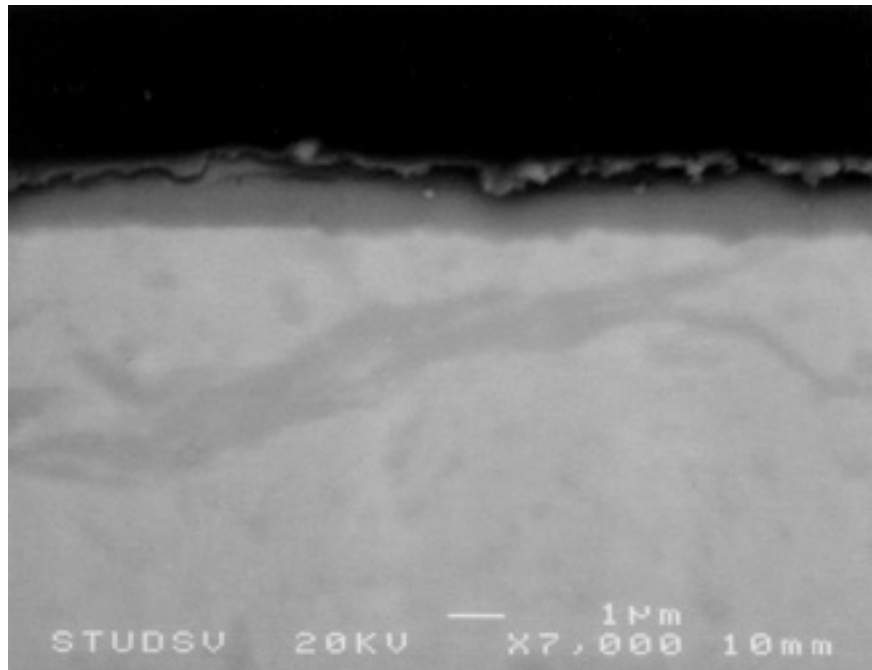


Figure 35
SEM micrograph of the LK3 material after the experiment.

Effective donor density and oxide capacitance

Capacitance versus voltage profiles were measured at one occasion, just before lowering the temperature at the end of the experiment. NaNO_3 was added to the water at the time of the measurements. Mott-Schottky plots (MS-plots) at three different frequencies from these measurements at 288°C are shown in Figure 6. The effective donor densities derived from these plots are given in Table . It can be seen that the values at the different frequencies are in good agreement, and that there is no systematic variation in the values when going from low to high frequencies (or vice versa). In Figure 36, the MS-plot based on α -corrected capacitances is also shown.

The oxide capacitance, C_{ox} , calculated from the slope of the Mott-Schottky plot and its intercept on the potential axis using Eq 6 is given in Table . The intercept and slope was calculated from the MS-plot constructed from α -corrected (extrapolated) capacitances, as explained in section 5.1. The plot made from the α -corrected capacitances was, however, not linear over the whole potential region considered. Therefore, only potentials of 0 and over were used to calculate the slope and intercept of the MS-plot.

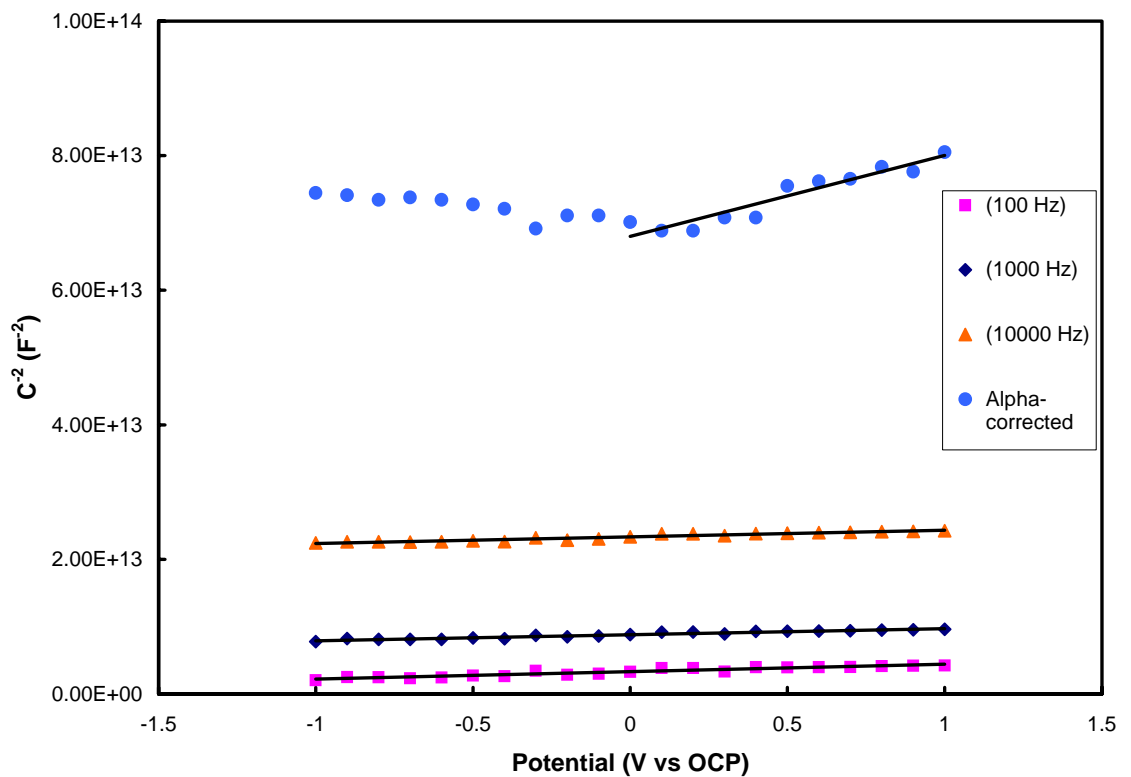


Figure 36

Mott-Schottky plots for the LK3 arterial at 288°C . The measurements were conducted at a total test time of 127 days.

Table 8

Effective donor density calculated for the LK3 material.

Test time (days)	Temperature (°C)	Frequency (Hz)	Effective donor density $N_D \times 10^{-23}$ (m ⁻³)
127	288	100	1.316
127	288	1000	1.606
127	288	10 000	1.470

The oxide capacitance obtained by considering the total measured capacitance, C_{tot} , as originating from a series combination of the oxide capacitance and the double layer capacitance of the electrolyte, C_{dl} , is also given in Table 9 (for details see section 4.1). The total measured capacitance given in the table is the α -corrected (extrapolated) capacitance. The calculated value of C_{dl} in our electrolyte (0.15 mM NaNO₃ at room temperature) is 9.194×10^{-3} F/m². The values of the oxide capacitance derived by the two methods described above are in reasonable good agreement.

The oxide thickness calculated from the total capacitance and the oxide capacitance, respectively, are also given in Table 9. The thickness was obtained using the expression for a parallel plate capacitor (Eqs 19 and 36). The values calculated from the total capacitance and the oxide capacitance are in good agreement. These values also agree with the thickness measured by SEM. Since the oxide capacitance, C_{ox} , is close to the measured total capacitance, C_{tot} , the error when using C_{tot} instead of C_{ox} for the calculation of oxide thickness is small.

Table 9

Oxide capacitance and derived values of the oxide thickness for the LK3 material at 288°C.

Test time (days)	Total capacitance $C_{tot} \times 10^7$ (F)	Oxide capacitance $C_{ox} \times 10^7$ (F)		Oxide thickness (nm)		
		From MS	From C_{dl}	From C_{tot}	From C_{ox}^a	From C_{ox}^b
127	1.377	1.342	1.409	938	963	917

^a Oxide capacitance from Mott-Schottky plot

^b Oxide capacitance from C_{dl} (Eq 35)

5 Discussion

Impedance spectra for the three materials investigated in the present work are compared in Figure 37. The measurements displayed were performed at 288°C at the end of the experiments. The total test time was 62, 56 and 115 days for the LK2, LK2+ and LK3 material, respectively. It can be seen that there are no major differences between the materials, neither regarding the magnitude of the impedance nor the positions of the time constants. When the oxide grows thicker during the experiments, a layered structure is formed as is evident from the appearance of a second time constant for the oxide at low frequencies. This was observed for all three materials although, for the LK2+ sample, only one time constant is distinguishable in the spectra after a temporary shutdown of the experiment (see section 4.2). The test time required for the second time constant for the oxide to appear was, however, different for the materials and amounted to about 18, 17 and 83 days for the LK2, LK2+ and LK3 material, respectively.

From Table 3 it can be seen that, for the LK2 and LK2+ material, the oxide thicknesses at the end of the experiments are virtually identical. The test time at 288°C is the same for these two materials. Unfortunately, the oxide thickness of the LK3 material at this test time is not known. This is due to the fact that the calculated oxide thickness is too large when supporting electrolyte is not added to the water. After a total test time of 127 days at 288°C, the oxide thickness calculated from the impedance data amounts to 930-1030 nm for the LK3 material (see Table 3). For the LK2 and LK2+ material, the oxide growth was fitted to a mathematical function describing its time dependence. These functions predict an oxide thickness of about 840 and 870 nm for the LK2 and LK2+ material, respectively, after a test time of 127 days at 288°C. In Figure 38, the oxide thickness, calculated from the α -corrected (extrapolated) capacitance as described in section 2.4, is shown as a function of test time for the three materials. For the LK3 material, the calculated thickness is too large prior to the start of addition of supporting electrolyte (at day 111), and some data points fall outside the scale of the diagram. It can be concluded that the difference in oxide growth rate between the three materials is very small in the pre-transition region.

The hydrogen contents given in Table 3 indicate that the hydrogen uptake of the LK2 material is slightly higher than for the LK2+ material. The difference is, however, within the uncertainty of the measurements. The tabulated hydrogen content of the LK3 material is somewhat higher than for the other materials. This is expected since the test time at 288°C is more than twice as long for the LK3 material compared to the other two materials. It is difficult, however, to compare the LK3 material with the LK2 and LK2+ materials, since the LK3 material was “pre-oxidized” without dosage of H₂O₂ and NaNO₃ in the spring of 2001 (see section 4.3). Due to this “pre-oxidation,” one would expect that the hydrogen uptake of the LK3 material would be low during the second exposure in the autumn of 2001.

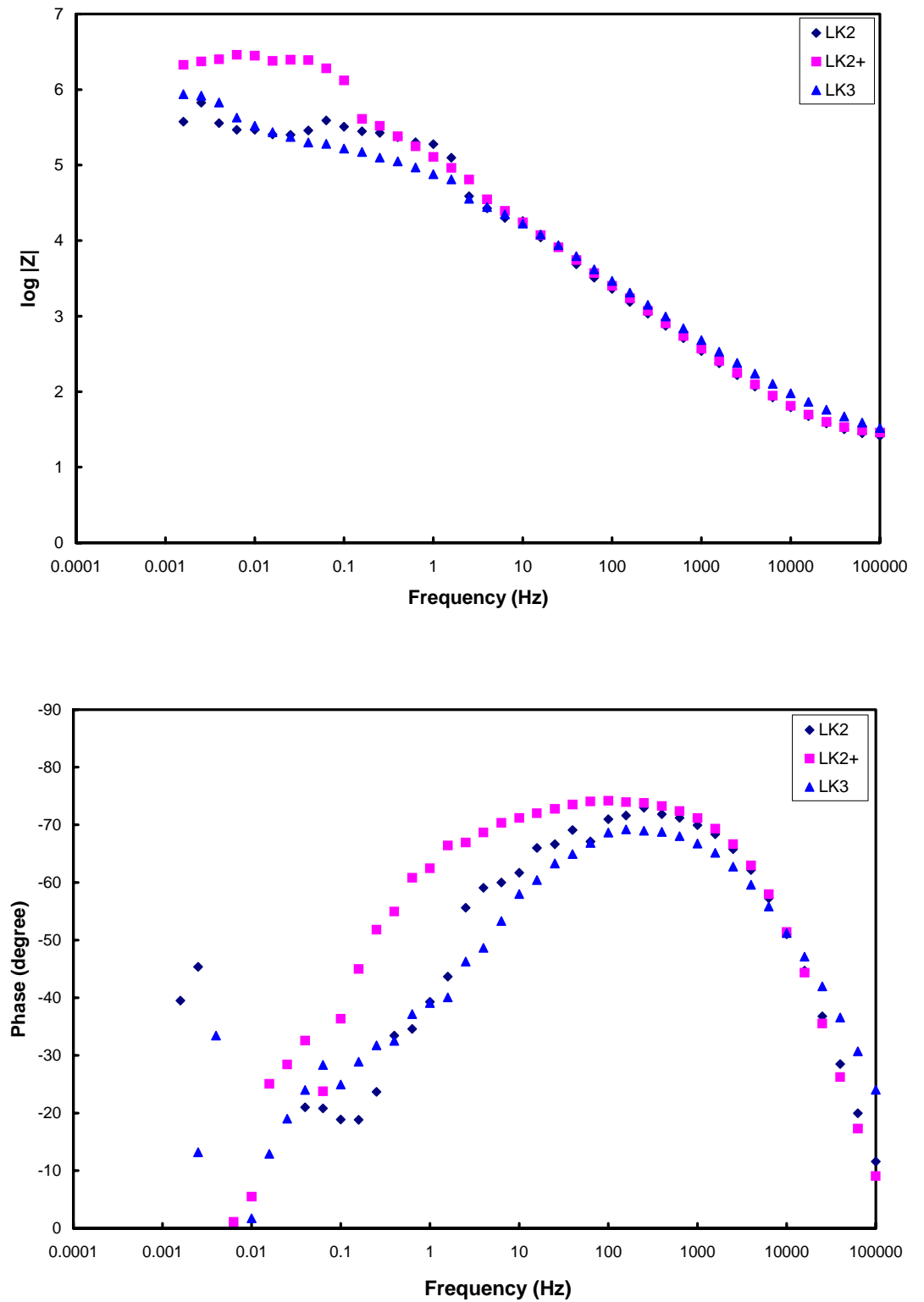


Figure 37

Impedance spectra of the investigated materials at the end of the experiments. The temperature was 288°C.

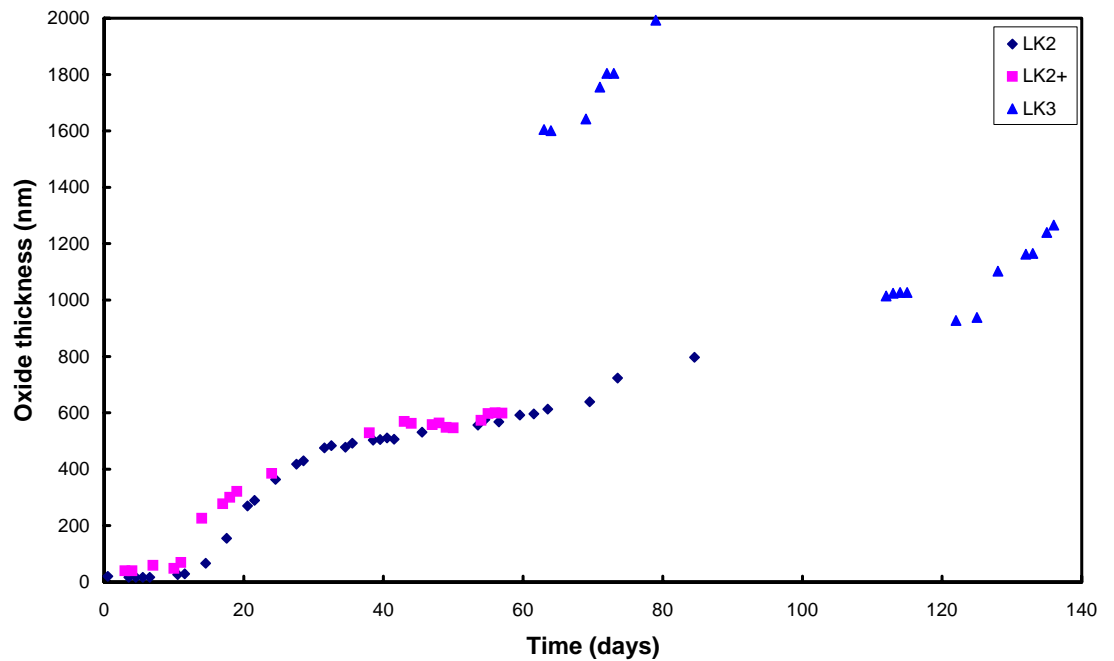


Figure 38

Oxide thickness, calculated from α -corrected (extrapolated) capacitances, as a function of test time for the investigated materials.

ABB-Atom-SVEA-96 fuel rods with LK2, LK2+ and LK3 cladding from Forsmark 3, irradiated for three and four years, have previously been examined in Studsvik. The results show that the LK3 material had the best corrosion resistance (thinnest oxide) and the LK2 material the least corrosion resistance (thickest oxide) after a burn-up of about 40 MWd/kgU [2]. The difference in corrosion behaviour was, however, not as significant as the difference in hydrogen uptake. The LK3 material had the lowest hydrogen uptake and the LK2 material the highest hydrogen uptake. The results from the present investigation indicate that it is not possible to predict the post-transition (and in-reactor) oxidation kinetics from measurements of the oxide growth rate in the pre-transition region.

In Figure 39, the oxide conductivity calculated from the thickness and resistance obtained from the impedance measurements is shown as a function of test time for the investigated materials. For the LK2 and LK2+ materials, the temperature was lower than 288°C at the beginning of the experiments. The temperature was raised to 288°C at day 21 and 12 for the LK2 and LK2+ material, respectively. The calculated conductivity of the materials is of comparable magnitude. The conductivity of the LK2+ material seem to be somewhat lower than for the other two materials at 288°C. The resistances determined from the equivalent circuit analysis (R2 and R3 in Figure 6) are, however, afflicted with some uncertainty. Thus, the

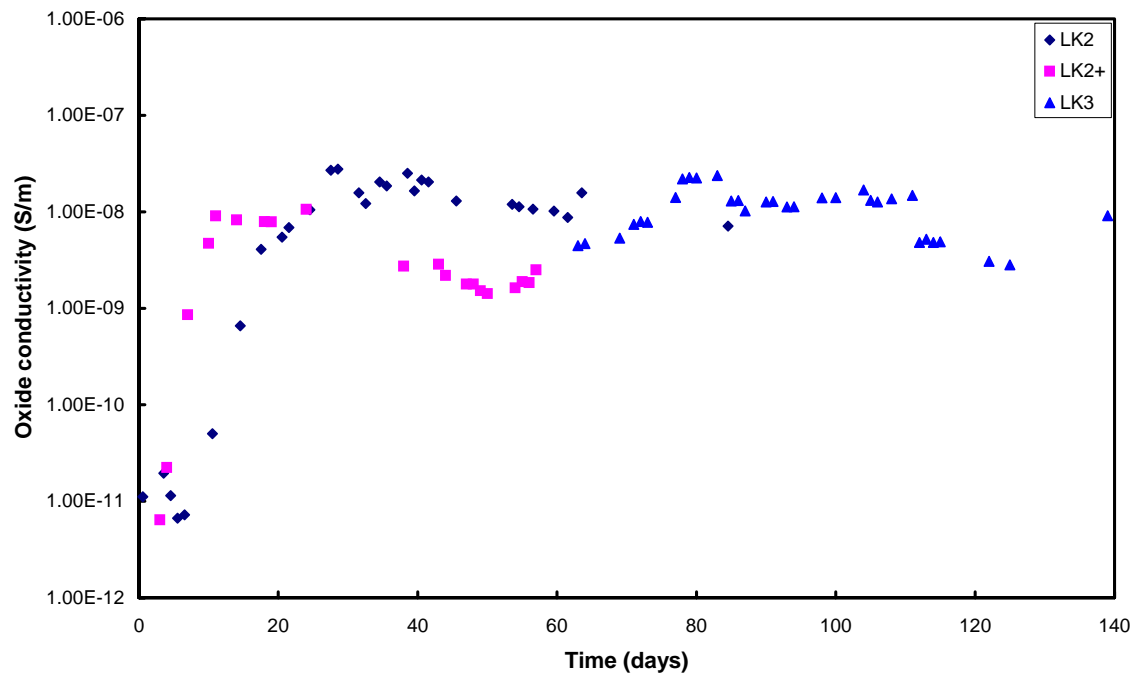


Figure 39

Calculated oxide conductivity for the investigated materials as a function of test time.

differences seen in Figure 39 are probably within the uncertainty of the calculated values. It can also be seen that, at 288°C, the conductivity decreases with time (this is least obvious for the LK3 material). The activation energies for conduction given in section 4.1 and 4.2 are in close agreement and amount to 34.4 and 33.4 kJ mol⁻¹ for the LK2 and LK2+ material, respectively. For the LK3 material, the activation energy is not available since no measurements were performed when raising the temperature at the beginning of the experiment.

The effective donor densities for the different materials at 288°C, are collected in Table 10. For the LK2+ material, the lower value at 100 Hz may be less reliable than the other two values, as explained in section 4.2. Disregarding this value, the effective donor density is $4.8\text{-}5.5 \times 10^{23} \text{ m}^{-3}$ for the LK2+ material. The effective donor density for the LK2+ material has also been measured by Andersson and Ahlberg [9]. These measurements were performed at 280°C in simulated PWR-environment (1000 ppm B, 3 ppm Li, 0.1 mM NaNO₃) on a specimen that had not been pre-oxidized. The effective donor density found varied between $15\text{-}39 \times 10^{23} \text{ m}^{-3}$ after 4-10 days of exposure.

Table 10

Effective donor densities for the investigated materials at 288°C.

Material	Test time (days)	Effective donor density $N_D \times 10^{-23} \text{ (m}^{-3}\text{)}$
LK2	43 and 67	3.4 – 4.4
LK2+	56	3.6 – 5.5
LK3	127	1.3 – 1.6

From Table 10 it is seen that the effective donor density of the LK3 material is lower than for the other two materials. This lower value for the electronic conductivity of the LK3 material may be one explanation as to why the corrosion resistance of the LK3 material in actual plant is better than for the other two materials. On the other hand, the poorer performance of the LK2 material has been attributed to the disappearance of the SPPs at high burn-ups (the particles dissolve), resulting in increased corrosion rate after 3-4 years of service in a reactor. The effect of the SPPs on the corrosion properties of Zircaloy is not fully understood. It has been proposed that the increased corrosion resistance is attributed to anodic protection provided by the SPP precipitates [18].

6 Conclusions

- It has been clearly demonstrated that impedance spectroscopy can be used for in-situ studies of the corrosion of Zircaloy cladding materials in the pre-transition region at temperatures up to 288°C.
- It was found that supporting electrolyte must be added to the water in order to follow the oxidation.
- When the oxide grows thicker during the experiments, a layered structure is formed.
- Nearly all impedance spectra have been successfully modelled using equivalent circuits with one or two time constants for the oxide.
- The following properties have been successfully evaluated from the impedance data:
 - oxide thickness
 - oxide conductivity
 - effective donor density
- The differences in oxide growth rate between the investigated materials are small in the pre-transition region.
- The oxide thickness measured using SEM is in good agreement with the thickness calculated from the impedance data.
- The effective donor density (a measure of the electronic conductivity) is lower for the LK3 material compared to the other two materials.

Acknowledgements

The authors would like to acknowledge the following persons:

Stig Karlgren, Studsvik Nuclear AB Sweden, for taking daily care of the experiments.

Eva Ögren, Studsvik Nuclear AB Sweden, for preparing solutions.

Roger Lundström, Studsvik Nuclear AB Sweden, for SEM work.

Sören Karlsson, Studsvik Nuclear AB Sweden, for measurements of hydrogen contents.

Seiji Yamamoto Toshiba Corporation, Japan for demonstrating how the experimental equipment works.

This work has been funded by the Swedish Nuclear Power Inspectorate, Sweden, Vattenfall Bränsle AB, Sweden, OKG AB, Sweden and Studsvik Nuclear AB, Sweden.

References

- [1] YAMAMOTO, S and PEIN, K
Studsvik Nuclear AB, Sweden 2001,
STUDSVIK/N(K)-01/016
- [2] NYSTRAND, A-C and LUNDSTRÖM, R
Studsvik Nuclear AB, Sweden 2000,
STUDSVIK/N(H)-00/020
- [3] BARD, A J and FAULKNER, L R
Electrochemical methods: Fundamentals and applications.
John Wiley & Sons, New York, 2001, Chap. 10.
ISBN 0-471-04372-9.
- [4] MACDONALD, J R, ed.
Impedance spectroscopy: Emphasizing Solid
Materials and Systems.
John Wiley & Sons, New York, 1987. ISBN 0-471-83122-0.
- [5] BOUKAMP, B A
Equivalent circuit. Users manual.
University of Twente, the Netherlands, 2nd edition, 1989.
- [6] OSKARSSON, M, AHLBERG, E, ANDERSSON, U and
PETTERSSON, K
Characterisation of pre-transition oxides on Zircalloys.
Journal of Nuclear Materials 297, 2001, p 77-88.
- [7] BARBERIS, P, AHLBERG, E, SIMIC, N, CHARQUET, D,
LEMAIGNAN, C, WIKMARK, G, DAHLBÄCK, M,
LIMBÄCK, M, TÄGTSTRÖM, P and LEHTINEN, B
Role of the second-phase particles in zirconium binary alloys.
Zirconium in the Nuclear Industry, ASTM STP 1423, 2002,
p 33-58.
- [8] OSKARSSON, M, AHLBERG, E and PETTERSSON, K
Oxidation of Zircaloy-2 and Zircaloy-4 in water and lithiated
water at 360°C.
Journal of Nuclear Materials 295, 2001, p 97-108.

- [9] ANDERSSON, U and AHLBERG, E
Departement of Chemistry, Göteborg University,
S-412 Göteborg, Sweden.
Manuscript in preparation.
- [10] GOOSSENS, A, VAZQUEZ, M, and MACDONALD, D D
The nature of electronic states in anodic zirconium oxide films.
Part 1: The potential distribution.
Electrochimica Acta 41, 1996, p 35-45.
- [11] GOMES, W P and VANMAEKELBERGH, D
Impedance spectroscopy at semiconductor electrodes: Review
and recent developments.
Electrochimica Acta 41, 1996, p 967-973.
- [12] NATARAJAN, A, OSKAM, G and SEARSON, P C
J. Phys. Chem. B 102, 1998, p 7793-7799.
- [13] HAMANN, C H, HAMNETT, A H, and VIELSTICH, W
Electrochemistry.
Wiley-VCH, Weinheim, 1998. ISBN 0-471-04372-9.
- [14] GUNNARSSON, M, ABBAS, Z, AHLBERG, E, GOBOM, S
and NORDHOLM, S
Corrected Debye-Hückel Analysis of Surface Complexation.
Journal of Colloid and Interface Science 249, 2002, p 52-61.
- [15] WEST, A R
Basic solid state chemistry.
John Wiley & Sons, 1988. ISBN 0-471-91798-2.
- [16] BERGSTRÖM, C and LUNDGREN, K
PEROX – Teoribeskrivning och användarhandledning.
ALARA Engineering, Report 98-0035R and 98-0036R, 1998,
in Swedish.
- [17] OSKARSSON, M
Study on the Mechanisms for Corrosion and Hydriding of
Zircaloy.
Doctoral Thesis, the Royal Institute of Technology,
Stockholm, Sweden, 2000.
- [18] ISOBE, T, MURAI, T and MAE, Y
Anodic protection provided by precipitates in aqueous
corrosion of Zircaloy.
Zirconium in the nuclear industry: 11th Int. Symp., ASTM,
1996, p 203-217.

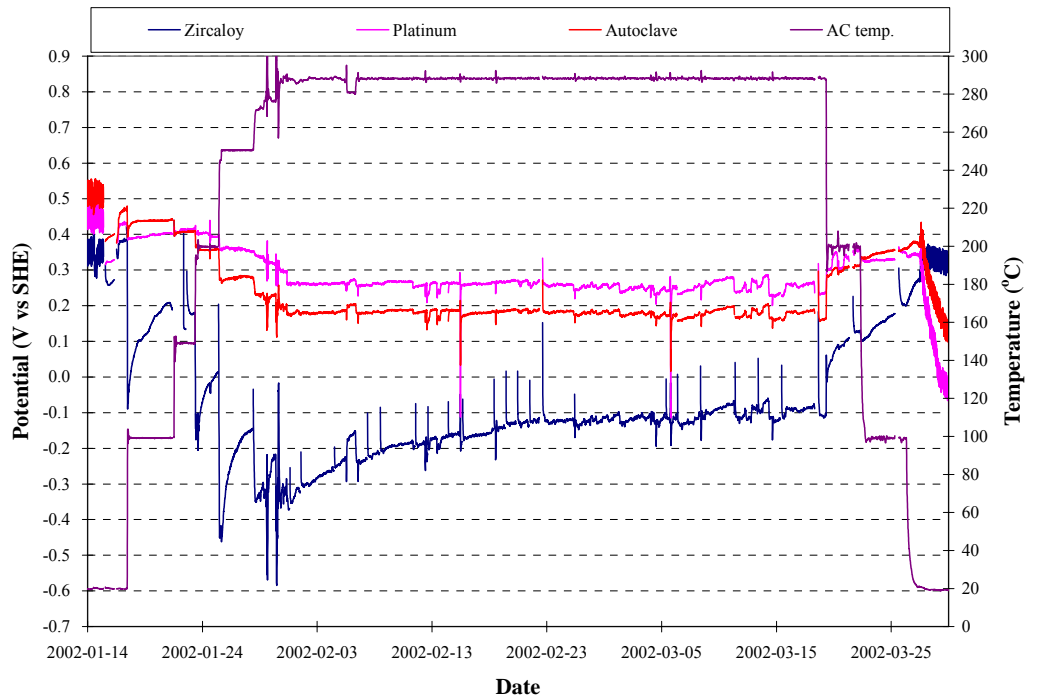


Figure A.1
Potentials measured during experiment with the LK2 material.

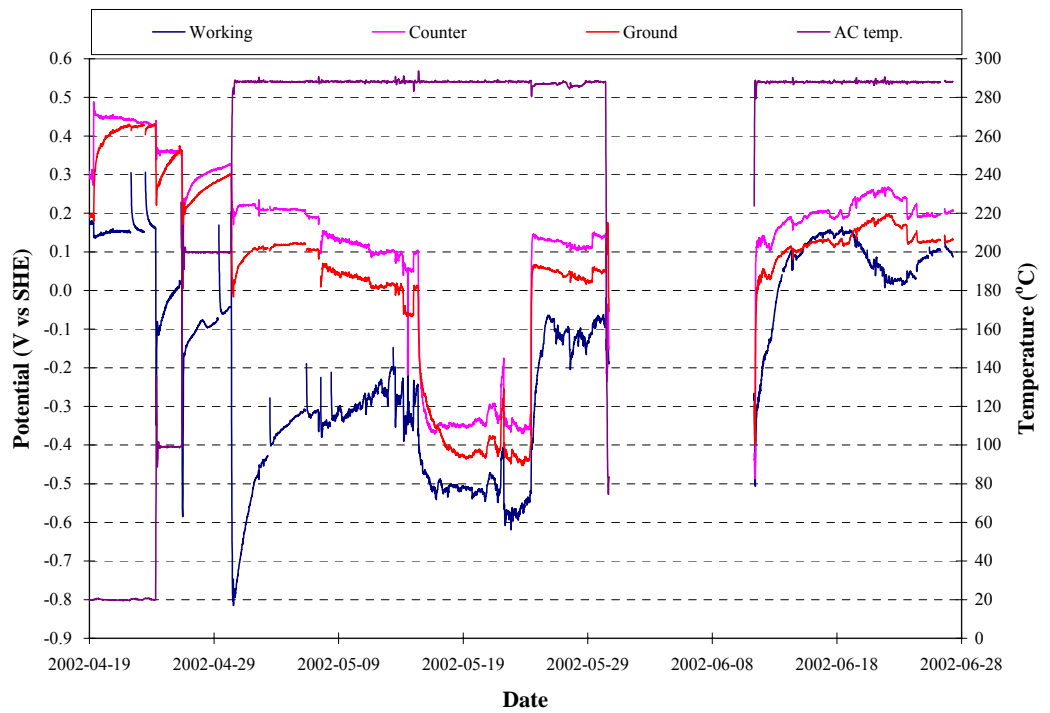


Figure A.2
Potentials measured during experiment with the LK2+ material.

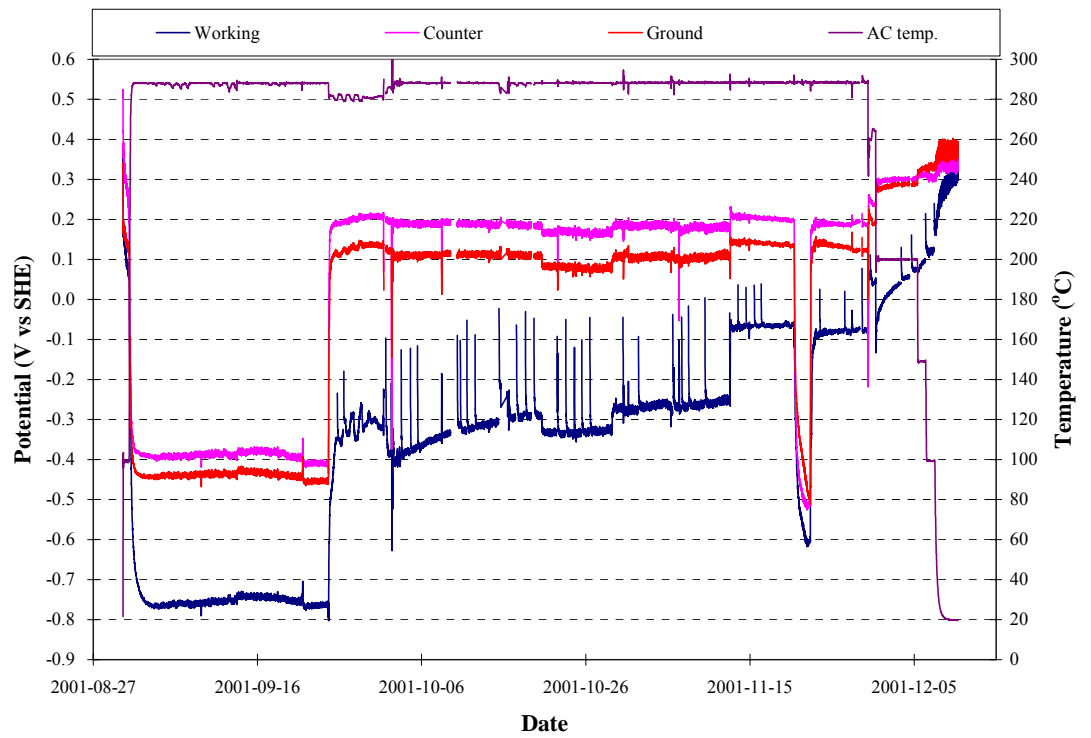
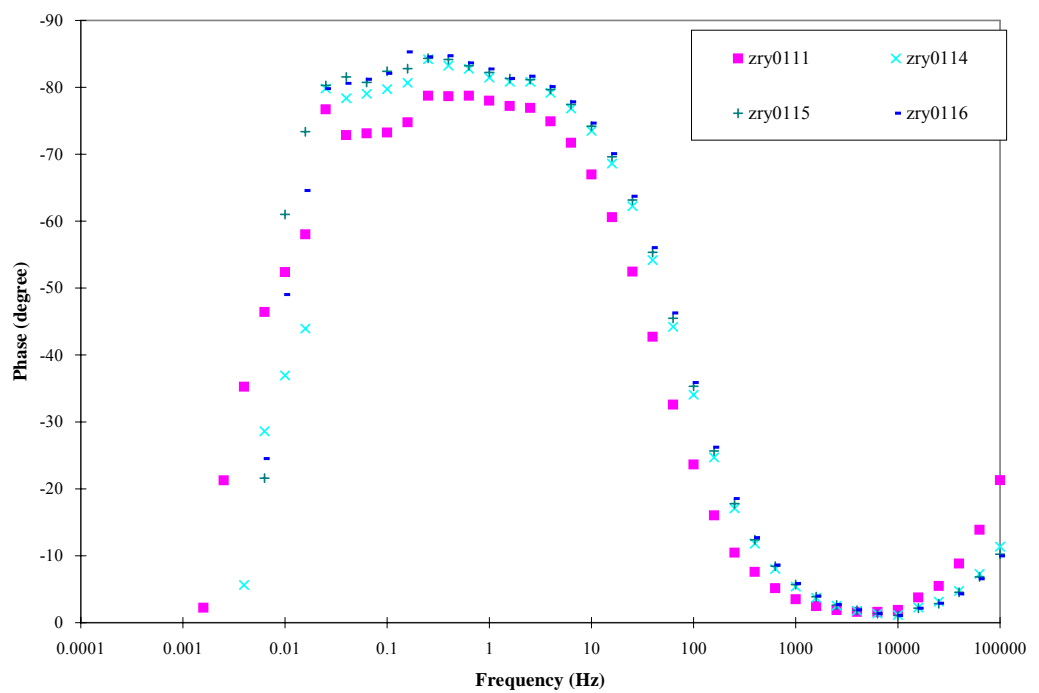
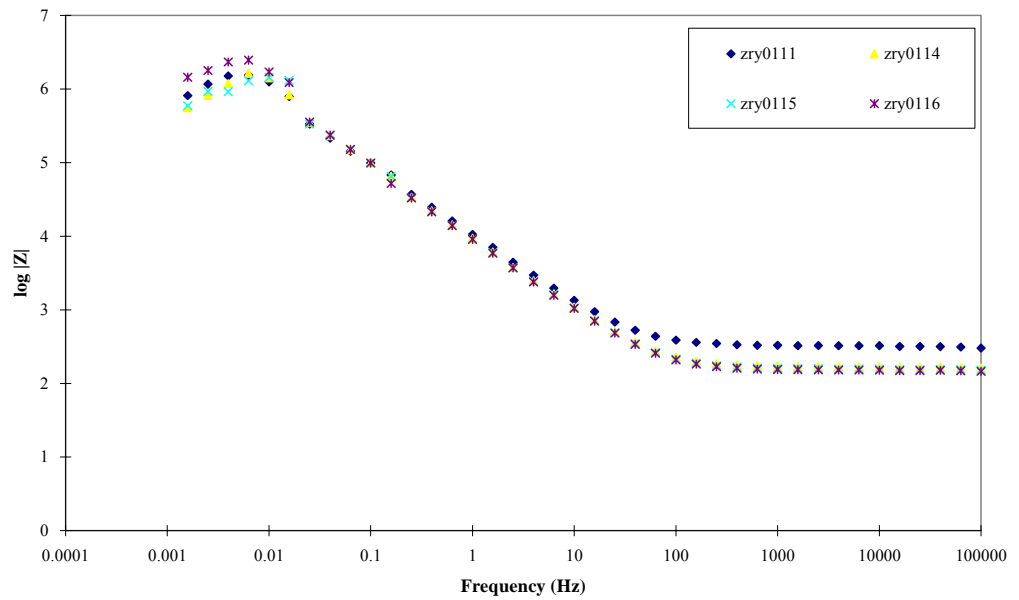
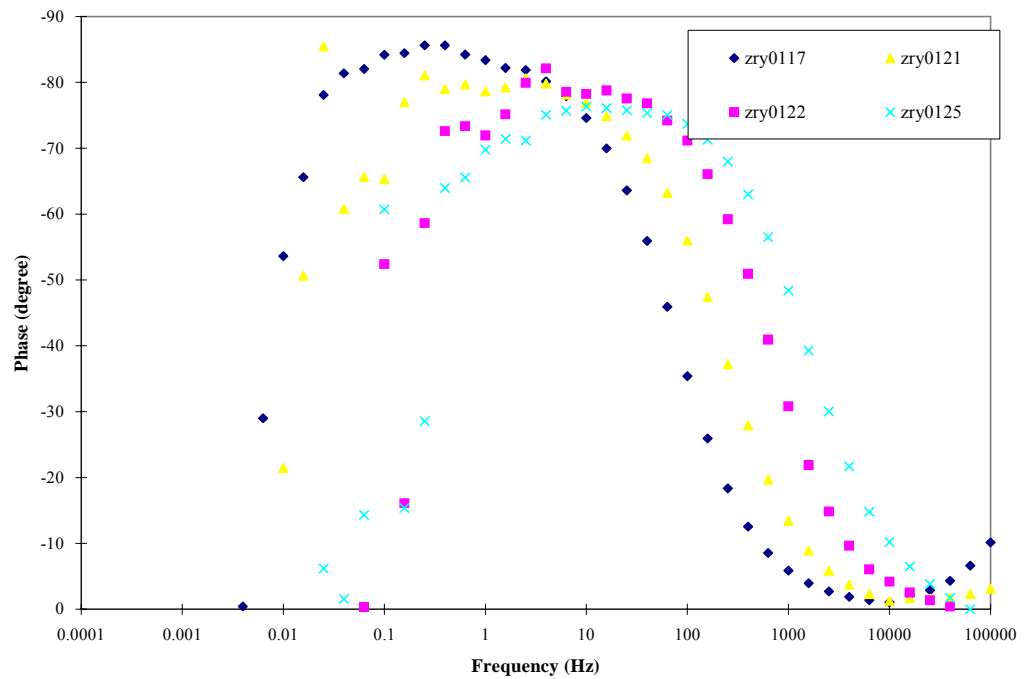
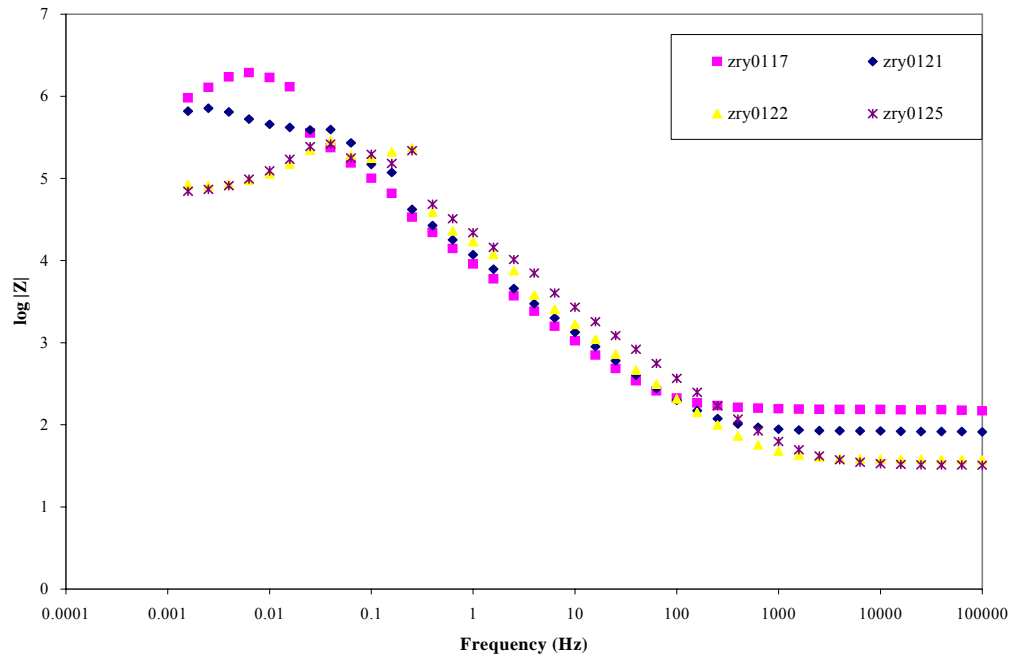


Figure A.3
Potentials measured during experiment with the LK3 material.

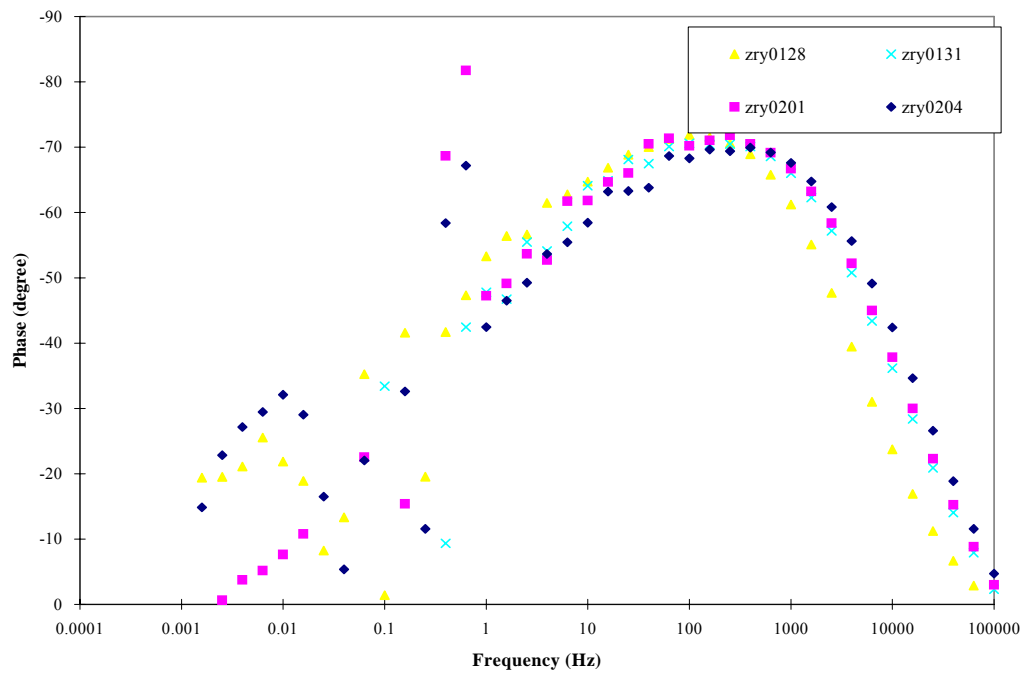
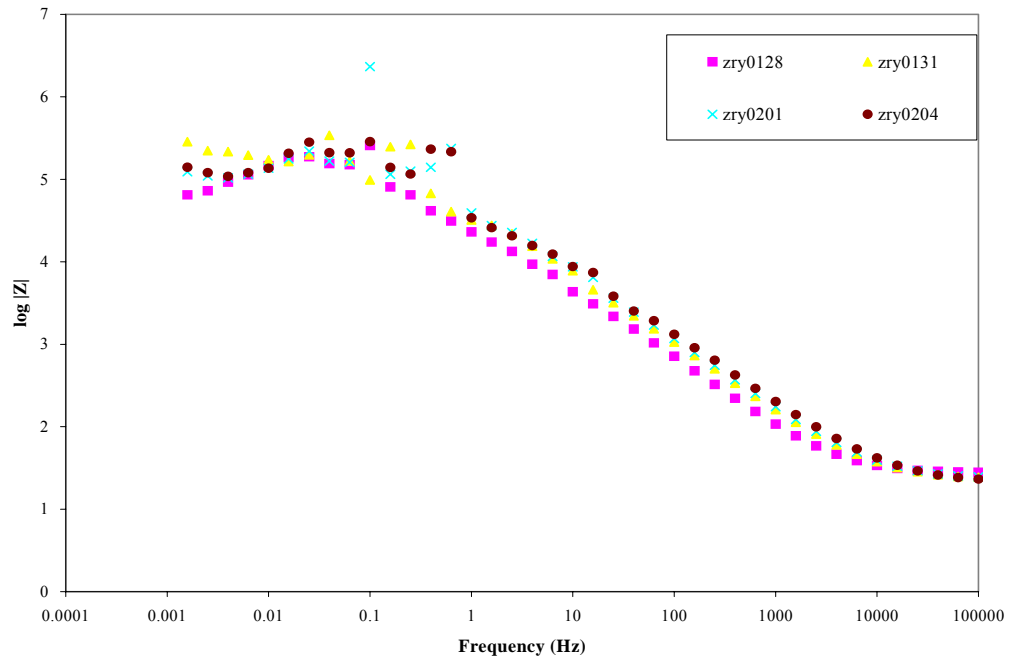
Impedance spectra measured during experiments with the LK2 material



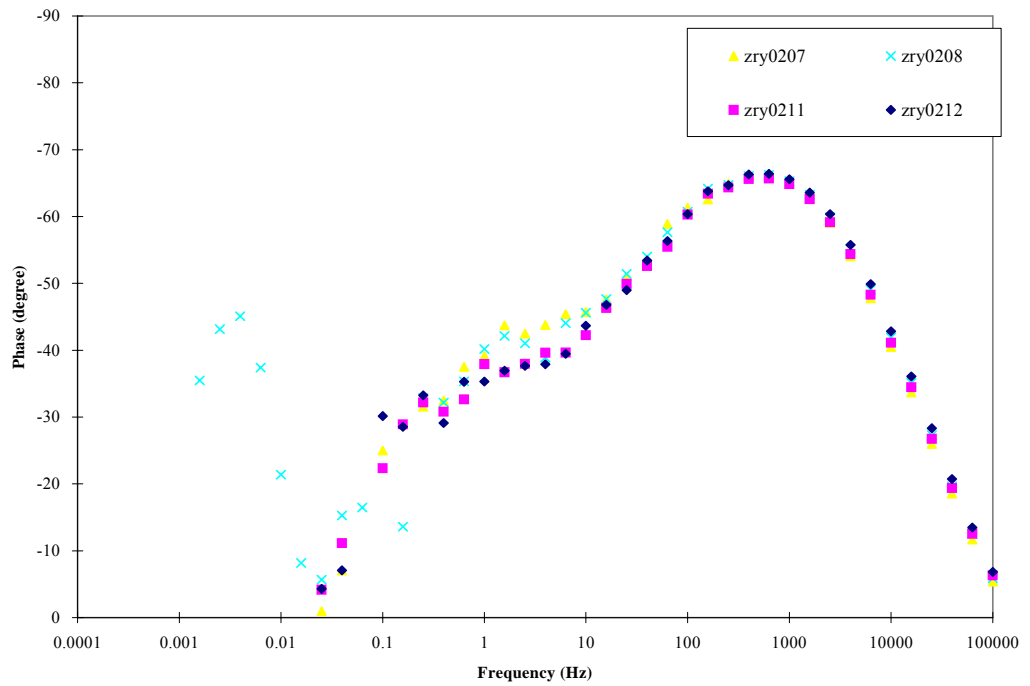
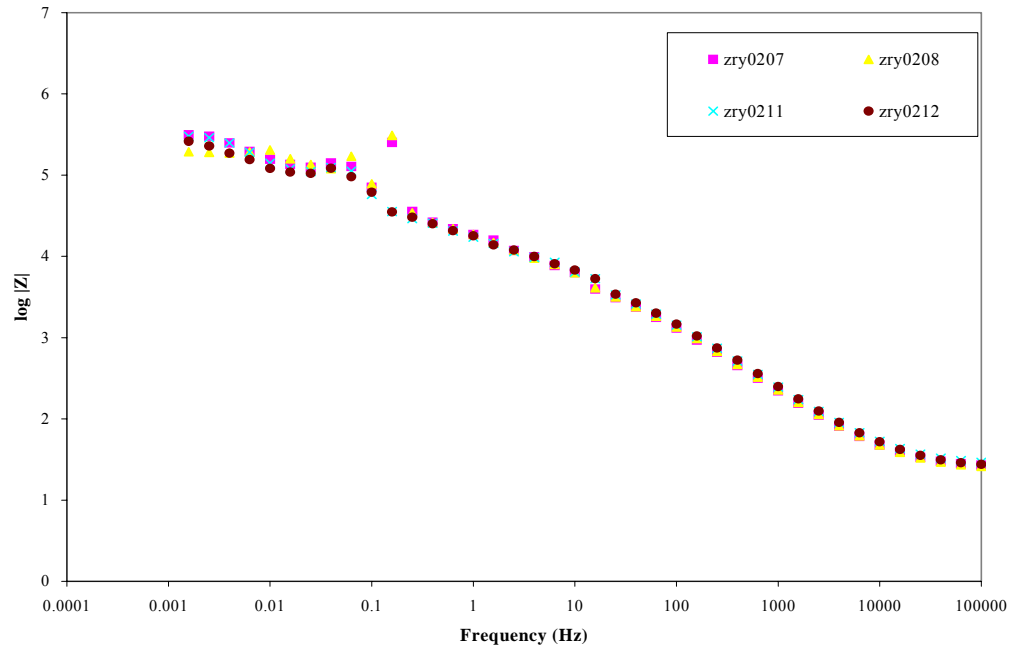
Impedance spectra measured during experiments with the LK2 material (cont.)



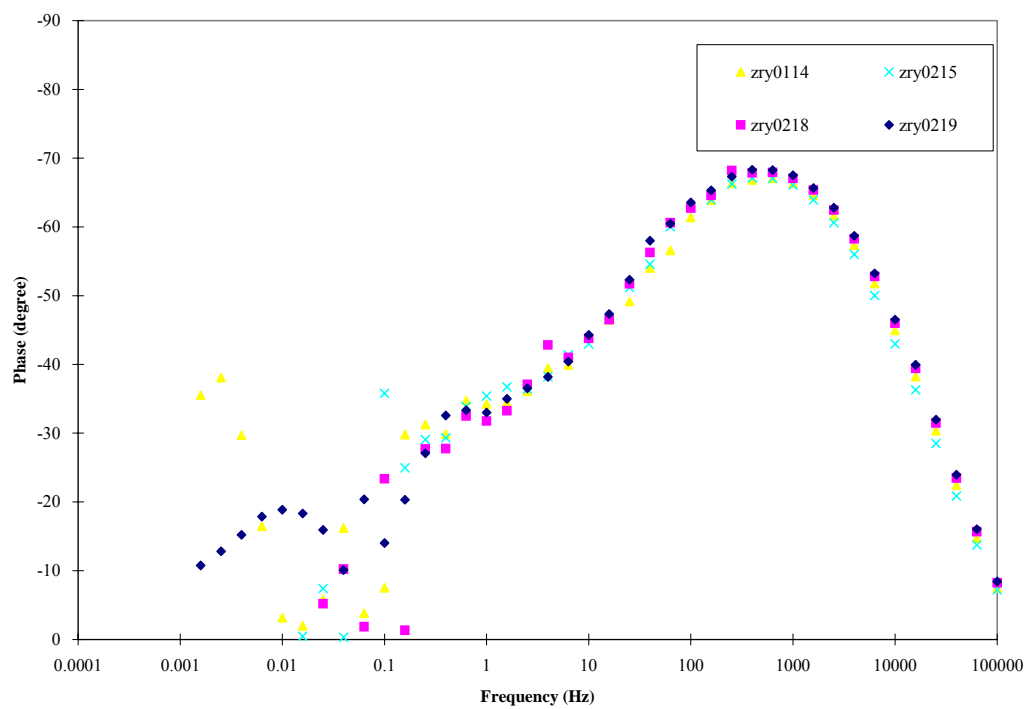
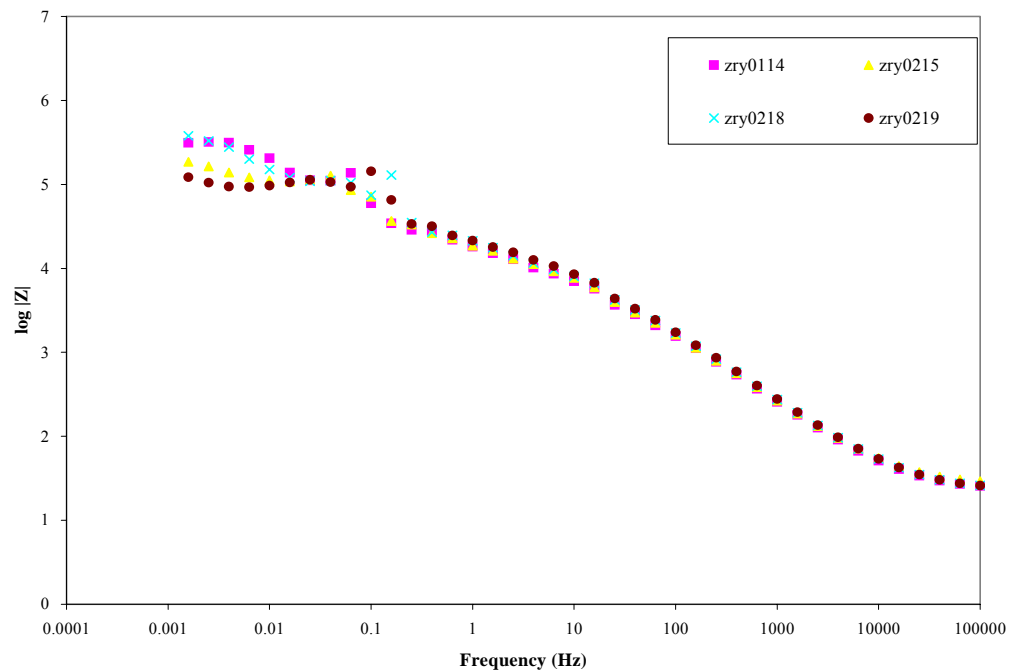
Impedance spectra measured during experiments with the LK2 material (cont.)



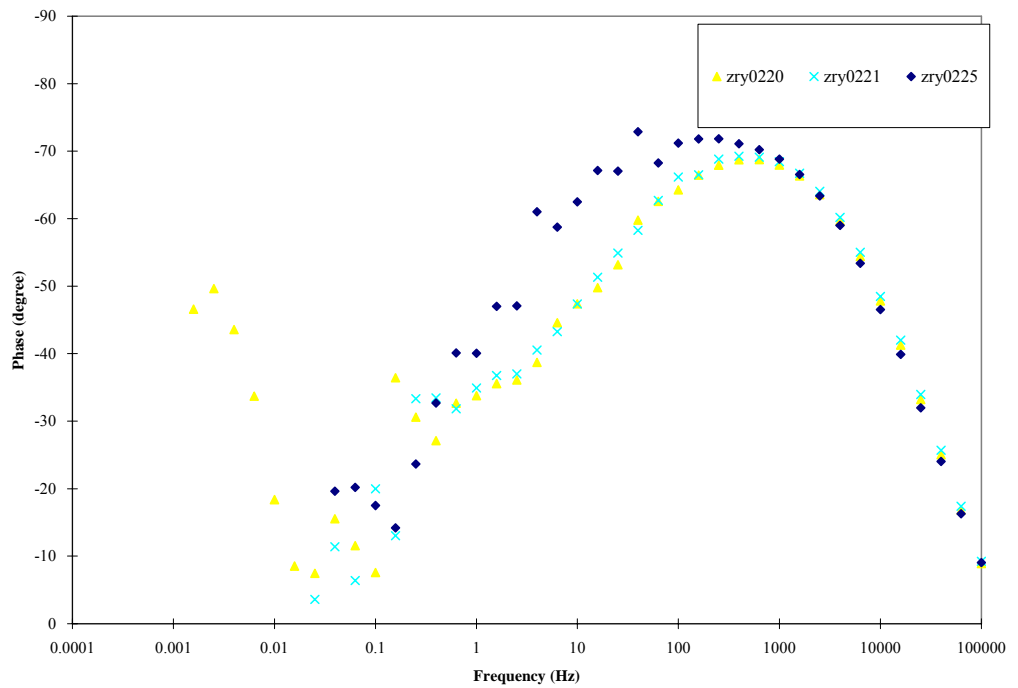
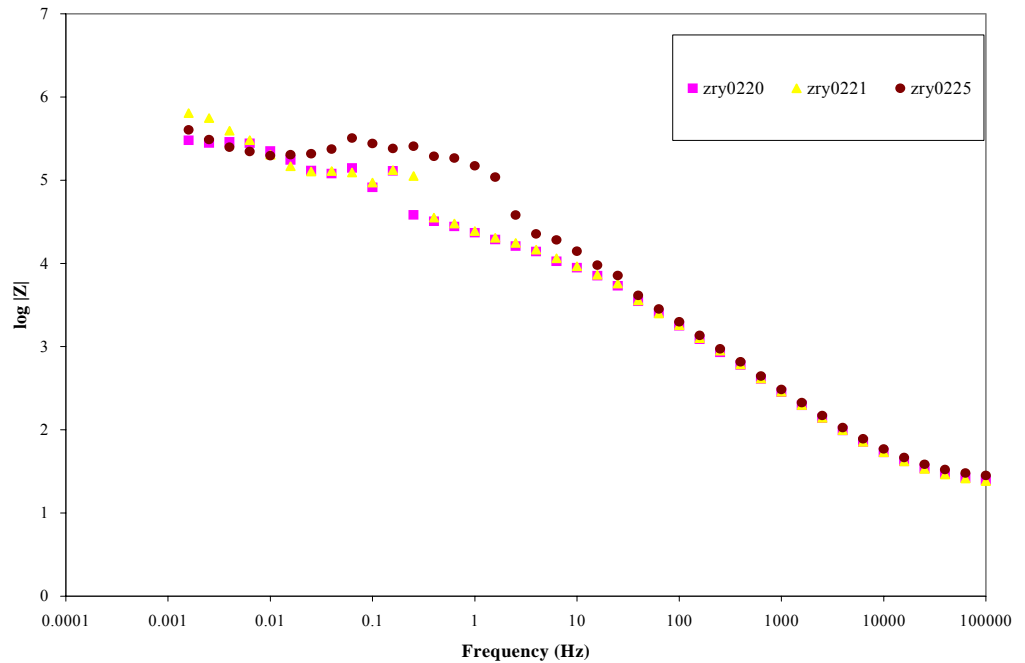
Impedance spectra measured during experiments with the LK2 material (cont.)



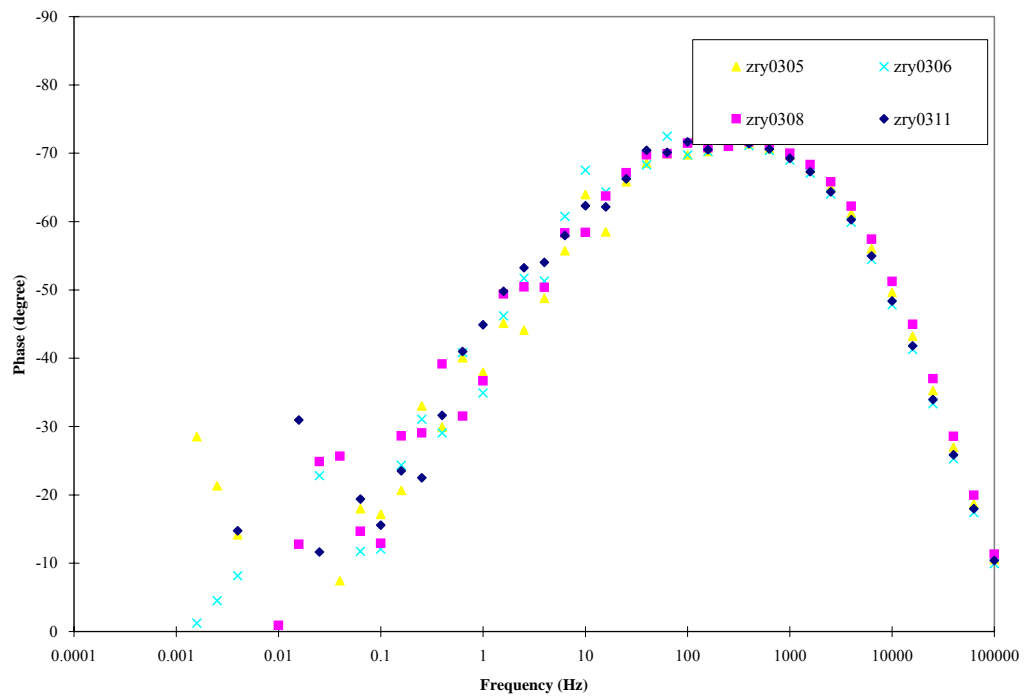
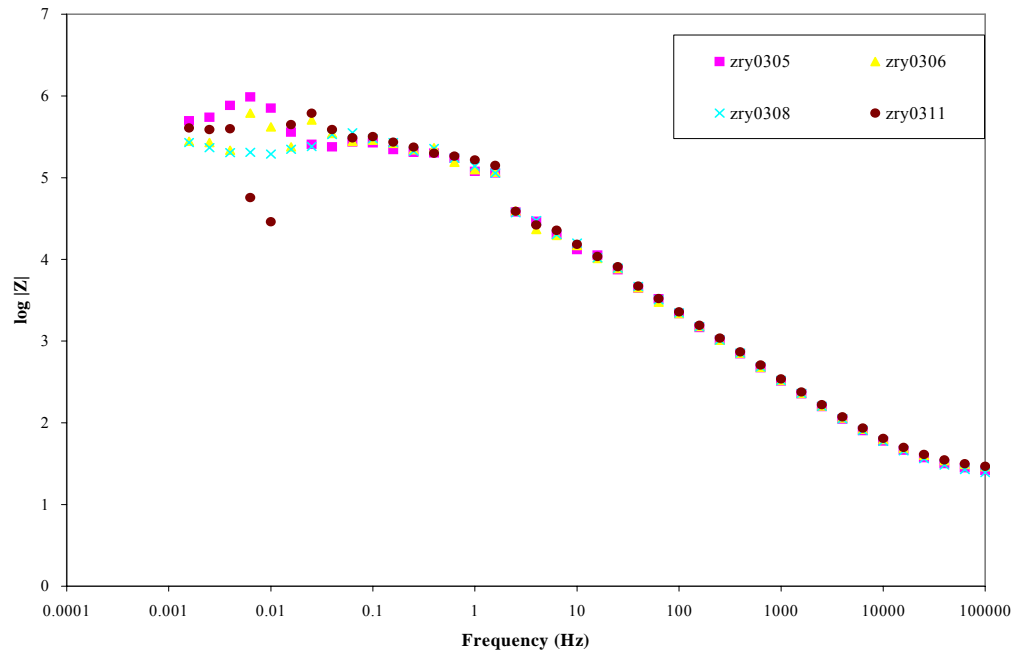
Impedance spectra measured during experiments with the LK2 material (cont.)



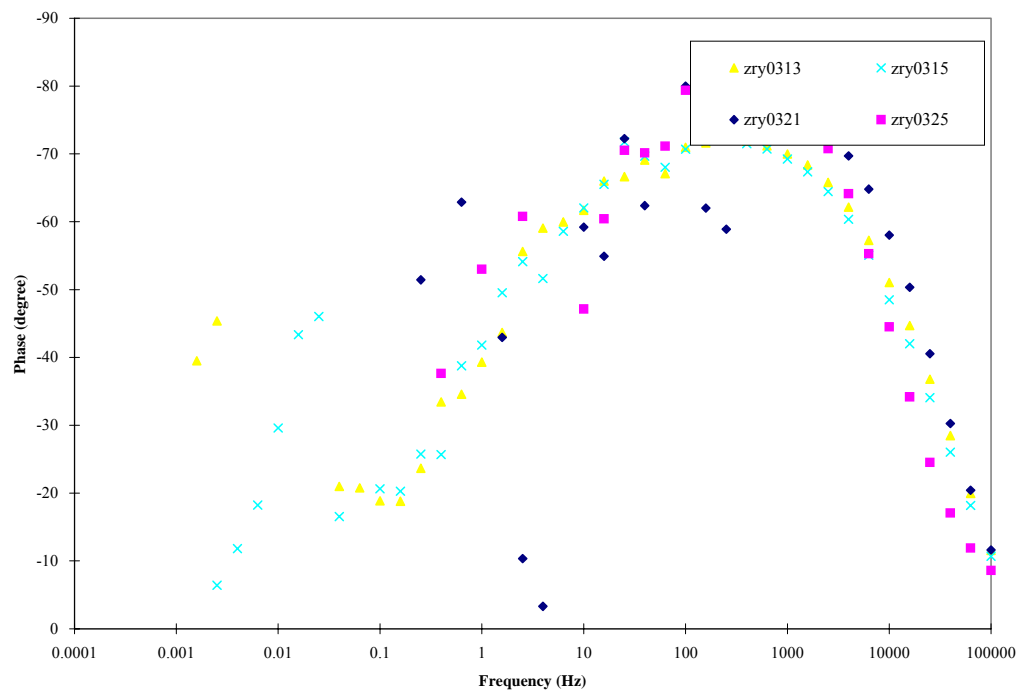
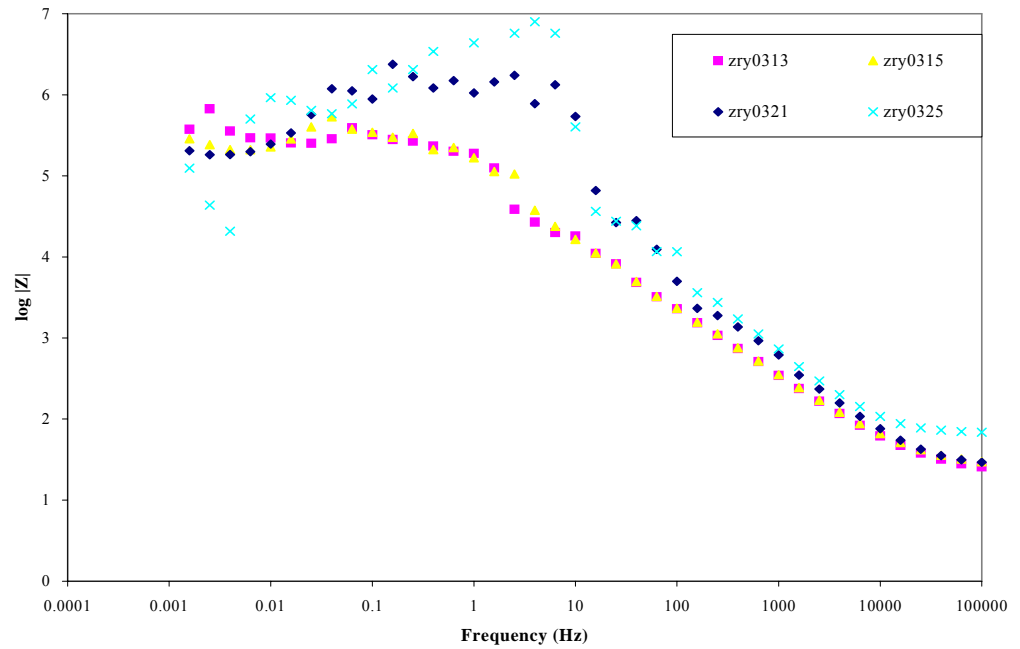
Impedance spectra measured during experiments with the LK2 material (cont.)

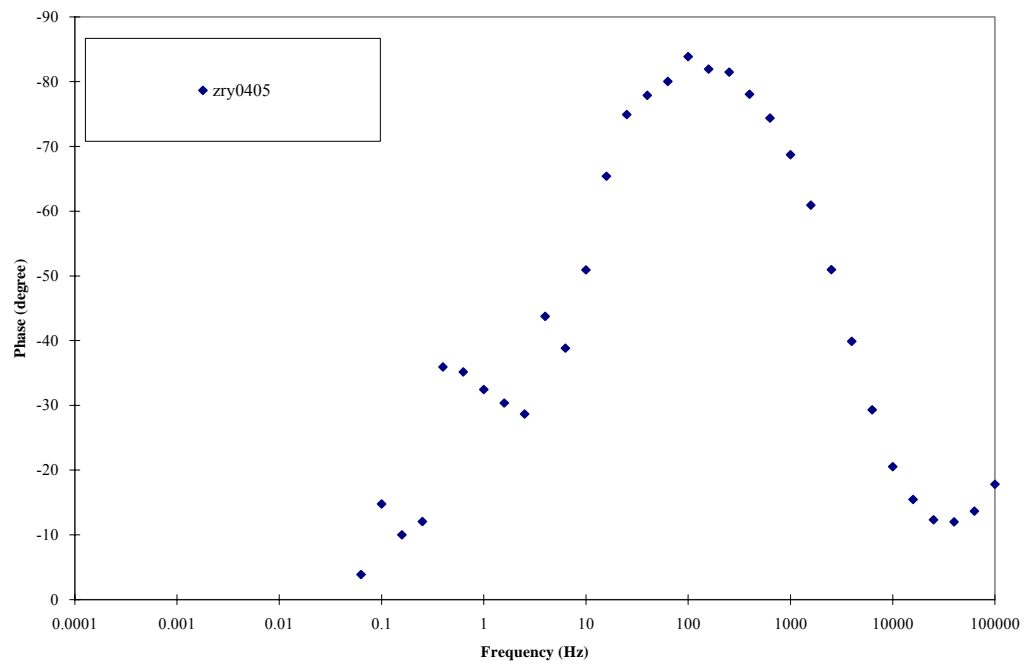
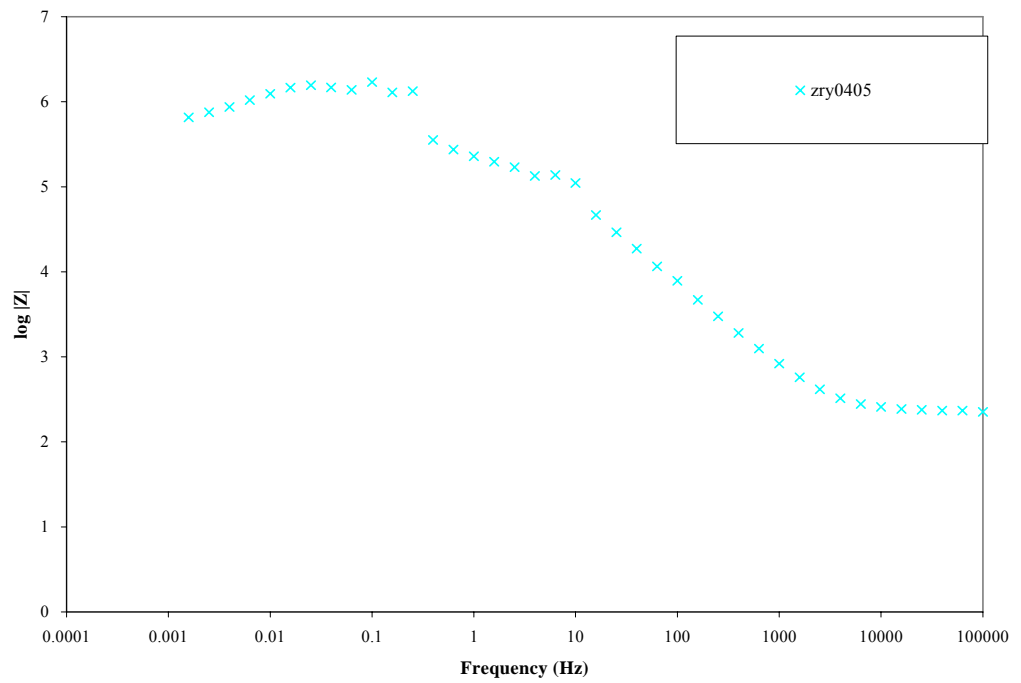


Impedance spectra measured during experiments with the LK2 material (cont.)

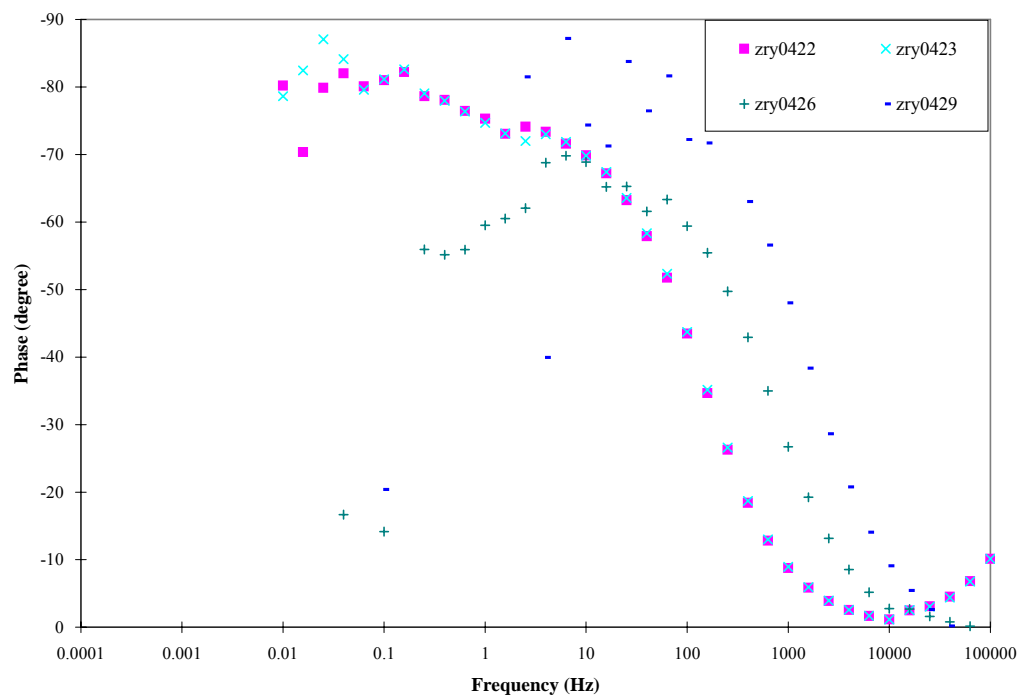
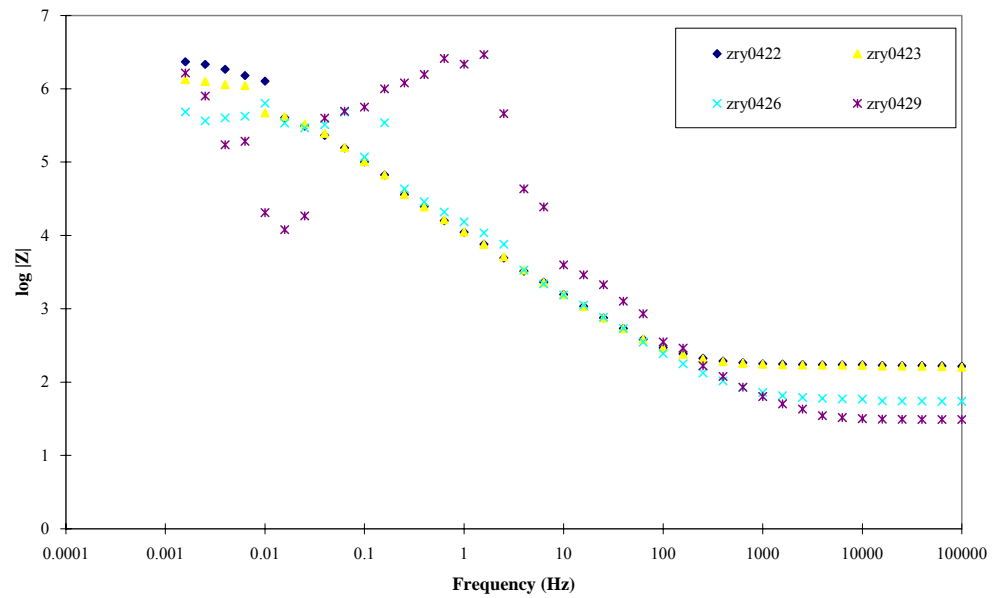


Impedance spectra measured during experiments with the LK2 material (cont.)

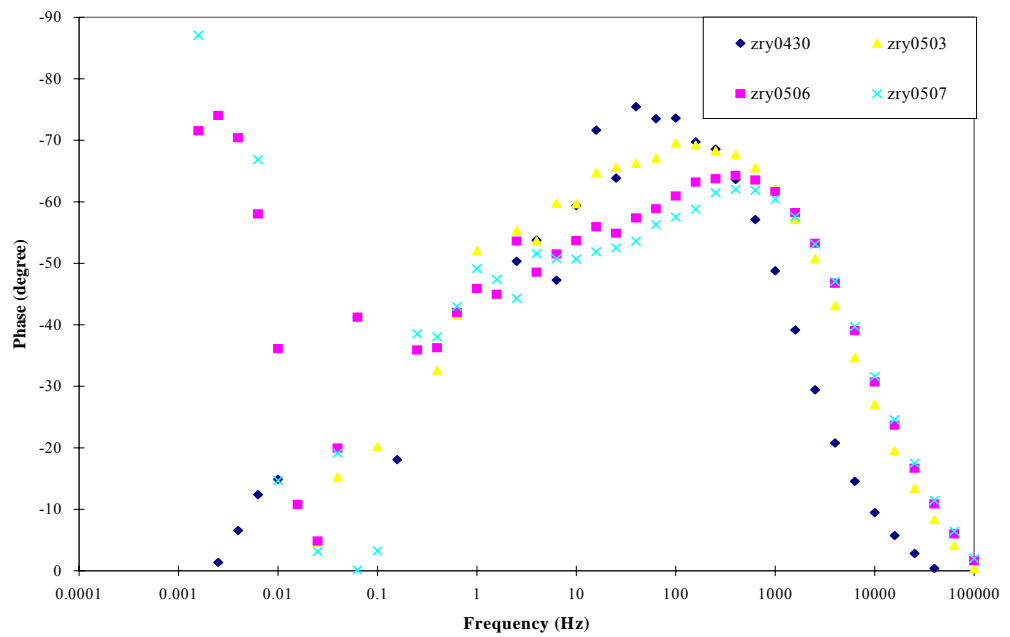
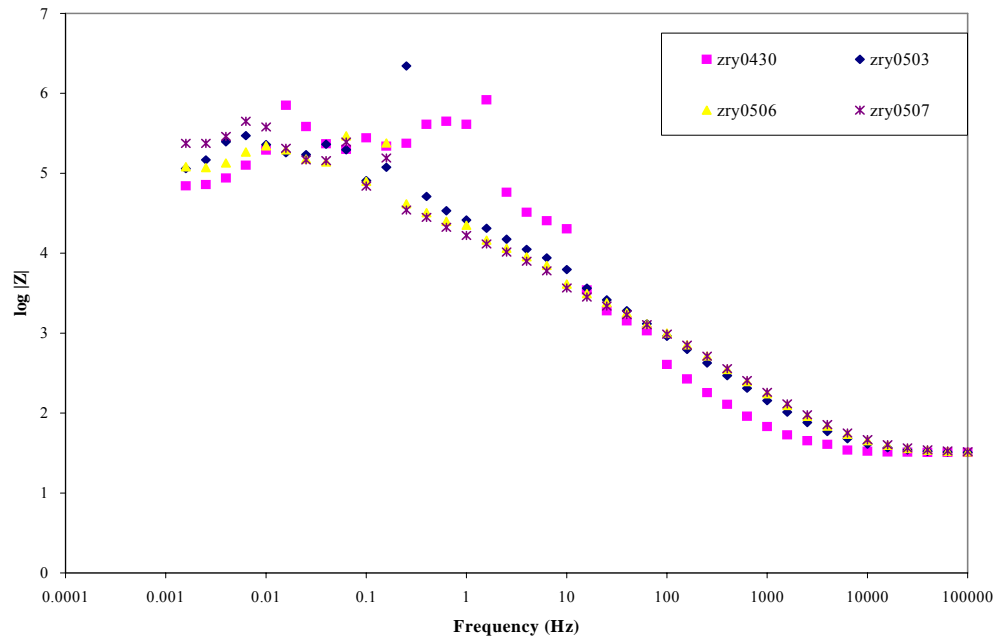


Impedance spectra measured during experiments with the LK2 material (cont.)

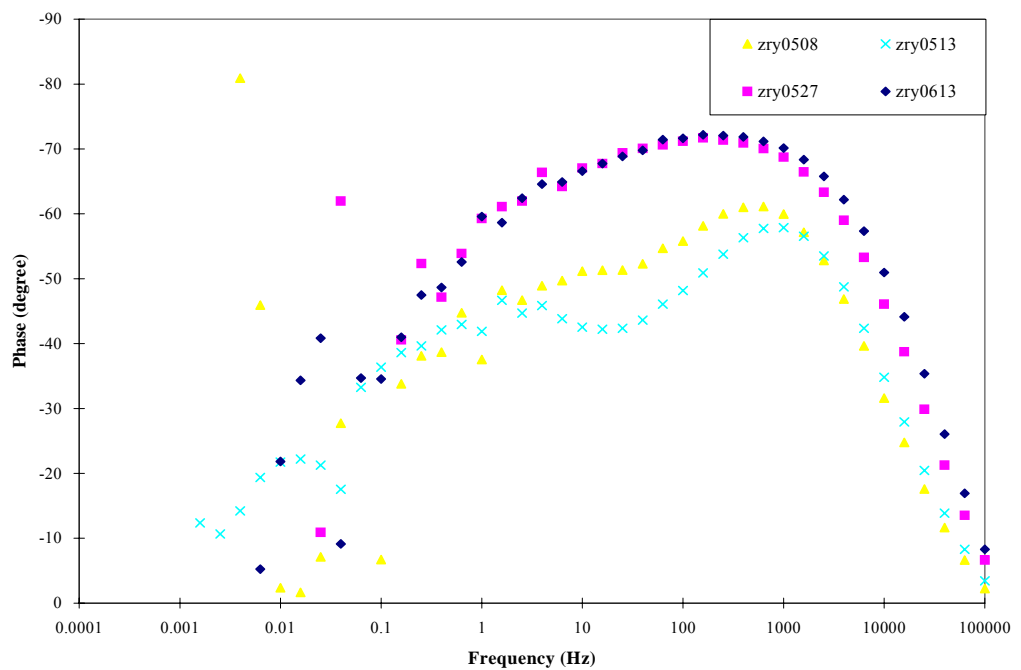
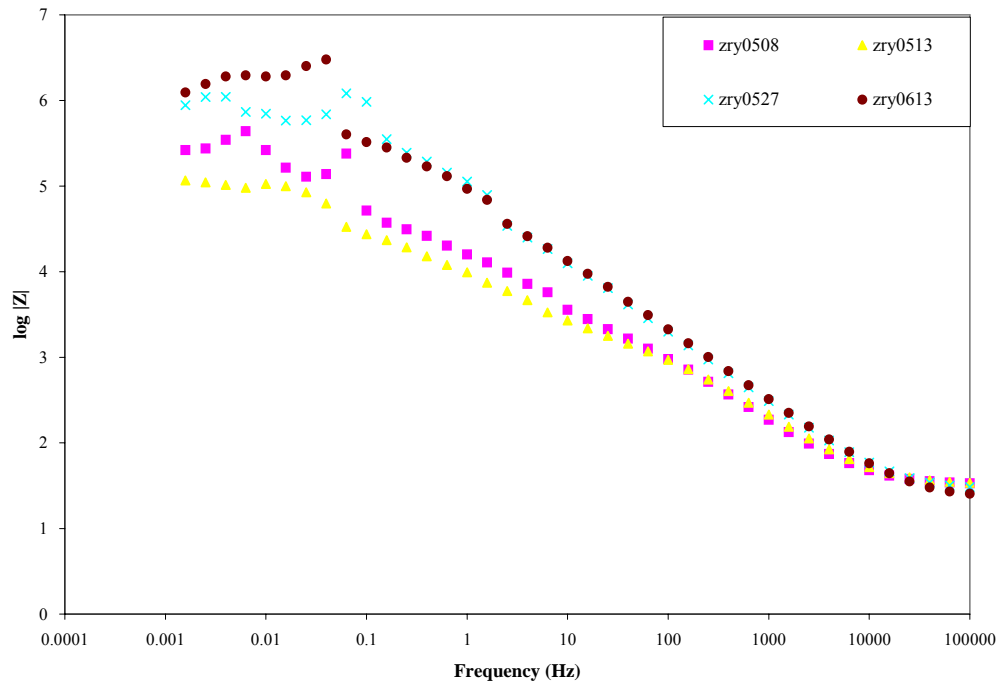
Impedance spectra measured during experiments with the LK2+ material



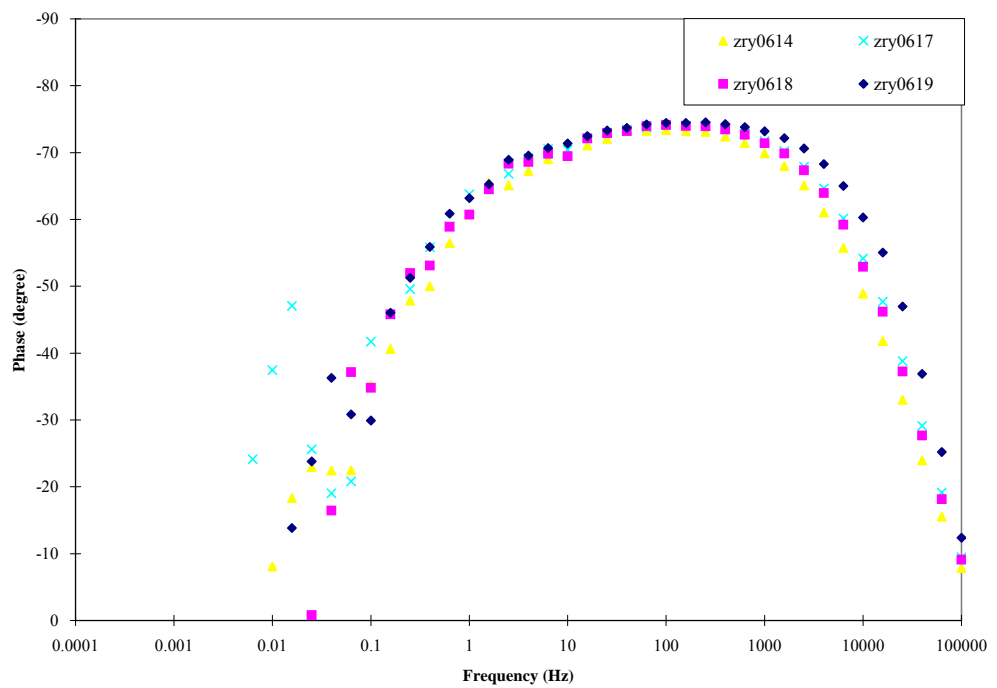
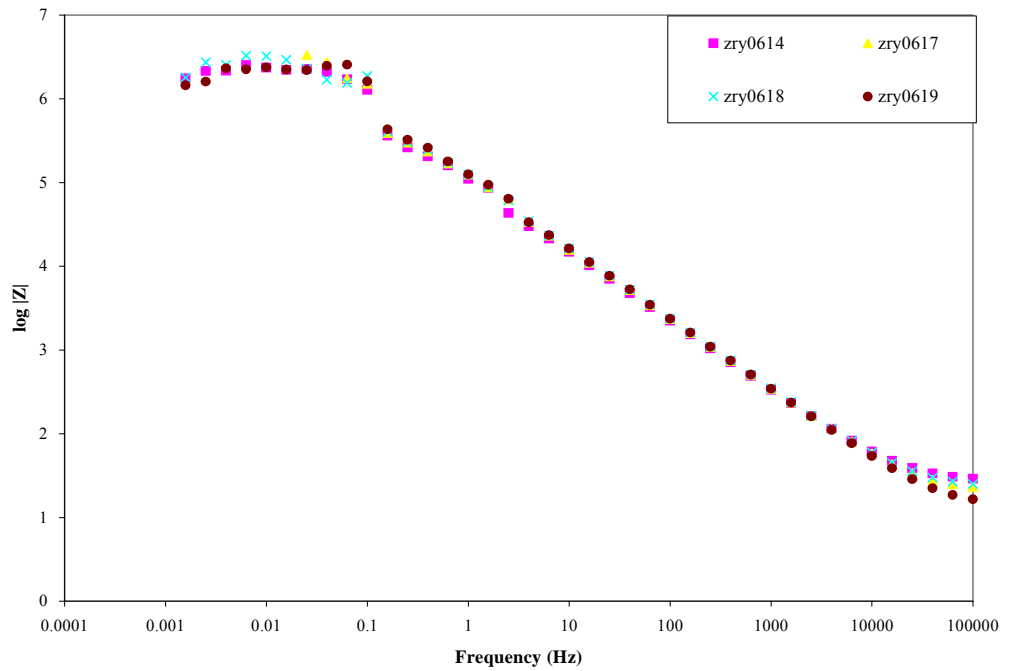
Impedance spectra measured during experiments with the LK2+ material (cont.)

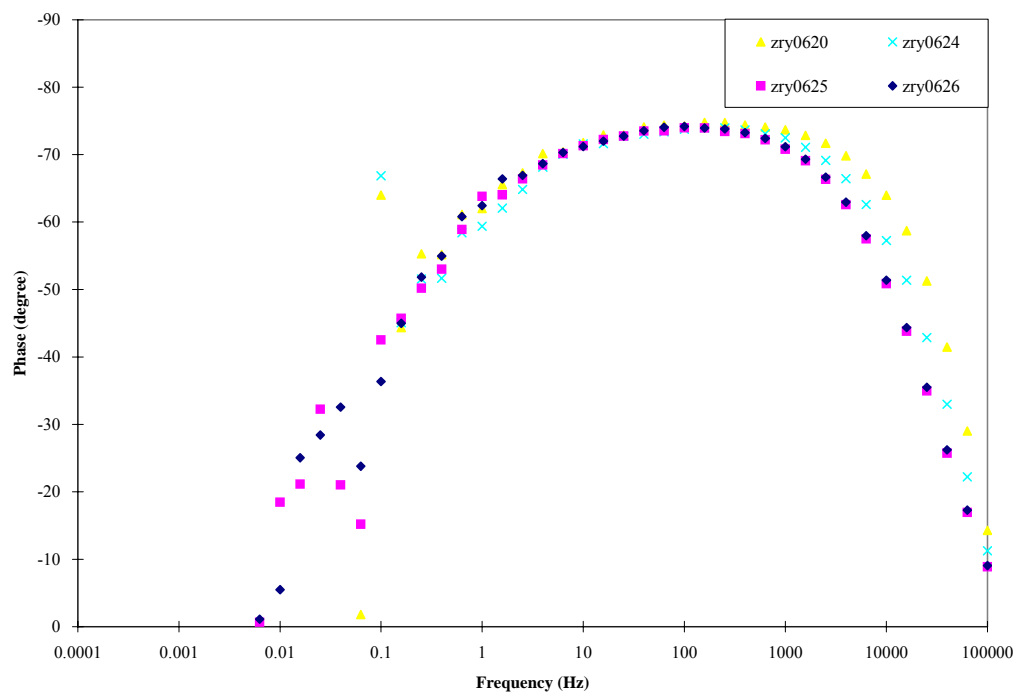
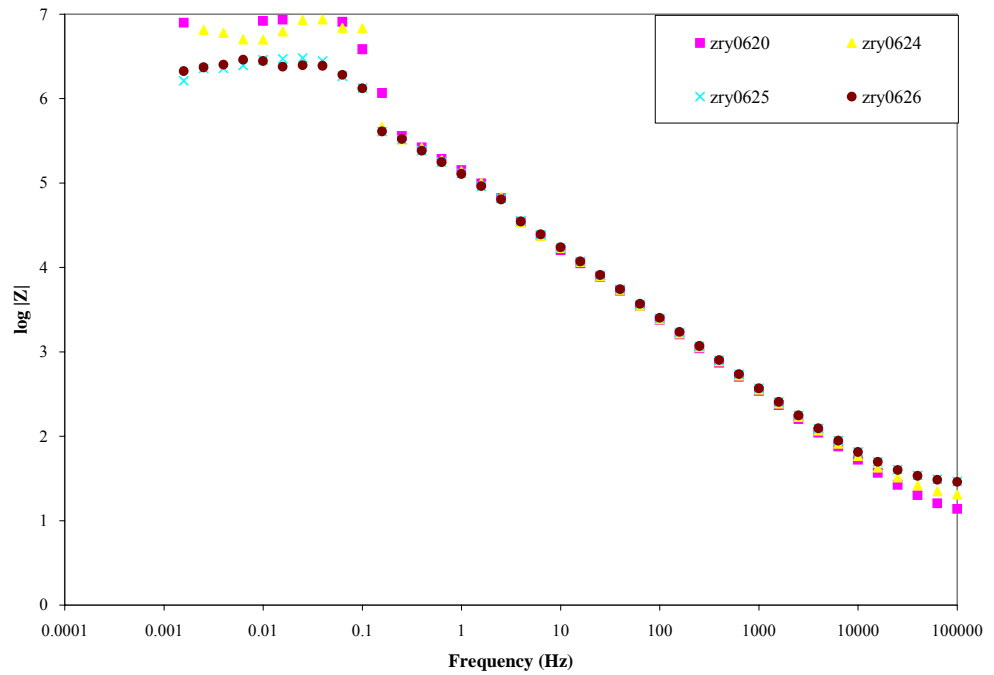


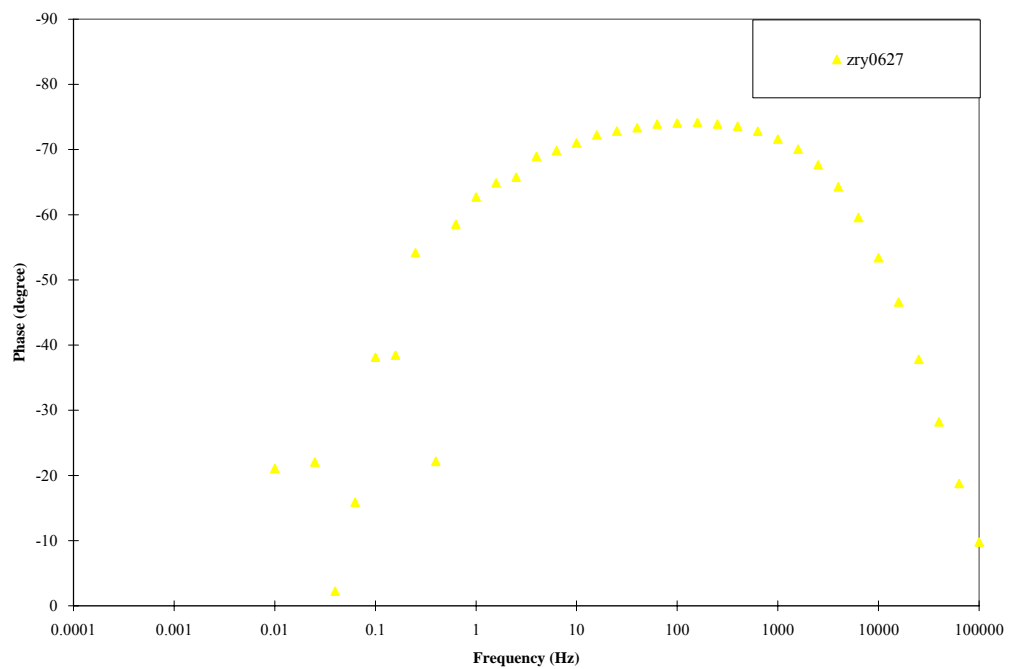
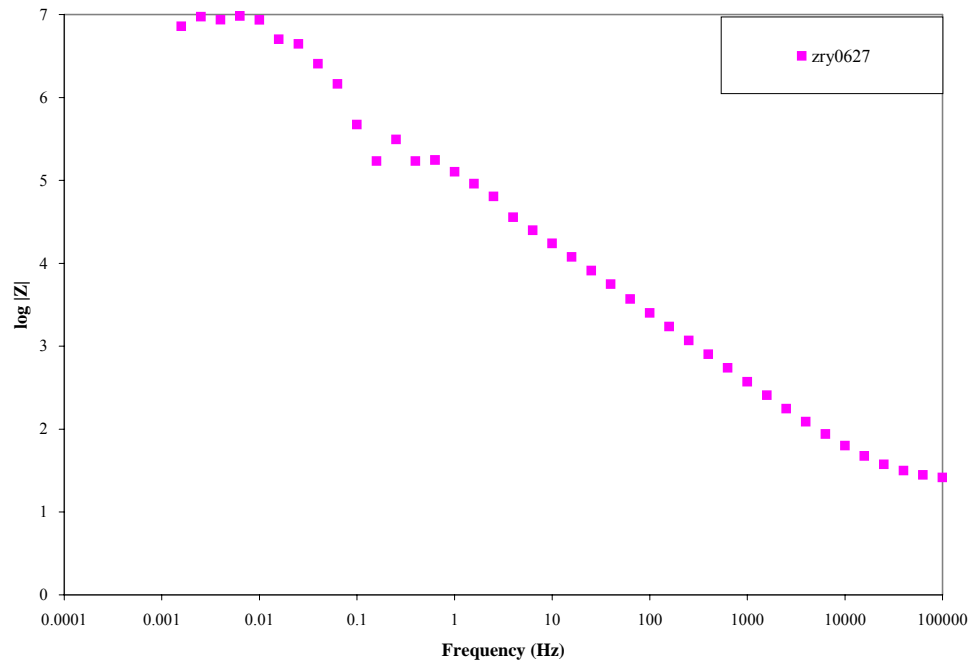
Impedance spectra measured during experiments with the LK2+ material (cont.)



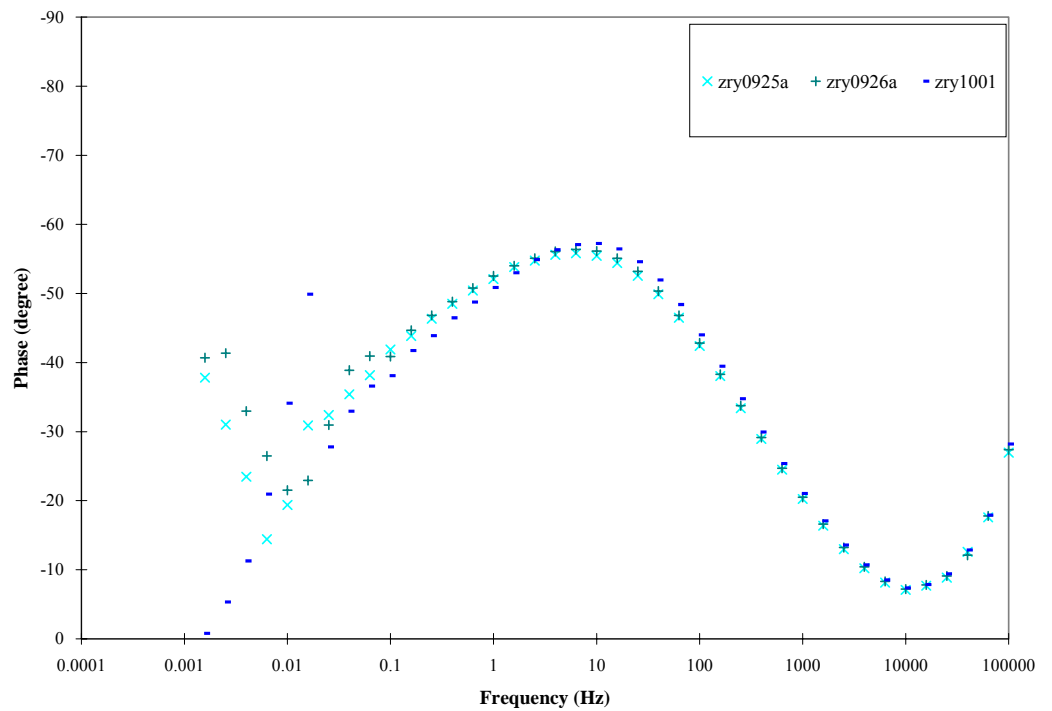
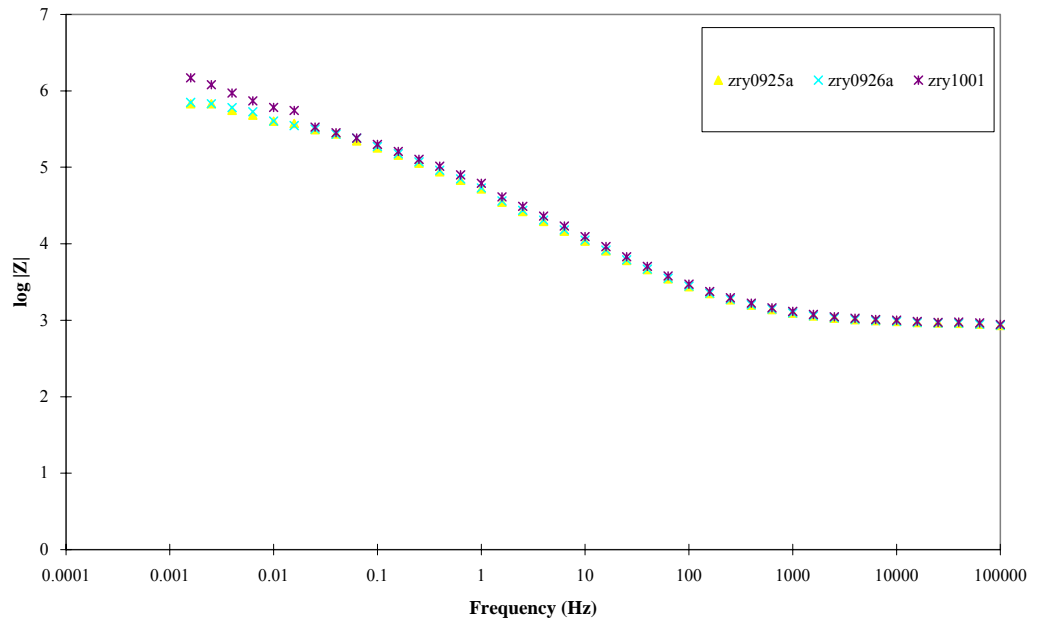
Impedance spectra measured during experiments with the LK2+ material (cont.)



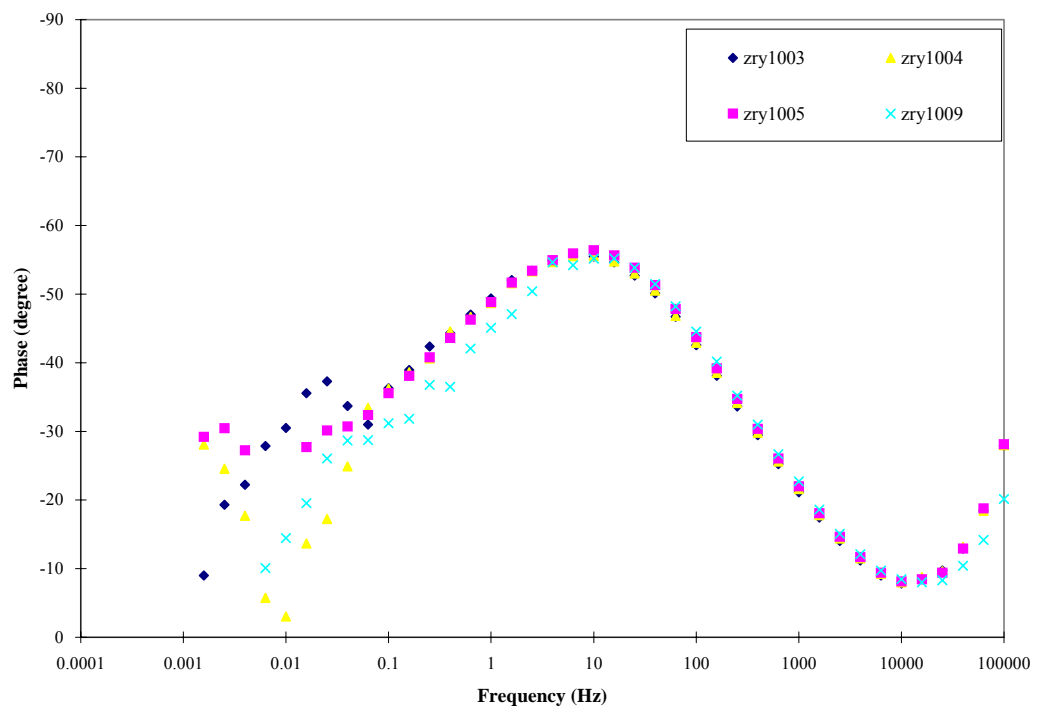
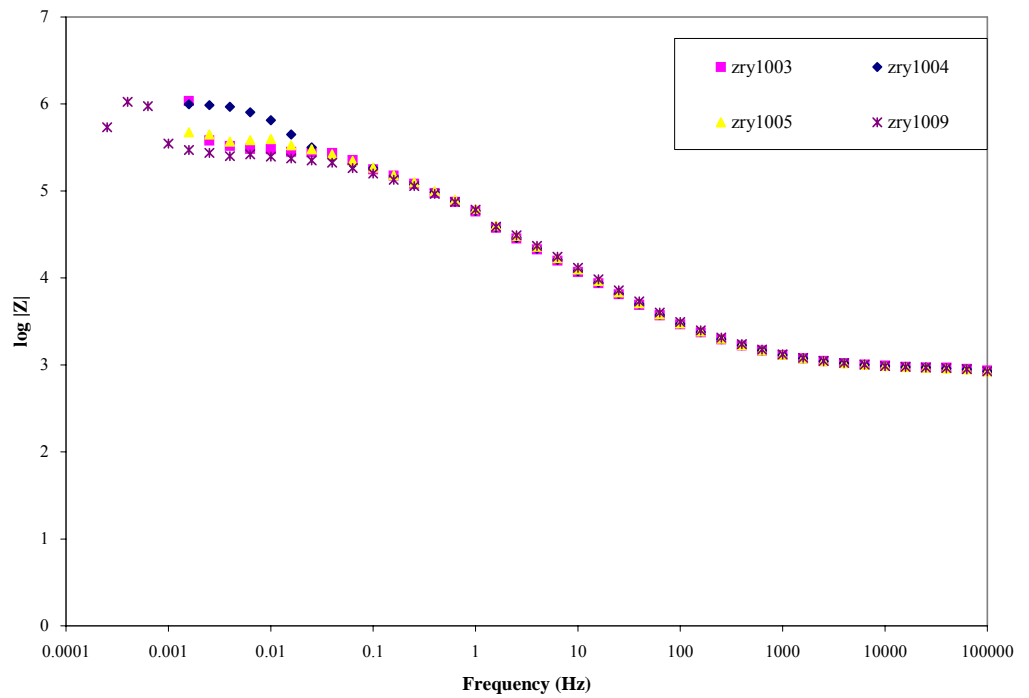
Impedance spectra measured during experiments with the LK2+ material (cont.)

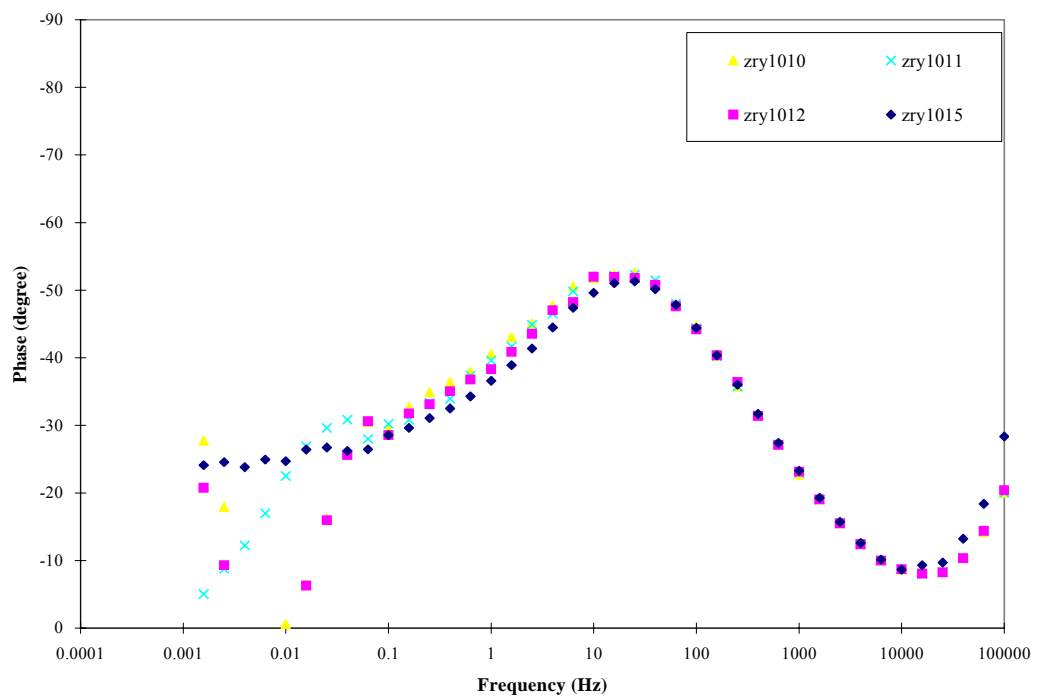
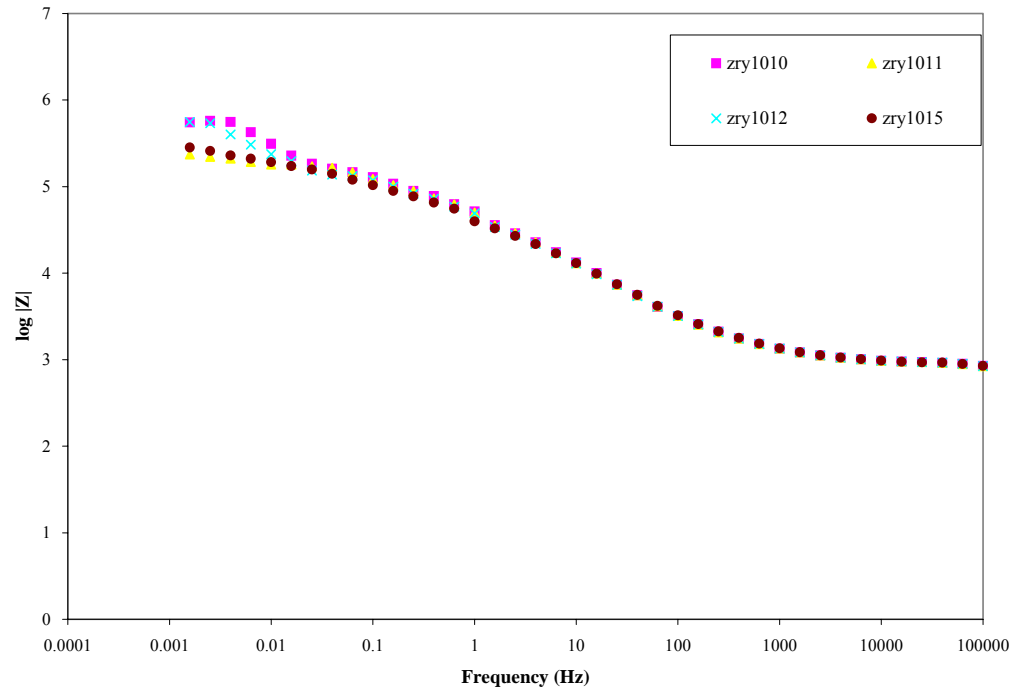
Impedance spectra measured during experiments with the LK2+ material (cont.)

Impedance spectra measured during experiments with the LK3 material

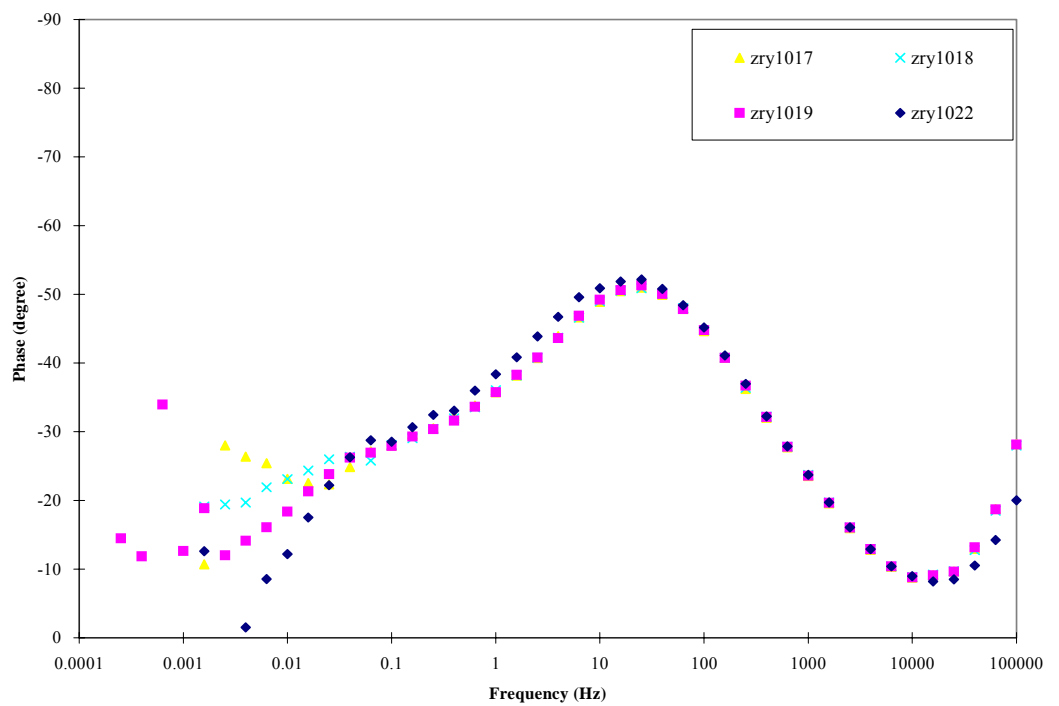
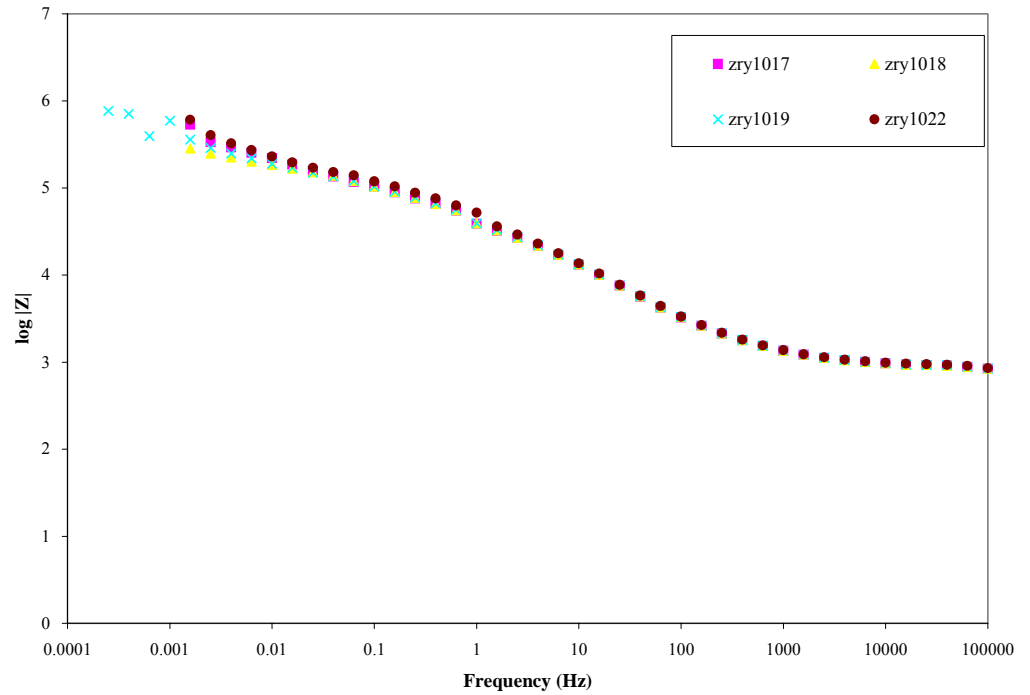


Impedance spectra measured during experiments with the LK3 material (cont.)

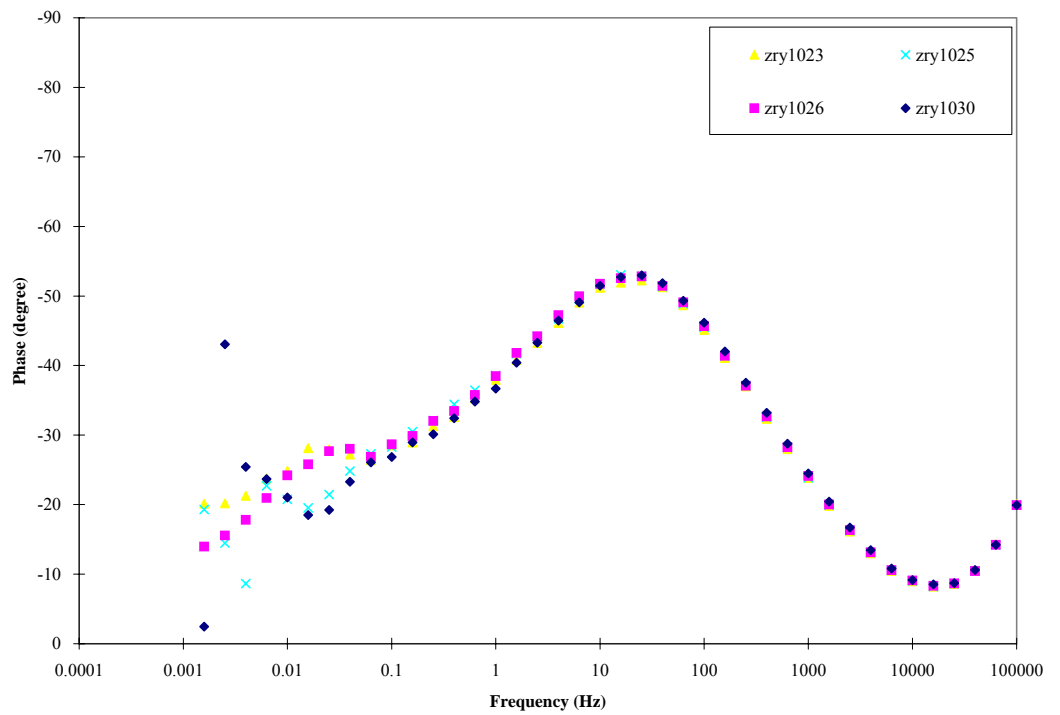
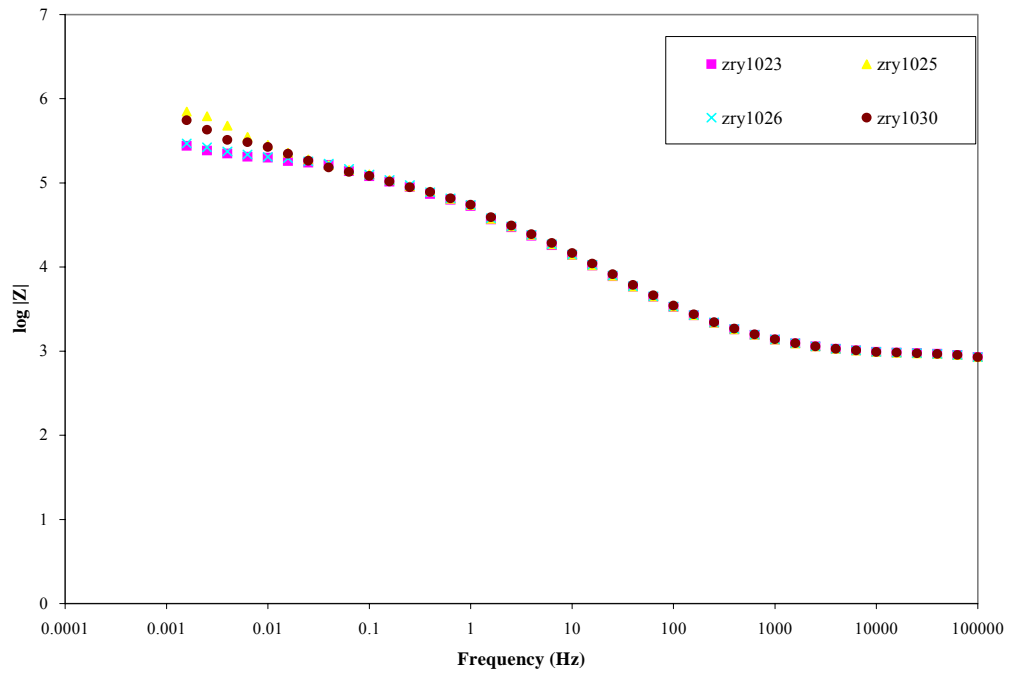


Impedance spectra measured during experiments with the LK3 material (cont.)

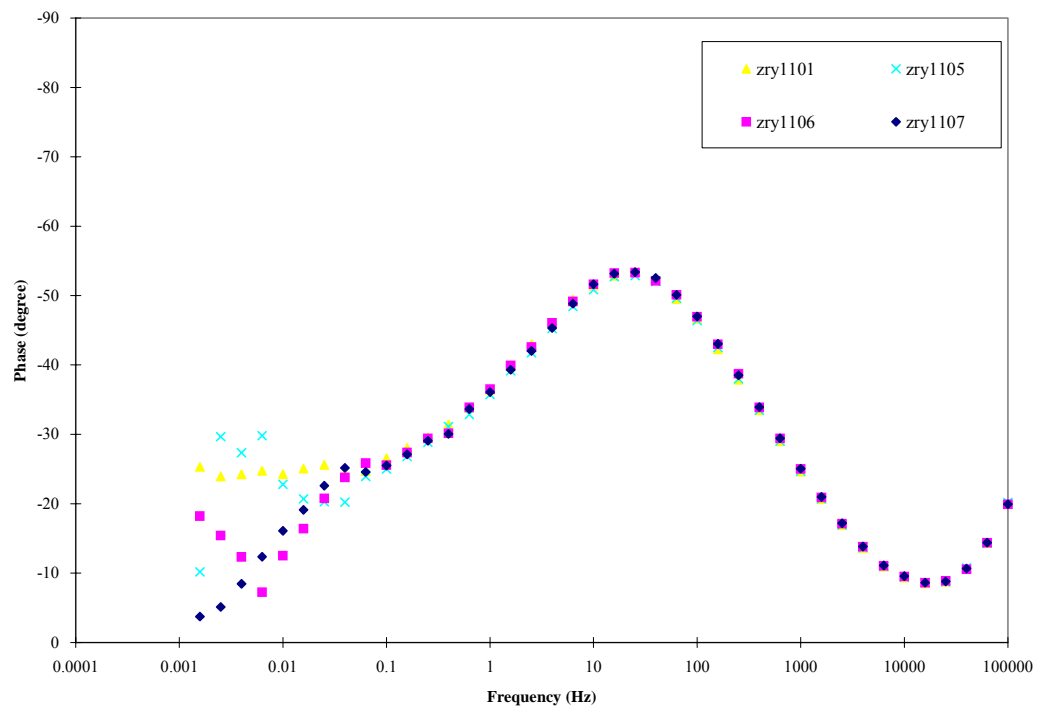
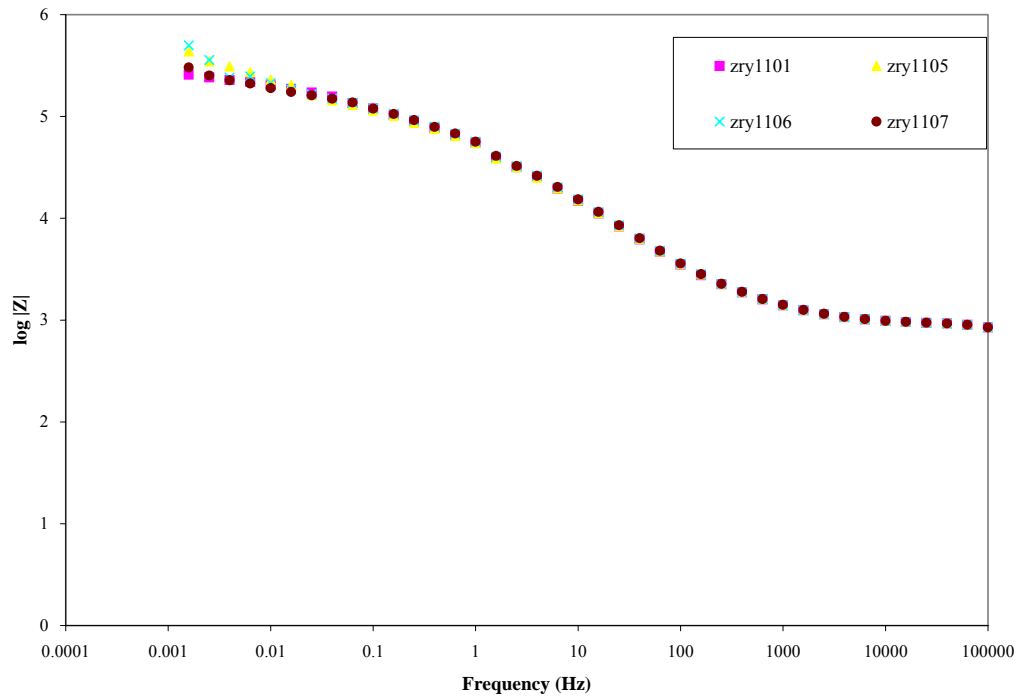
Impedance spectra measured during experiments with the LK3 material (cont.)



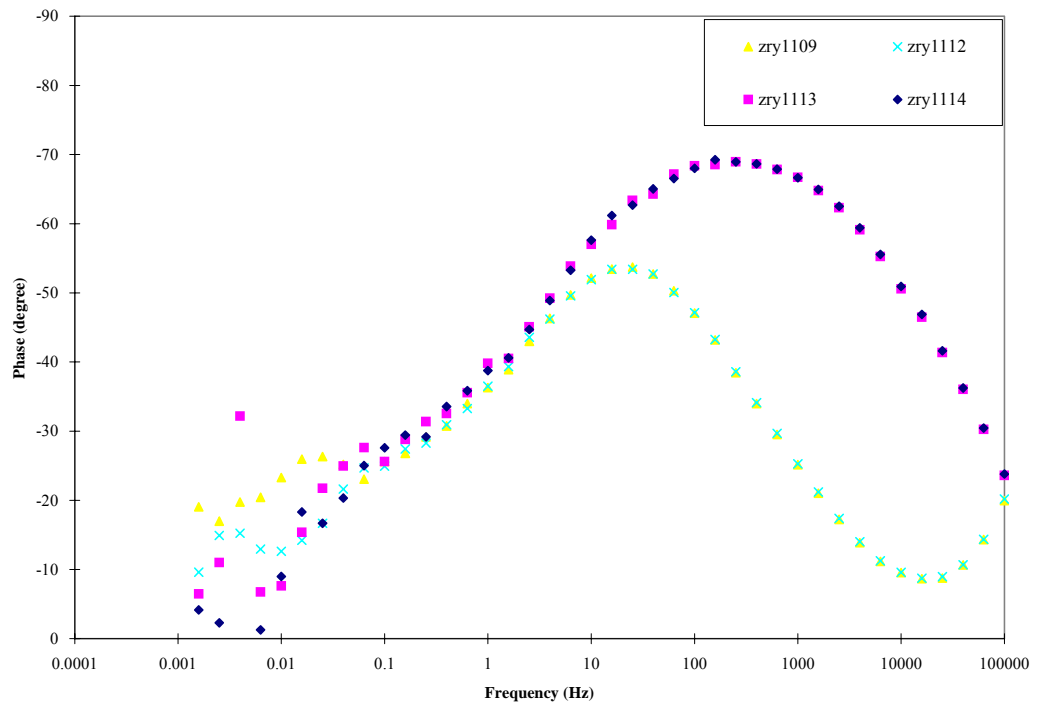
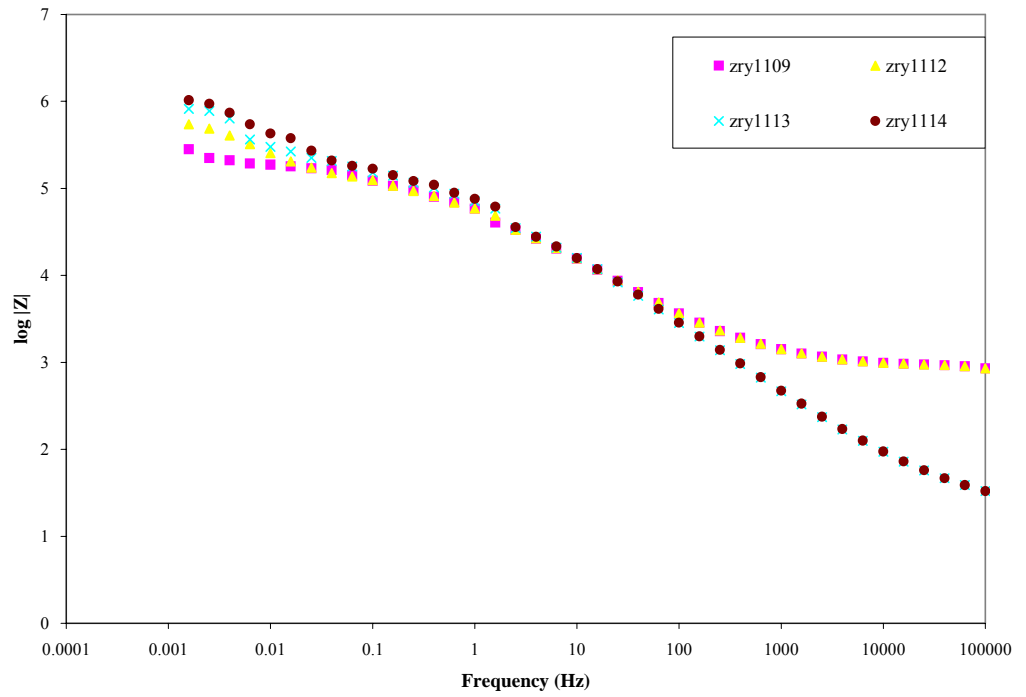
Impedance spectra measured during experiments with the LK3 material (cont.)



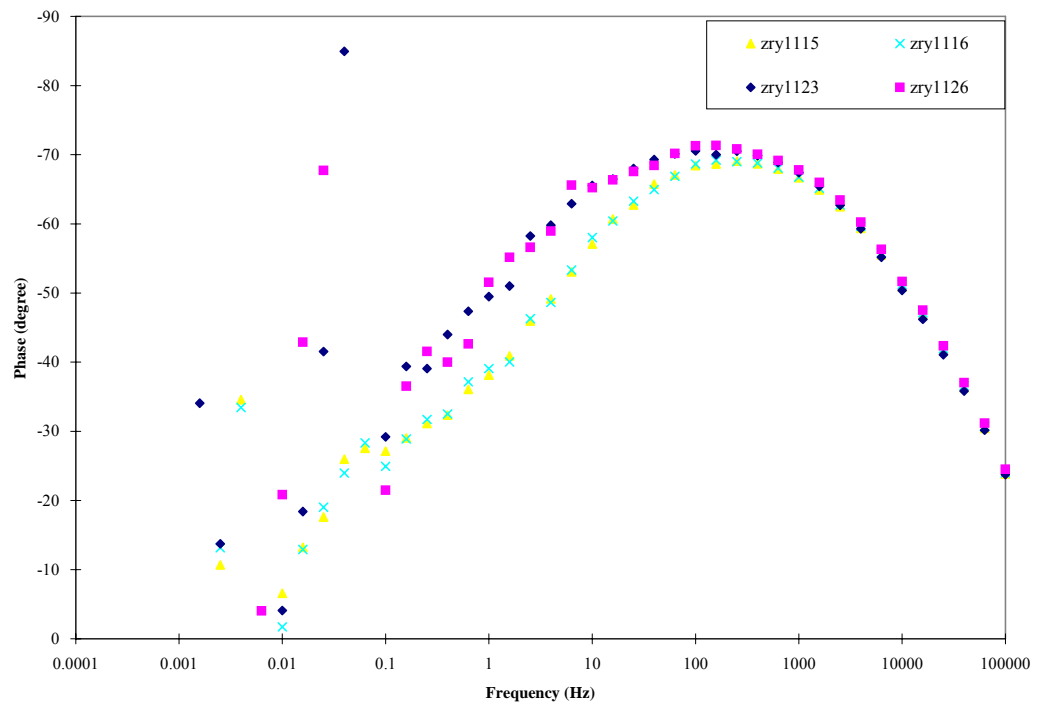
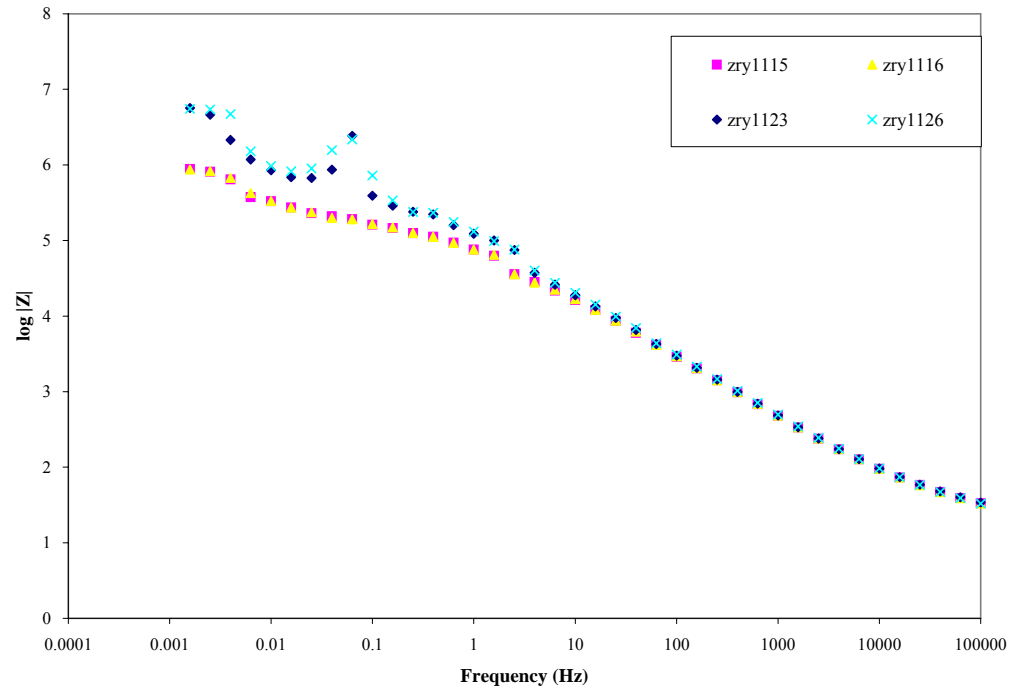
Impedance spectra measured during experiments with the LK3 material (cont.)



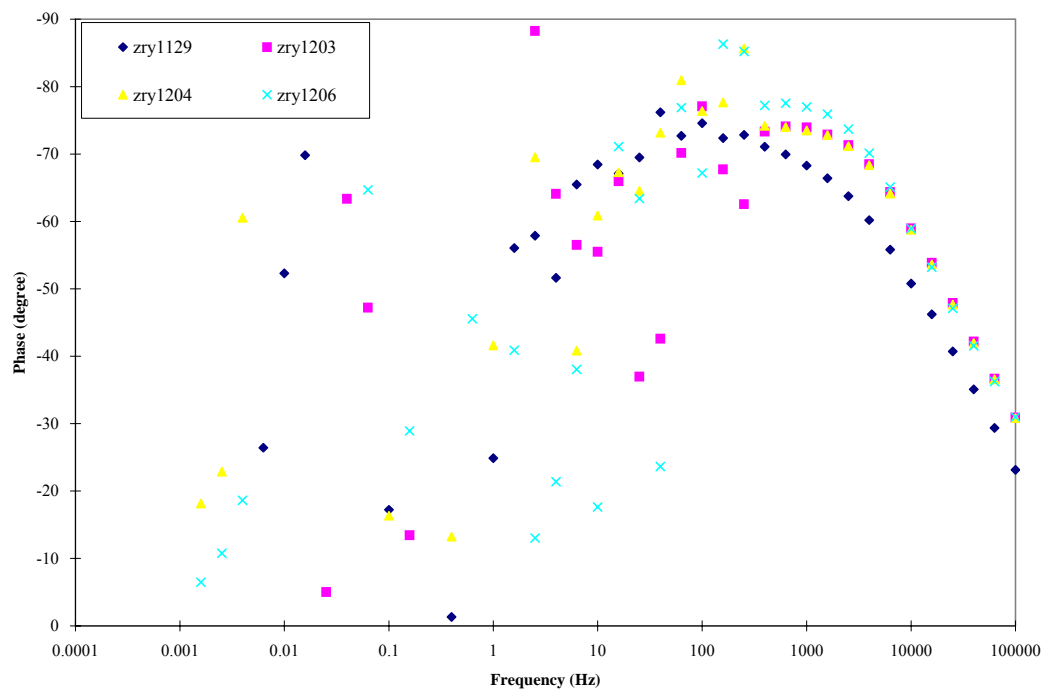
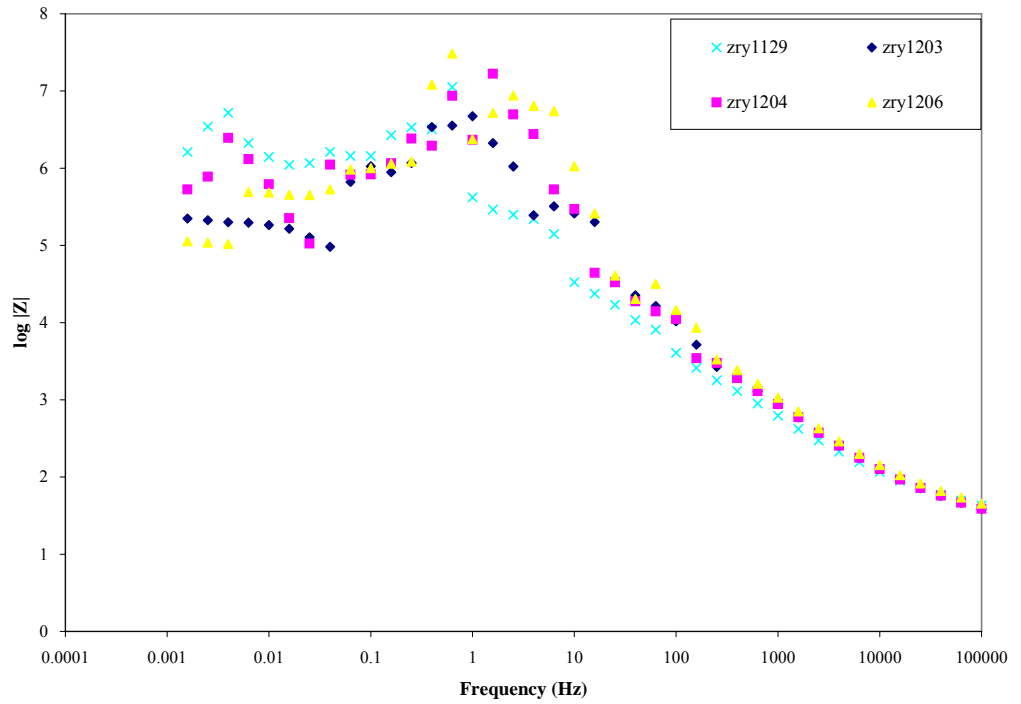
Impedance spectra measured during experiments with the LK3 material (cont.)



Impedance spectra measured during experiments with the LK3 material (cont.)



Impedance spectra measured during experiments with the LK3 material (cont.)



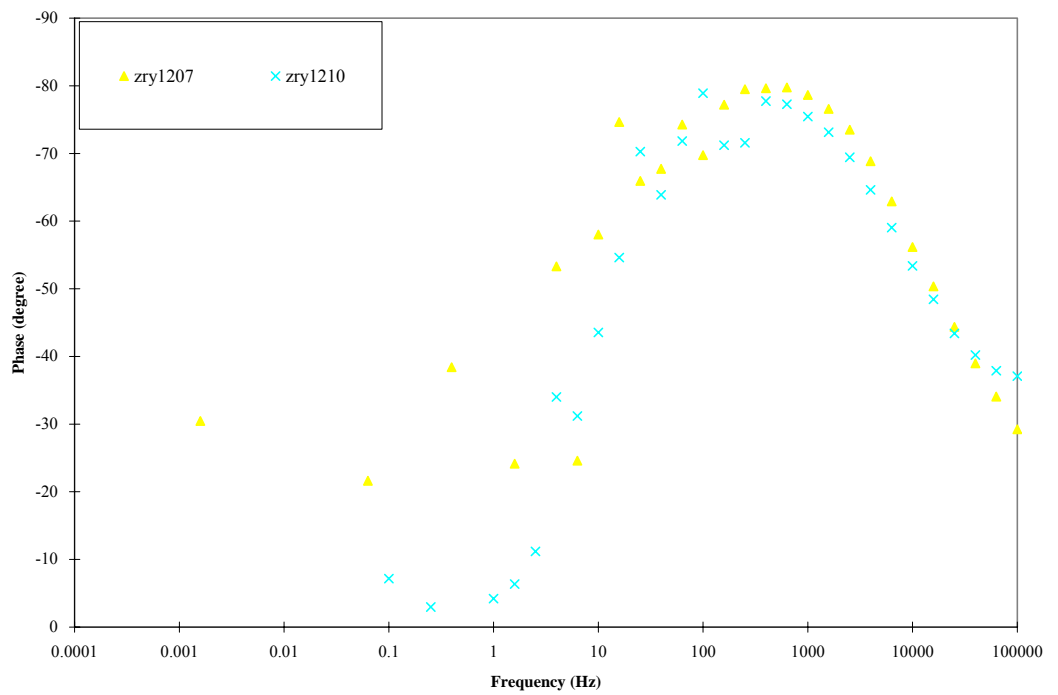
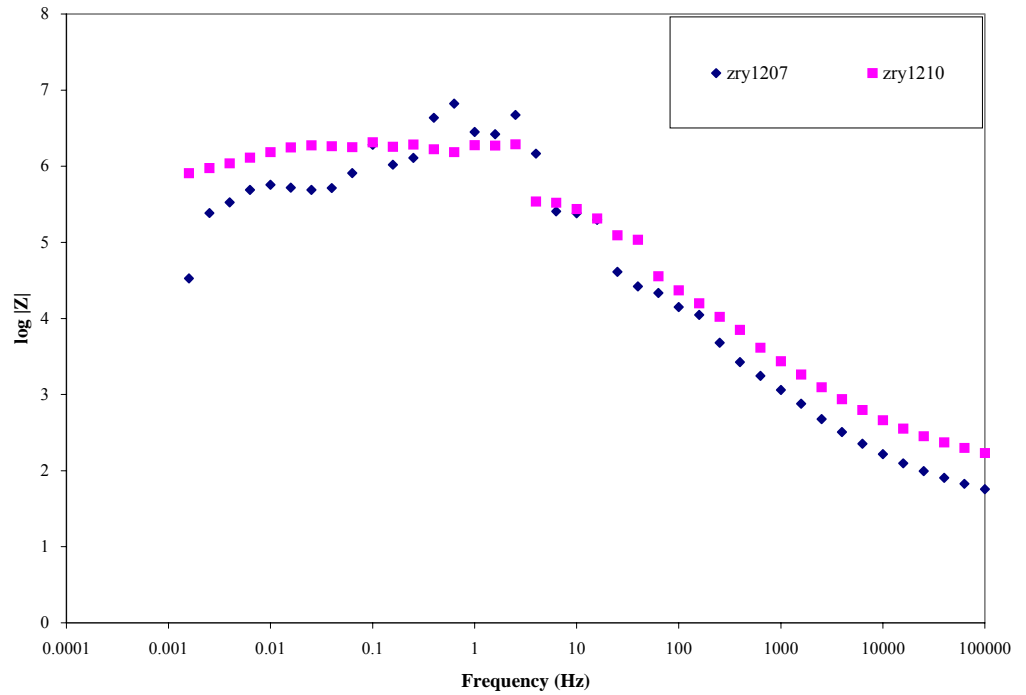
Impedance spectra measured during experiments with the LK3 material (cont.)

Table C.1

Parameter values from the equivalent circuit analysis for the LK2 material.

Date	Temp. (°C)	R1 (Ω)	C1 (F)	Q1 - C _Q (F)	Q1 - α	R2 (Ω)	Q2 - C _Q (F)	Q2 - α	R3 (Ω)
2002-01-11	20	325	1.99E-09	1.44E-05	0.974	1631700			
2002-01-14	20	170	1.94E-09	1.80E-05	0.949	998590			
2002-01-15	20	159	1.90E-09	1.79E-05	0.956	1578000			
2002-01-16	20	153	1.90E-09	1.79E-05	0.960	2568900			
2002-01-17	20	156	1.91E-09	1.73E-05	0.966	2302600			
2002-01-21	100	84		1.27E-05	0.965	458400			
2002-01-22	150								
2002-01-25	200	32		8.75E-06	0.890	142380			
2002-01-28	250	28		6.10E-06	0.848	33340	5.88E-06	1.000	34164
2002-01-31	288	24		4.02E-06	0.843	51886	1.30E-05	1.000	37409
2002-02-01	288	25		3.37E-06	0.852	46126	5.53E-06	1.000	28860
2002-02-04	288	23		3.28E-06	0.839	35150	5.58E-06	1.000	28179
2002-02-07	288	25		4.41E-06	0.798	11814	8.53E-06	0.900	25719
2002-02-08	288	24		4.23E-06	0.799	11799	9.74E-06	0.900	25619
2002-02-11	288	27		3.72E-06	0.804	10915	1.84E-05	0.697	59722
2002-02-12	288	25		3.57E-06	0.806	10662	2.01E-05	0.656	80684
2002-02-14	288	24		3.28E-06	0.812	11356	1.86E-05	0.700	42725
2002-02-15	288	28		3.05E-06	0.816	11415	1.90E-05	0.637	49244
2002-02-18	288	25		2.93E-06	0.817	14220	1.37E-05	0.800	31436
2002-02-19	288	25		2.71E-06	0.824	13567	1.87E-05	0.625	54767
2002-02-20	288	23		2.61E-06	0.826	16110	1.38E-05	0.737	36279
2002-02-21	288	23		2.51E-06	0.828	17734	1.22E-05	0.766	37259
2002-02-25	288	28		1.00E-06	0.898	281	1.18E-06	0.768	71368
2002-03-05	288	26		3.58E-07	0.976	129	1.77E-06	0.774	65135
2002-03-06	288	29		3.74E-07	0.970	116	2.11E-06	0.751	72039
2002-03-08	288	24		3.71E-07	0.971	119	1.88E-06	0.761	76391
2002-03-11	288	29		4.60E-07	0.950	126	1.90E-06	0.742	89472
2002-03-13	288	25		4.58E-07	0.950	119	1.95E-06	0.737	104960
2002-03-15	288	29		1.20E-06	0.873	675	3.97E-07	0.832	75355
2002-03-21	200								
2002-03-25	100								
2002-04-05	20	233	1.87E-09	2.16E-07	0.980	172840			

Table C.2

Parameter values from the equivalent circuit analysis for the LK2+ material.

Date	Temp. (°C)	R1 (Ω)	C1 (F)	Q1 - C _Q (F)	Q1 - α	R2 (Ω)	Q2 - C _Q (F)	Q2 - α	R3 (Ω)
2002-04-22	20	171	1.70E-09	1.67E-05	0.884	7678700			
2002-04-23	20	167	1.74E-09	1.64E-05	0.892	2000000			
2002-04-26	100	56		1.42E-05	0.880	73054			
2002-04-29	200	33		4.13E-06	0.972	14300			
2002-04-30	200	35		3.60E-06	0.978	7909			
2002-05-03	288	31		6.04E-06	0.813	61865			
2002-05-06	288	32		3.43E-06	0.852	2261	9.17E-06	0.635	67020
2002-05-07	288	32		3.51E-06	0.844	1731	1.30E-05	0.610	70174
2002-05-08	288	34		3.18E-06	0.850	1342	1.50E-05	0.594	70958
2002-05-13	288	33		3.30E-06	0.830	1251	3.26E-05	0.579	72632
2002-05-27	288	29		2.14E-06	0.843	380210			
2002-06-13	288	24		2.06E-06	0.838	68000	3.81E-07	0.846	345120
2002-06-14	288	28		1.93E-06	0.842	537460			
2002-06-17	288	22		1.73E-06	0.851	642420			
2002-06-18	288	23		1.71E-06	0.850	661210			
2002-06-19	288	15		1.64E-06	0.857	718680			
2002-06-20	288	12		1.55E-06	0.864	723210			
2002-06-24	288	19		1.57E-06	0.859	689950			
2002-06-25	288	28		1.65E-06	0.848	675360			
2002-06-26	288	27		1.66E-06	0.847	705550			
2002-06-27	288	24		1.61E-06	0.851	502220			

Table C.3

Parameter values from the equivalent circuit analysis for the LK3 material.

Date	Temp. (°C)	R1 (Ω)	C1 (F)	Q1 - C _Q (F)	Q1 - α	R2 (Ω)	Q2 - C _Q (F)	Q2 - α	R3 (Ω)
2001-09-25	288	916	7.90E-10	5.95E-06	0.669	542710			
2001-09-26	288	921	8.04E-10	5.61E-06	0.676	513830			
2001-10-01	288	952	8.01E-10	4.83E-06	0.685	464470			
2001-10-03	288	949	8.29E-10	5.02E-06	0.684	357440			
2001-10-04	288	938	8.43E-10	4.98E-06	0.682	341990			
2001-10-05	288	937	8.44E-10	4.70E-06	0.686	348230			
2001-10-09	288	928	6.16E-10	4.48E-06	0.686	223760			
2001-10-10	288	910	5.95E-10	4.97E-06	0.664	158140			
2001-10-11	288	914	5.99E-10	4.80E-06	0.670	132280			
2001-10-12	288	908	5.99E-10	5.16E-06	0.659	138970			
2001-10-15	288	916	8.67E-10	4.52E-06	0.676	79946	9.46E-06	0.877	57048
2001-10-17	288	906	8.73E-10	4.45E-06	0.675	72530	1.34E-05	0.555	184130
2001-10-18	288	902	8.66E-10	4.42E-06	0.675	72568	1.32E-05	0.543	183550
2001-10-19	288	909	8.66E-10	4.46E-06	0.674	77719	1.55E-05	0.513	249910
2001-10-22	288	907	6.16E-10	4.63E-06	0.666	137460	2.81E-05	0.835	120440
2001-10-23	288	908	6.20E-10	4.49E-06	0.670	132930	2.65E-05	0.858	119440
2001-10-25	288	907	6.18E-10	4.40E-06	0.671	142230	2.52E-05	0.807	141530
2001-10-26	288	909	6.16E-10	4.35E-06	0.673	140830	2.45E-05	0.808	143740
2001-10-30	288	906	6.18E-10	4.13E-06	0.676	128750	2.82E-05	0.868	103550
2001-11-01	288	907	6.21E-10	3.98E-06	0.679	122550	2.60E-05	0.814	111610
2001-11-05	288	919	6.18E-10	3.94E-06	0.678	112820	2.48E-05	0.768	89660
2001-11-06	288	906	6.18E-10	3.86E-06	0.680	127060	3.11E-05	0.810	124200
2001-11-07	288	909	6.20E-10	3.78E-06	0.682	118430	2.79E-05	0.674	144870
2001-11-09	288	910	6.19E-10	3.79E-06	0.681	128720	2.81E-05	0.820	114640
2001-11-12	288	916	6.23E-10	3.63E-06	0.685	129150	3.24E-05	0.875	97406
2001-11-13	288	28		2.39E-06	0.775	126800	1.52E-05	0.775	191010
2001-11-14	288	27		2.32E-06	0.777	135190	1.44E-05	0.818	162590
2001-11-15	288	28		2.31E-06	0.777	143340	1.71E-05	0.845	176910
2001-11-16	288	27		2.28E-06	0.778	143700	1.64E-05	0.843	172170
2001-11-23	288	30		1.87E-06	0.798	456574			
2001-11-26	288	29		1.74E-06	0.803	501144			
2001-11-29	250								
2001-12-03	200								
2001-12-04	200								
2001-12-06	150								
2001-12-07	100								
2001-12-10	20	163		9.62E-08	0.925	573660			

Table D.1

Values of α -corrected (extrapolated) capacitance and accompanying values of the dispersion factor for the LK2 material.

Date	Temp. (°C)	log $C_{\alpha\text{-corr}}$	$C_{\alpha\text{-corr}}$ (F)	α
2002-01-11	20	-5.198	6.339E-06	0.925
2002-01-14	20	-5.115	7.674E-06	0.929
2002-01-15	20	-5.114	7.691E-06	0.927
2002-01-16	20	-5.112	7.727E-06	0.927
2002-01-17	20	-5.118	7.621E-06	0.926
2002-01-21	100	-5.307	4.932E-06	0.902
2002-01-22	150	-5.347	4.498E-06	0.916
2002-01-25	200	-5.711	1.945E-06	0.878
2002-01-28	250	-6.079	8.337E-07	0.848
2002-01-31	288	-6.320	4.786E-07	0.824
2002-02-01	288	-6.350	4.467E-07	0.828
2002-02-04	288	-6.449	3.556E-07	0.807
2002-02-07	288	-6.510	3.090E-07	0.790
2002-02-08	288	-6.522	3.006E-07	0.792
2002-02-11	288	-6.566	2.716E-07	0.786
2002-02-12	288	-6.573	2.673E-07	0.787
2002-02-14	288	-6.568	2.704E-07	0.797
2002-02-15	288	-6.581	2.624E-07	0.798
2002-02-18	288	-6.590	2.570E-07	0.802
2002-02-19	288	-6.592	2.559E-07	0.806
2002-02-20	288	-6.597	2.529E-07	0.806
2002-02-21	288	-6.593	2.553E-07	0.813
2002-02-25	288	-6.614	2.432E-07	0.819
2002-03-05	288	-6.634	2.323E-07	0.824
2002-03-06	288	-6.649	2.244E-07	0.819
2002-03-08	288	-6.643	2.275E-07	0.824
2002-03-11	288	-6.661	2.183E-07	0.823
2002-03-13	288	-6.664	2.168E-07	0.822
2002-03-15	288	-6.676	2.109E-07	0.820
2002-03-21	200	-6.694	2.023E-07	0.910
2002-03-25	100	-6.748	1.786E-07	0.934
2002-04-05	20	-6.790	1.622E-07	0.952

Table D.2

Values of α -corrected (extrapolated) capacitance and accompanying values of the dispersion factor for the LK2+ material.

Date	Temp. (°C)	log C_{α-corr}	C_{α-corr} (F)	α
2002-04-22	20	-5.486	3.266E-06	0.869
2002-04-23	20	-5.483	3.289E-06	0.871
2002-04-26	100	-5.660	2.188E-06	0.825
2002-04-29	200	-5.569	2.698E-06	0.947
2002-04-30	200	-5.727	1.875E-06	0.886
2002-05-03	288	-6.242	5.728E-07	0.827
2002-05-06	288	-6.332	4.656E-07	0.828
2002-05-07	288	-6.366	4.305E-07	0.817
2002-05-08	288	-6.396	4.018E-07	0.803
2002-05-13	288	-6.474	3.357E-07	0.798
2002-05-27	288	-6.612	2.443E-07	0.819
2002-06-13	288	-6.644	2.270E-07	0.816
2002-06-14	288	-6.639	2.296E-07	0.828
2002-06-17	288	-6.635	2.317E-07	0.839
2002-06-18	288	-6.640	2.291E-07	0.839
2002-06-19	288	-6.628	2.355E-07	0.843
2002-06-20	288	-6.626	2.366E-07	0.844
2002-06-24	288	-6.647	2.254E-07	0.840
2002-06-25	288	-6.665	2.163E-07	0.837
2002-06-26	288	-6.667	2.153E-07	0.838
2002-06-27	288	-6.666	2.158E-07	0.840

Table D.3

Values of α -corrected (extrapolated) capacitance and accompanying values of the dispersion factor for the LK3 material.

Date	Temp. (°C)	log $C_{\alpha\text{-corr}}$	$C_{\alpha\text{-corr}}$ (F)	α
2001-09-25	288	-7.094	8.054E-08	0.661
2001-09-26	288	-7.093	8.072E-08	0.665
2001-10-01	288	-7.104	7.870E-08	0.674
2001-10-03	288	-7.133	7.362E-08	0.659
2001-10-04	288	-7.145	7.161E-08	0.658
2001-10-05	288	-7.145	7.161E-08	0.663
2001-10-09	288	-7.208	6.194E-08	0.647
2001-10-10	288	-7.250	5.623E-08	0.635
2001-10-11	288	-7.188	6.486E-08	0.657
2001-10-12	288	-7.204	6.252E-08	0.651
2001-10-15	288	-7.222	5.998E-08	0.646
2001-10-17	288	-7.233	5.848E-08	0.644
2001-10-18	288	-7.236	5.808E-08	0.644
2001-10-19	288	-7.235	5.821E-08	0.645
2001-10-22	288	-7.224	5.970E-08	0.653
2001-10-23	288	-7.219	6.039E-08	0.655
2001-10-25	288	-7.215	6.095E-08	0.658
2001-10-26	288	-7.218	6.053E-08	0.658
2001-10-30	288	-7.221	6.012E-08	0.661
2001-11-01	288	-7.226	5.943E-08	0.662
2001-11-05	288	-7.242	5.728E-08	0.659
2001-11-06	288	-7.229	5.902E-08	0.665
2001-11-07	288	-7.233	5.848E-08	0.664
2001-11-09	288	-7.232	5.861E-08	0.666
2001-11-12	288	-7.236	5.808E-08	0.666
2001-11-13	288	-6.895	1.274E-07	0.768
2001-11-14	288	-6.899	1.262E-07	0.769
2001-11-15	288	-6.900	1.259E-07	0.771
2001-11-16	288	-6.900	1.259E-07	0.773
2001-11-23	288	-6.856	1.393E-07	0.798
2001-11-26	288	-6.861	1.377E-07	0.802
2001-11-29	250	-6.931	1.172E-07	0.813
2001-12-03	200	-6.954	1.112E-07	0.880
2001-12-04	200	-6.955	1.109E-07	0.880
2001-12-06	150	-6.982	1.042E-07	0.909
2001-12-07	100	-6.991	1.021E-07	0.927
2001-12-10	20	-7.428	3.733E-08	0.907

www.ski.se

STATENS KÄRNKRAFTINSPEKTION
Swedish Nuclear Power Inspectorate

POST/POSTAL ADDRESS SE-106 58 Stockholm

BESÖK/OFFICE Klarabergsviadukten 90

TELEFON/TELEPHONE +46 (0)8 698 84 00

TELEFAX +46 (0)8 661 90 86

E-POST/E-MAIL ski@ski.se

WEBBPLATS/WEB SITE www.ski.se